Development and evaluation of meropenem encapsulated nanostructured lipid carriers as an antimicrobial treatment of *Pseudomonas aeruginosa*

By

Charlotte Elizabeth Wilson

Submitted in partial fulfilment of the Master of Science (by research)
School of Pharmacy and Biomedical Science, University of Central Lancashire

Date of submission: October 2023

Declaration

RESEARCH STUDENT DECLARATION FORM

Type of Award Master's by Research

School Pharmacy and Biomedical Science

1. Concurrent registration for two or more academic awards

I declare that while registered as a candidate for the research degree, I have not been a registered candidate or enrolled student for another award of the University or other academic or professional institution.

_____

2. Material submitted for another award

I declare that no material contained in the thesis has been used in any other submission for an academic award and is solely my own work.

_____

3. Collaboration

Where a candidate's research programme is part of a collaborative project, the thesis must indicate in addition clearly the candidate's individual contribution and the extent of the collaboration. Please state below:

_____

4. Use of a Proof-reader

No proof-reading service was used in the compilation of this thesis.

Signature of Candidate _____ 

Print name: ___Charlotte Elizabeth Wilson_____

Table of Contents

List of Tables

List of Figures

List of abbreviations

ABC	**ATP-binding cassette**
ACBT	Active cycle of breathing techniques
ACT	Airway clearance techniques
BCC	Burkholderia cepacia complex
CF	Cystic Fibrosis
CFTR	Cystic fibrosis transmembrane conductance regulatory
CLED	Cystine-Lactose-electrolyte- deficient agar
DD-transpeptidase	D-alanyl-D-alanine transpeptidase
DSC	Differential scanning calorimetry
EE	Entrapment Efficiency
FD	Free drug
FTIR	Fourier transform infrared spectroscopy
HPLC	High performance liquid chromatography
ICH	International Conference on Harmonisation
MATE	Multidrug and toxic compound extrusion
MBC	Minimum bactericidal concentration
MDR	Multi drug resistant
ME-NLCs	Meropenem loaded nanostructured lipid carrier
MFS	Major facilitator superfamily
MIC	Minimum inhibitory concentration
NETs	Neutrophil extracellular traps
NLC	Nanostructured lipid carrier
PBP	Penicillin binding protein
PBP3	Penicillin binding protein 3
PDI	Polydispersion Index
PEP	Positive expiratory pressure
RND	Resistance-nodulation-division
RT	Retention time
RSD	Relative standard deviation
SLN	Solid lipid nanoparticle
SMR	Small multidrug resistance
WHO	World Health Organisation
XDR	Extensive drug resistance
ZP	Zeta potential

Abstract

Pseudomonas aeruginosa (*P. aeruginosa*) is a Gram-negative bacterium which most commonly causes opportunistic infections in immunocompromised individuals including those with cystic fibrosis. Meropenem is a carbapenem antibiotic with a beta lactam structure which is recommended as a treatment for meropenem-susceptible *P. aeruginosa* infections *P. aeruginosa* has developed multiple resistance mechanisms including resistance to beta lactam antibiotics such as meropenem.

Nanoparticles can be used as a targeted treatment therapy by utilizing a controlled delivery and release of active pharmaceutical ingredient at a specific target site. Therefore, encapsulating antibiotics, such as meropenem, which has high renal elimination, a short half-life and is unstable in aqueous solutions, could provide an alternative drug delivery pathway for treatment of sensitive strains of *P. aeruginosa*, improving pharmacokinetic outcomes.

Meropenem-encapsulated nanostructured lipid carriers (ME-NLCs) were formulated using Sodium Cholate as a surfactant, Dynasan 114 as a solid lipid, Capryol 90, oleic acid, lipoid E80 and lipoid S75 as liquid lipids, and Kolliphor HS 15 as a solubiliser. A hot homogenisation method followed by probe sonication was used for preparation of NLCs. Optimisation of product parameters (surfactant, liquid and solid lipids, solubiliser and drug concentration) and process parameter (sonication time) was carried out to obtain NLCs with desired physicochemical properties in terms of particle size, polydispersity index, zeta potential and drug entrapment. Increasing the concentration of surfactant sodium cholate resulted in an increase in particle size (<200nm) and poly dispersity index (<0.3) of the NLCs. Similarly, the loading of meropenem in NLCs resulted in an increase of particle size but interestingly did not

affect the PDI. Meropenem-loaded NLCs produced a particle size of 178.8nm , poly dispersity index 0.283 and zeta potential -31mV.

A high performance liquid chromatography (HPLC) method was developed and validated to quantify meropenem in the NLCs formulations and drug encapsulation was calculated to be 85.72%. Additionally in vitro drug dissolution studies of the ME-NLCs revealed an initial fast release of 30% of the drug in the first thirty minutes and a sustained release of drug from NLCs with 70% of the drug being released for 8 hours which then remained steady until 24 hours.

Reference isolates of *P. aeruginosa* ATCC 27853 were tested for minimum inhibitory concentration (MIC) and minimum bactericidal concentration (MBC) using – ISO-20776-1 method recommended by EUCAST - using the ME-NLCs. The minimum inhibitory concentration for ME-NLC for *P. aeruginosa* was 2 μg/ml. The ME-NLCs was bactericidal at a concentration of 8 μg/ml, compared to free drug which has a MIC of 0.5 μg/ml and MBC of 4 μg/ml.

Interactions between ME-NLCs and *P. aeruginosa* cells were investigated using fluorescence microscopy. Morphological changes were observed in the bacterial cells which showed an increase in the number of elongated rod-shaped cells.

The use of meropenem encapsulated NLCs may provide an alternative drug delivery system with the potential to optimise therapeutic dosage without increasing nephrotoxicity.

Acknowledgements

I would like to acknowledge with sincere appreciation my director of study Dr David Wareing and co-supervisor Professor Kamalinder Singh for excellent scientific guidance, advice, support, and encouragement throughout my research. Working with you both has been a fantastic and educational experience; you have made me become a better researcher.

I would like to express my gratitude and thanks to my parents Darrel and Andrea Wilson I could never reach this far without your support in every possible way.

Thank you to my partner Micheál for his continuous support and encouragement throughout this time.

I would also like to thank all of my family and friends for their motivation and support. I am grateful for each and every one of you.

Finally, I would like to express my gratitude towards A1 Skip Hire Ltd for the funding to allow me to fulfil this degree.

Chapter 1: Introduction

1.1 Introduction to *Pseudomonas aeruginosa*

Pseudomonas aeruginosa (P. aeruginosa) was first described in 1882 by Carle Gessard a French pharmacist, during his investigation 'On the blue and green coloration of bandages' (Diggle and Whiteley 2020).

The Gram negative bacillus, monoflagellated, non-sporing, obligate aerobic bacterium that optimally grows at 37°C after 24-48hrs, also has the ability to grow at temperatures between 4°C and 42°C, which aids in distinguishing it from other *Pseudomonas* species (Diggle and Whiteley 2020). The colonies produced are of opaque and pearlescent appearance with a characteristic fruity smell when cultured on nutrient agar (LaBauve and Wargo, 2012). *P. aeruginosa* also has the ability to produce one or multiple pigments when growing on different culture media. The pigments can include pyorubin (red), pyocyanin (blue/green) and pyoverdine (yellow/green, fluorescent) (Abdelaziz, Kamer *et al.,* 2023). *P. aeruginosa* is an opportunistic pathogen which predominantly inhabits soil, water and host-associated environments such as plants, animals and humans (Diggle and Whiteley 2020). In a clinical background *P. aeruginosa* is globally recognised as a cause of hospital-acquired infections, in immunocompromised individuals. In 2018 Public Health England (PHE) reported that *P. aeruginosa* infections were responsible for 7.8 cases per 100,00 population, with 37.8% being hospital-acquired infections (PHE, 2018).

Reynolds and Kollef (2021) reported in an international observational point prevalence study that of all *P. aeruginosa* infects, 16.2% were community-acquired infections and 23% were hospital-acquired infections.

1.1.2 Infection scenarios of *Pseudomonas aeruginosa*

Hospital-acquired infections caused by *P. aeruginosa* can arise due to bacterial reservoirs in the clinical setting such as taps, sinks, icemakers, sanitizers and respiratory therapy equipment including ventilators and endoscopes (Kanamori, Weber *et al.,* 2016). The transmission of the bacterium within the clinical setting is problematic due to the risk of infection to the immunocompromised patients because of the opportunistic nature of *P. aeruginosa*, which can cause systemic infections in severe cases (Qin, Xiao *et al.,* 2022). This includes patients with conditions such as burns and wounds, organ transplants, HIV/AIDS and cystic fibrosis (Qin, Xiao *et al.,* 2022).

Burns and wounds cause damage to the epidermis and dermis, allowing the first line of defence of the immune system to be breached, inducing colonisation in the damaged tissue. this can be either acute infection such as cellulitis (Bassetti, Vena *et al.,* 2018) or severe infections including sepsis (Reynolds and Kollef 2021). A study from 1999-2009 found that *P. aeruginosa* was responsible for 64% of deaths in paediatric intensive care due to sepsis (Reynolds and Kollef 2021).

In addition, patients with invasive devices such as endotracheal tubes, urinary and other indwelling catheters and joint replacements are at risk of infections caused by *P. aeruginosa* due the ability of the bacterium to form a biofilm (Mulcahy, Isabella *et al.,* 2014). *P. aeruginosa* has the ability to survive up to sixteen months on dry inanimate surfaces such as food packaging and up to five weeks on flooring (Kramer, Schwebke *et al.,* 2006), and in water

taps due to the alginate slime formed in the biofilm matrix. This colonisation of *P. aeruginosa* in biofilm form can be impenetrable to disinfectants and antipseudomonal agents (Aziz et al. 2022).

However, the most recognised opportunistic infection of *P. aeruginosa* is within the pulmonary system of those with cystic fibrosis (CF). Over a six-year period between 2006-2012, it was reported by the cystic fibrosis foundation patient registry, that *P. aeruginosa* had a prevalence of 49.6% within CF patients (Reynolds and Kollef 2021). This is further increased within older patients where 74.1% of cultures were positive for *P. aeruginosa*.

1.1.3. Virulence factors of Pseudomonas aeruginosa

Virulence factors of *P. aeruginosa* can be classified into three categories: bacterial surface structures, secreted factors and bacterial cell-to-cell interaction (Liao, Huang *et al.,* 2022). Bacterial surface structures allow for interaction with the human host lung epithelium by using the bacterium's flagellum and pili for motility and adhesion while also utilising other virulence factors to bind to the host cells (Liao, Huang *et al.,* 2022). During adhesion the flagellar cap protein FliD is used to bind to mucins in the airways (Haiko and Westerlund-Wikström 2013). The lipopolysaccharide (LPS) located in the outer membrane of Gram negative bacteria is an activator of the host immune response, stimulating neutrophils to release neutrophil extracellular traps (NETs) (Liao, Huang *et al.,* 2022). White blood cells, including neutrophils engulf invading pathogens in the body to undergo phagocytosis. *P. aeruginosa* utilises this process by stimulating NETs to capture other invading pathogens such

as *Staphylococcus aureus* in the lung microbiome thereby preventing phagocytosis of *P. aeruginosa*, allowing for production of a biofilm matrix.

P. aeruginosa uses five different types of secretory systems to transport and release bacterial proteins and other virulence factors directly into targeted cells and or the extracellular space: type I, type II, type III, type V and type VI (Qin, Xiao *et al.,* 2022). Types II and III are the secretory systems which the main virulence factors are released (Liao, Huang et al., 2022). The type II system is responsible for the secretion of various lytic enzymes, whereas type III is responsible for the virulent effectors used in the host cells (Liao, Huang *et al.,* 2022).

The secreted factors can be classified into four categories: exopolysaccharides, siderophores, proteases and toxins.

Exopolysaccharides are a highly viscous carbohydrate macromolecules found in the extracellular matrix, that are used by *P. aeruginosa* to increase tolerance to harsh environments, for example the host defence/immune response, by the formation of microcolonies within biofilm (Liao, Huang *et al.,* 2022), which in turn increases the pathogenesis of the bacteria by inhibiting the action of the immune response consequently aiding the survival. Additionally, exopolysaccharides are primary parts of the extracellular matrix structure, which are essential for the structure and integrity of formation and maintenance of *P. aeruginosa* biofilm (Flemming, Niese *et al.,* 2022).

Siderophores are compounds secreted by the bacterium to aid with iron accumulation.

P. aeruginosa produces two siderophores, pyoverdine and pyochelin. Pyoverdine and pyochelin are used to promote bacterial growth by chelating iron molecules, particularly Fe^{3+}

from transferrin and lactoferrin in the host environment (Liao, Huang *et al.,* 2022). Both siderophores are required for full impact virulence.

Proteases are used to interfere with host cell immunity. In particular the serine protease IV has the ability to degrade molecules such as immunoglobulins, collagen-containing surfactant proteins and to damage host cells and tissues (Liao, Huang *et al.,* 2022), consequently allowing for increased spread of bacterial infection in the host.

Toxins, ExoS, ExoT, ExoU and ExoY are secreted via the type III secretory system, (Horna and Ruiz 2021). The primary actions of these toxins include the disruptions of the host's actin cytoskeleton which simultaneously interferes with the cell-cell adhesion and promotes apoptosis of the host cell.

P. aeruginosa uses quorum sensing to provide bacterial cell-to-cell interactions. Quorum sensing controls transcription of toxicity genes, and the regulation of the other virulence factors such as proteases and toxins, while also stimulating the maturation of the biofilm within the host (Qin, Xiao *et al.,* 2022).

1.1.4. Treatments for *P. aeruginosa* infections

Treatment of *P. aeruginosa* infection is dependent on the intrinsic and or acquired antimicrobial resistance of the strain causing infection. The co-morbidities of the individual can also be a contributing factor to the treatment of an infection. There are eight categories of antibiotic that are used to treat *P. aeruginosa* infections: aminoglycosides, carbapenems, cephalosporins, fluoroquinolones, penicillin with beta-lactamase inhibitors, monobactams,

fosfomycin and polymyxins (Pottier, Gravey *et al.,* 2023). The antipseudomonal agents suggested as a first line treatment for respiratory *P. aeruginosa* infections is an aminoglycoside with a beta-lactam penicillin (Bassetti, Vena *et al.,* 2018). First line treatment for skin and soft tissue infections with *P. aeruginosa* is directly dependent on the results of the in vitro susceptibility testing and is generally treated with a beta lactam antibiotic (cefepime), a carbapenem (meropenem) or a fluoroquinolone (ciprofloxacin), (Bassetti, Vena et al., 2018)

1.1.5. Resistance mechanisms of *Pseudomonas aeruginosa*

Resistance can be categorised into multi drug-resistant (MDR), extensively drug-resistant (XDR) and pandrug-resistant (PDR). Multidrug resistance is defined as resistance being observed in one or more agents in three categories (Magiorakos, Srinivasan *et al.,* 2012). XDR is determined by resistance being observed in in at least one agent in six or more categories and PDR is determined by the resistance being observed in all agents in each respective category (Basak, Singh et al., 2016).

1.1.6 Intrinsic resistance

P. aeruginosa has intrinsic antimicrobial resistance methods including reduced outer membrane permeability, efflux systems and antibiotic-inactivating enzymes, to decrease the efficacy of individual or multiple antimicrobial agents (Pachori, Gothalwal *et al.,* 2019).

Alterations in the outer membrane permeability directly impact the ability for the antibiotics to pass through the cell membrane (Delcour, 2009). This decreases the efficacy of antibiotics with modes of action inside the cell and periplasmic space, such as inhibiting bacterial protein synthesis, interfering DNA replication and blocking bacterial cell wall biosynthesis. Penicillin-binding protein 3 (PBP3) is essential for the growth and remodelling of peptidoglycan in the cell wall of *P. aeruginosa* (Chen, Zhang *et al.,* 2017). Mutations within the gene *ftsI* which encodes for PBP3 have undergone selective pressure to alter the active site of the PBP to reduce binding affinity and decrease the efficacy of beta-lactam antibiotics for cell lysis (Horcajada, Montero *et al.,* 2019).

Porin channels used for the uptake of molecules into the cell, are used by some classes of antibiotics to gain entry to bacterial cells. Mutations within the genes *parR* and *parS* in *P. aeruginosa* cause a downregulation of the narrow outer membrane porin protein *OprD* which provides a specific channel for basic amino acids and small peptides (Li, Luo *et al.,* 2012). Carbapenems share a similar structural composition to amino acids and small peptides, which enables the uptake through *OprD* (Delcour, 2009). Therefore, decreasing the permeability of the outer cell membrane, decreases antibiotic action and uptake and further contributing to resistance in *P. aeruginosa*.

Efflux systems allow the bacterium to eject toxic compounds, macromolecules and antibiotics from the intracellular matrix and periplasmic space to prevent cell death. There are five families of bacterial efflux pumps: resistance-nodulation-division (RND), major facilitator superfamily (MFS), ATP-binding cassette (ABC), small multidrug resistance (SMR) and multidrug and toxic compound extrusion (MATE) (Sharma, Gupta *et al.,* 2019). Antibiotic

resistance due to the efflux pump family RND in which *P. aeruginosa* expresses twelve efflux pumps in total with four which give rise to further antibiotic resistance; *MexAB-OprM, MexCD-OprJ, MexEF-OprN*, and *MexXY-OprM* (Lorusso, Carrara *et al.,* 2022).

In particular the hyperproduction of the RND transporter *MexAB-OprM*, encoded for on genes *mexR*, *nalC* and *nalD* is used to transport fluroquinolones, carbapenems and carboxypenicillins out of the cell (Pang, Raudonis *et al.,* 2019), whereas *MexCD-OprJ* is able to expel beta-lactams, *MexEF-OprN* can remove quinolones and *MexXY-OprM* eliminates aminoglycosides. This decreases the antibiotics action and contributes to increased resistance (Lorusso, Carrara *et al.,* 2022).

Beta-lactamase and aminoglycoside-modifying enzymes hydrolyse amide and ester bonds and are able to inactivate antibiotics. (Pang, Raudonis *et al.,* 2019).

The beta-lactam enzymes can be categorised into four classes (A, B, C and D) depending on the amino acid sequence (Tooke, Hinchliffe *et al.,* 2019). *P. aeruginosa* utilises the enzyme beta-lactamase, which is encoded by the *ampC* gene (Glen and Lamont 2021). The enzyme hydrolyses the amide bond within the beta-lactam ring inactivating the antibiotic, which consequently is no longer able to inhibit bacterial wall synthesis. Class C beta-lactamase enzymes inhibit antipseudomonal agents such as cephalosporins by hydrolysing the beta lactam rings with active sites containing serine (Tooke, Hinchliffe *et al.,* 2019). However, it has been shown that some *P. aeruginosa* strains can produce extended-spectrum-beta lactamase enzymes (ESBLs), which are part of the enzyme classes A and D (Glen and Lamont 2021), further increasing the resistance to beta-lactam antibiotics including penicillins, cephalosporins and aztreonam.

1.1.7. Acquired resistance.

Acquired antibiotic resistance in bacteria can arise through mutation of genes or the acquisition of resistance genes through horizontal gene transfer.

Gene mutations can cause cellular changes such as the overexpression of efflux pumps, production of antibiotic – inactivating enzymes or modifications of antibiotic targets. Mutations within the genes *parR* and *parS* in *P. aeruginosa* causes a downregulation of the membrane porin protein *OprD* (Pang, Raudonis *et al.,* 2019).

Horizontal transfer of resistance genes is a result of the movement of genetic information between organisms. Resistance genes can be carried on plasmids, transposons, integrons and prophages. The horizontal gene transfer mechanisms are transformation, conjugation and transduction. Transformation occurs when there is an uptake of DNA from the surrounding environment into the bacterium. When the gene is directly transferred from one cell to another cell, this is the mechanism conjugation. Furthermore, the final mechanism is transduction, which occurs when bacteriophages move genetic information from one cell to another (Pang, Raudonis *et al.,* 2019).

1.1.8. Adaptive resistance

The bacterium has the ability to adapt to survive within environments that are less than optimal, such as introducing antibiotics to the environment. Environmental stimuli to *P. aeruginosa* can result in the formation of a biofilm and the generation of persister cells. Persister cells are responsible for approximately 1% of the bacterial population, which can increase in exponential and stationary phase cultures (Lewis, 2008). Research suggests that

the increase of persister cells in cultures can be attributed to oxidative stress, DNA damage and the presence of antibiotics (Grassi, Di Luca *et al.,* 2017). Persister cells contribute to chronic infections and increasing antibiotic resistance as the cells allow for regrowth and recolonisation after initial antibiotic treatment, therefore presenting further challenges for the treatment of infections including that of *P. aeruginosa (*Grassi, Di Luca *et al., 2017).*

1.2.1. Introduction to Cystic fibrosis

Cystic Fibrosis (CF) is a recessive autosomal disease, that is characterised by the mutation of the cystic fibrosis transmembrane conductance regulatory (*CFTR*) gene on chromosome 7 that encodes for the *CFTR* protein (Manos, 2021).

CF predominantly occurs within the Caucasian population with 1 in 2,500-3,500 new-borns diagnosed each year (Nayak, 2012). Mutations in the *CFTR* gene cause either the production of malfunctional proteins or absent CFTR protein to be synthesised (Manos, 2021). The CFTR protein is responsible for the movement of chloride and bicarbonate ions and regulates the sodium and potassium ion channels within the epithelial cell membrane of the respiratory, gastrointestinal, and reproductive system (Liou, 2019). Without the functional CFTR protein the pathophysiology presented by CF is the secretion of abnormal dehydrated viscous mucus that coats the walls of the lungs (Clunes and Boucher 2007). The large amounts of viscous mucus present in the lungs provides an optimum environment for bacterial colonisation by species such as *Pseudomonas aeruginosa* (Figure 1.1). Therefore, frequent use of antibiotics in bacterial infections for CF patients promotes the colonisation of increasingly resistant

strains of organisms on the sticky mucus coating the upper and lower respiratory tract along with the lungs.

The ecology of the cystic fibrosis pulmonary microbiome is highly diverse and includes bacteria, viruses, fungi and archaea. The cystic fibrosis ecological succession model described by Khanolkar (2020), identifies five clear stages: barren, pioneer, intermediate, climax and perturbation. This is also associated with six age ranges. The barren stage is associated with the neonatal period in which colonisation of the neonate can arise during delivery and is related to the different methods of delivery (Khanolkar, Clark *et al.,* 2020). The pioneer stage, associated with infancy is responsible for colonisation by multiple strains including *Staphylococcus aureus, Haemophilus influenzae* and *Streptococcus spp*. in the upper respiratory system (Khanolkar, Clark *et al.,* 2020). Once the individual has reached childhood and progresses to adolescence and further to adulthood the microbiome succession goes from intermediate to climax. 'Intermediate' is characterised by the increased incidence of *Pseudomonas aeruginosa, Burkholderia cepacia complex* (BCC*), Stenotrophomonas* sp*.* and *Achromobacter* sp. (Khanolkar, Clark *et al.,* 2020). The climax phase is typically represented by colonisation with *P. aeruginosa* and *Burkholderia cepacia complex* (Khanolkar, Clark *et al.,* 2020). Furthermore, succession can then increase to perturbation during the stage of exacerbation, in which growth of anaerobes such as *Prevotella* spp. (Khanolkar, Clark *et al.,* 2020), can result in a significant health challenge to the individual and can provide the conditions for adaptive resistance of the overall microbiome.

Factors that can affect the microbiome of the CF lung include age, pulmonary exacerbations, antibiotic exposure, host immunity, genetic background, disease state, and lung function of

the individual (Françoise and Héry-Arnaud 2020). The lung function of an individual is measured by forced expiratory volume, which decreases with increased age. This also correlates to the ecological succession stage of climax because with decreased lung capacity, there is a decrease in the diversity of the microbiome and the dominance of *P. aeruginosa* and *Burkholderia cepacia complex* occurs (Françoise and Héry-Arnaud 2020). Similarly, exposure to antibiotics can also decrease the diversity of the microbiome as the susceptible organisms will be killed by the antibiotic, and the selective pressure will allow for the increase of antibiotic resistant bacteria in the microbiome (Khanolkar, Clark *et al.,* 2020). In parallel to this, the increase of pulmonary exacerbations relates to the decrease of lung function, hence a decrease in the overall diversity of the microbiome but an increase in the dominant pathogenic bacteria (Françoise and Héry-Arnaud 2020).

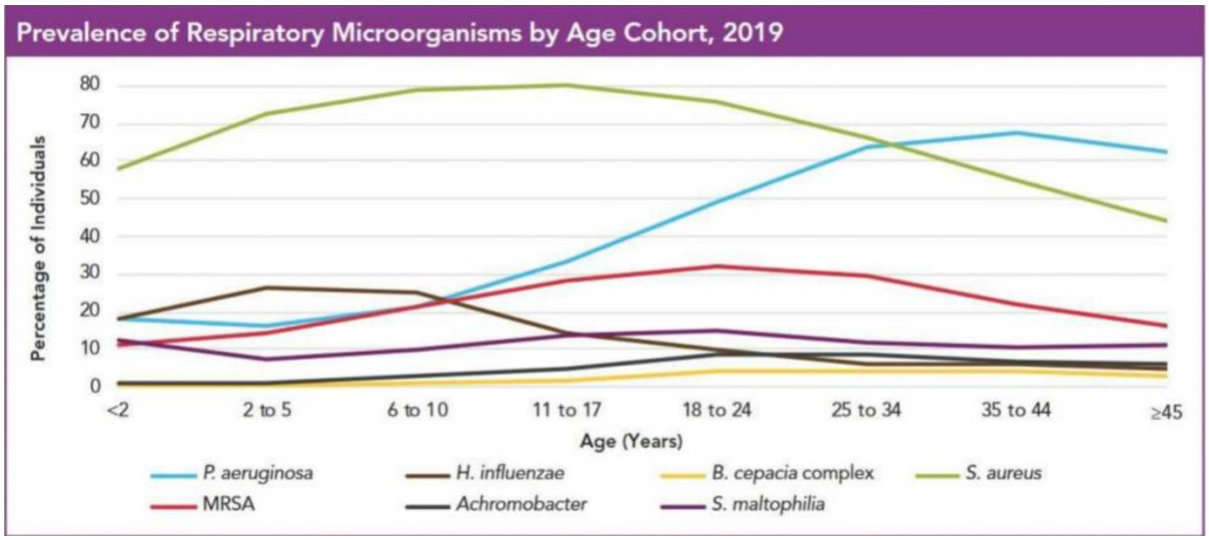

Figure 1. 1. The prevalence of bacterial respiratory infections in patients with cystic fibrosis in relation to age (Manos, 2021).

1.2.2 Current treatment methodologies for Cystic Fibrosis

Treatments for CF include preventative methods and therapeutic medication for infections (Döring *et al.,* 2012). Preventive methods include antibiotic prophylaxis, airway clearance techniques (ACT) such as lung lavages, active cycle of breathing techniques (ACBT), autogenic drainage, positive expiratory pressure (PEP) devices and bronchodilators (Lee, Button and Tannenbaum, 2017). These ACTs are used to dilate and expectorate excess mucus from the respiratory tracts, aiding in the reduction of bacterial infections in CF patients. A synergistic approach to support the reduction in mucus is the use of hypertonic saline and ivacaftor, which is a transmembrane conductance regulator potentiator (TCRP) (Donaldson *et al.,* 2018). A TRCP allows increased volume of chloride ions at the CSM which in turn thins the mucus (Tildy and Rogers, 2015). Furthermore, antibiotics are used as a prophylaxis for chest infections. Thus for *P. aeruginosa,* meropenem is given for susceptible strains but for meropenem resistant strains a treatment of ciprofloxacin or amikacin is given via intravenous injections (Doi, 2019).

1.3.1. Introduction to antimicrobial agents

Antibiotics can be grouped by the mode of action and the cellular synthesis they inhibit. Cell wall synthesis inhibition antibiotics are described as either beta-lactam e.g., meropenem or glycopeptides. There are five other antibiotic groups that inhibit either protein synthesis, DNA synthesis, folic acid synthesis, mRNA synthesis or DNA (damage) synthesis (Kapoor, Saigal *et al.,* 2017).

Beta lactam antibiotics are further split into four classifications: penicillin, cephalosporins, carbapenems, monobactams (Bush and Bradford, 2016). Beta-lactams have a mode of action which disrupts the bacterial cell wall formation via interfering with the synthesis of the cross linking in the peptidoglycan and weakening the cell wall to cause bacterial lysis and cell death (Kapoor, Saigal et *al.,* 2017), thereby classifying beta-lactams as bactericidal for susceptible strains of bacteria.

The bacterial cell walls consist of peptidoglycan which are linear chains of polysaccharides in the formation of a three-dimensional crystal lattice. Each polysaccharide chain consists of N-acetylglucosamine (NAG) and N- acetylmuramic acid (NAM) in an alternating pattern, along with pentapeptides forming cross links via the enzymatic action of D-alanyl-D-alanine-transpeptidases (DD-transpeptidases), commonly known as penicillin binding proteins (PBP) (Yadav, Espaillat and Cava, 2018). Beta lactam antibiotics cause the weakening of the cell wall by disabling DD-transpeptidases between each linear chain, in turn weakening the cross links and consequently the full bacterial cell wall causing cell lysis and cell death (Cho, Uehara and Bernhardt, 2014).

Resistance to beta-lactam antibiotics is rising due the horizontal transfer of genes coding for modification of penicillin binding proteins and the production of beta-lactamases enzymes.

The production of beta-lactamase enzymes which are an intrinsic resistance mechanism within *P. aeruginosa*, inactivates the antibiotic by hydrolysing the beta-lactam ring (Tooke *et al.,* 2019). In addition, the production of an altered form of the PBP caused by mutations in *ftsI* which encodes for PBP3 inhibits the action of beta-lactam antibiotics due to a lower binding affinity between the PBP active site and beta-lactam antibiotics. However, this limitation can be overcome by the use of beta-lactamase inhibitors in conjunction with beta-lactam antibiotics (Bush and Bradford, 2016) to prevent the hydrolysis of the beta-lactam ring,

therefore increasing the efficacy. An example of this is tazobactam and piperacillin for the treatment of P. *aeruginosa* infections (Bush and Bradford, 2016).

Glycopeptides e.g., vancomycin also inhibit cell wall synthesis in Gram positive bacteria. Similarly, to beta lactams, glycopeptides affect cell wall synthesis by the cyclic peptide of the glycopeptide binding to amino acids D-alanyl-D-alanine-transpeptidase preventing the addition of new units to form the crystalline lattice (Zeng, Debabov *et al.,* 2016). The difference between beta-lactams and glycopeptides is that they are only effective against Gram positive bacteria because the antibiotic is unable to penetrate the lipopolysaccharide containing outer membrane of Gram negative bacteria.

Limitations of glycopeptides include the poor penetration to body tissue, nephrotoxicity and administration via intravenously or orally for vancomycin, restricting the clinical use of glycopeptides (Ziglam and Finch, 2001).

Aminoglycosides, tetracyclines, macrolides and lincosamides inhibit bacterial protein synthesis. Protein synthesis inhibitors can act on the 30S/50s ribosomal subunit (Kapoor, Saigal *et al.,* 2017). This prevents the amino acids forming peptide bonds, consequently stopping the synthesis of proteins within the cell and causing cell lysis. Resistance to protein synthesis inhibitors is caused by alterations to the ribosomal binding site, inhibiting antibiotic binding. Limitations of the use of aminoglycosides include that of nephrotoxicity, neuromuscular blockade and increased resistance (Kapoor, Saigal *et al.,* 2017).

Fluoroquinolones are part of the DNA topoisomerase synthesis inhibitors.

Fluoroquinolones, act within the intracellular space of the bacterium, targeting DNA gyrase or topoisomerase to inhibit the supercoiling within the bacterial cell (Hooper and Jacoby, 2016);which is used to maintain the proper chromosomal structure within the DNA strand. Limitations of fluoroquinolones include adverse side effects, toxicity and increased resistance (Hooper and Jacoby, 2016).

Furthermore, limitations to the use of antibiotics are the increasing resistance among *P. aeruginosa* with 93% being resistant to ampicillin, 89.5 % resistant to gentamicin and 2.9% resistant to imipenem (Ahmadi, Hashemian *et al.,* 2016).

1.4.1. Meropenem

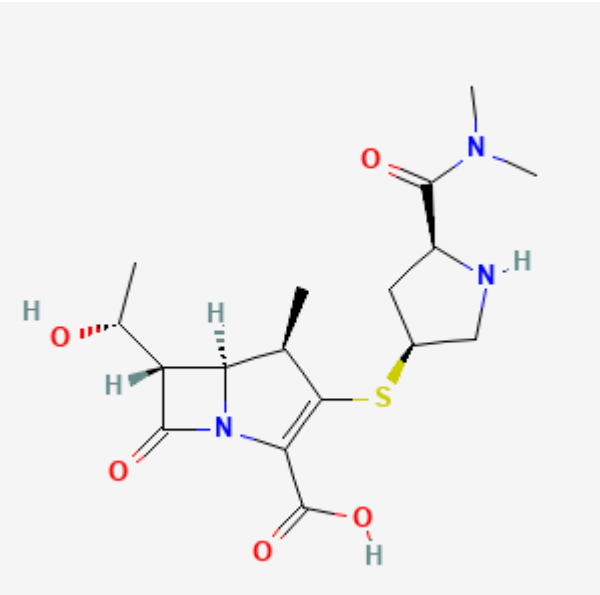

Figure 1. 2. Diagram to show the chemical structure of meropenem (National Center for Biotechnology Information 2023).

Meropenem, is a broad-spectrum carbapenem antibiotic effective against Gram positive and Gram negative bacteria. The meropenem molecule is sparingly soluble in water with a solubility value of 5.36mg/mL and a partition coefficient (LogP) of -0.46. The strongest acidic

pKa for meropenem in a crystalline powdered form is 2.9 and the strongest basic pKa is 7.4. Research conducted by (Fawaz *et al.,* 2019) showed that once meropenem is reconstituted that the 90% of the molecule is intact after 7.4 hours at 22 ° C, therefore the stability decreases after reconstitution and kept before use in crystalline form to increase stability. Meropenem inhibits cell wall synthesis by blocking the activity of DD-transpeptidase in the peri-plasmic space between the cell wall and cell membrane (Meletis, 2016). Dosages are dependent on the age of the individual and the infection. The National Institute for Health and Care Excellence (NICE, 2023) advises that for adults with lower respiratory-tract infection in cystic fibrosis, meningitis and endocarditis, two grams of meropenem should be infused every 8 hours. For infections caused by aerobic and anaerobic Gram positive and Gram negative bacteria and in hospital-acquired septicaemia, 0.5-1 gram is infused intravenously every 8 hours for an adult individual (NICE, 2023). The half-life of meropenem is approximately one hour within adults and with normal renal function (Fish, 2006). In neonates the half-life extends to approximately two hours and in preterm neonates to approximately three hours (Maria Pacifici 2019). Elimination of intravenous meropenem can be detected within the urine after 12 hours with approximately 70% unchanged (Thalhammer, Schenk *et al.,* 1998). The utility and administration in a clinical setting is limited due to the current prescribing information that a three-hour infusion must be completed within four hours upon reconstitution as meropenem is stable for ~4-6 hours when stored at 25° C (Fawaz, Barton *et al.,* 2019). This is due to the instability of meropenem in aqueous solution.

Meropenem is well tolerated within the body. Some patients experience adverse side effects including diarrhoea, rash, vomiting and inflammation at the injection site (Linden, 2007) or severe side effects for example seizures (NICE, 2023).

1.5.1 Introduction to antibiotic resistance

Antibiotic resistance is the result of the evolutionary and mutational changes within bacteria (Dadgostar, 2019). According to the English Surveillance Programme for Antimicrobial Utilisation and Resistance (ESPAUR) report, the number of severe antibiotic resistant infections in England rose by 2.2% in 2021, compared to 2020 (Ashiru-Oredope, Cunningham *et al.,* 2023). The ESPAUR study found that 20.9% of bloodstream infections, in patients with white ethnic background were caused by antibiotic resistant strains (Ashiru-Oredope, Cunningham *et al.,* 2023). Similarly, 32.8% of infections in patients from Asian or British Asian background and 31.8% of those with the Black, African, Caribbean or Black British ethnicities had infections caused by resistant strains (Ashiru-Oredope, Cunningham *et al.,* 2023).

The increased use and misuse of antibiotics within the health care system contributes to increased antibiotic resistant strains of bacteria. Antibiotic misuse in the clinical setting includes over prescribing for non-bacterial infections (Mohareb, Letourneau et al., 2021). Community scenarios of antibiotic misuse include the sharing of antibiotics between individuals or the reuse of left over antibiotics from a previous prescription (Wong, Alias *et al.,* 2021).

The use of antibiotics within the agricultural sector also contributes to the development of resistant bacterial strains. The agricultural sector uses antibiotics in the livestock feed as a prophylaxis to prevent and treats infections along with the abilities to promote growth (Kasimanickam, Kasimanickam *et al.,* 2021). Antibiotic and their metabolite residues can be found in animal manure which and can contaminate surfaces, soil and groundwater along

with wastewater and farm surface water that does not absorb into the ground due to irrigation (Manyi-Loh, Mamphweli *et al.,* 2018). The contamination of natural water reservoirs is particularly problematic due to antibiotics with high water solubility, which can lead to increased spread in the environment. Similarly, the use of animal manure to fertilise land can also contribute to the spread of antibiotics and metabolites (Manyi-Loh, Mamphweli *et al.,* 2018). This is a direct factor in the development of resistant strains of bacteria as the environmental leaching of antibiotics and metabolites affect environmental bacteria. The selective environmental pressure allows for adaptive and acquired resistance in bacteria.

The World Health Organisation (WHO) has highlighted ways each section within the clinical settings, agricultural settings, and individuals can do to prevent and control of antibiotic resistance (World Health Organisation, 2021). Prevention strategies for health care workers include the reporting of resistant strains and the regulation of appropriate use of antibiotics for suitable treatment of infections (Zanichelli, Sharland *et al.,* 2023). Strategies for individuals include the prevention of infection through good hygiene, the use of antibiotics that have been prescribed and to not share or reuse unused and leftover antibiotics (World Health Organisation, 2021). Those within the agricultural sector can aid in the prevention of antimicrobial resistance by the vaccination of animals, the administration of antibiotics to animals under veterinary supervision and eliminating the use of antibiotics for growth promotion or prophylaxis (Zanichelli, Sharland *et al.,* 2023).

Within the clinical setting, in order to treat antibiotic resistant strains, the use of antimicrobial susceptibility testing can allow for the appropriate selection of antibiotics instead of giving multiple dosages of multiple antibiotics. This principle is implemented within the United

Kingdom by the General Pharmaceutical Council with the 'Start smart then Focus' campaign (UK Health Security Agency, 2023).

In addition, as global antimicrobial resistance is increasing the development of new antibiotics and reservation of key antibiotics is becoming a requirement. This is important as it provides patients a viable treatment to multi drug resistant bacteria (World Health Organisation, 2021).

Furthermore, the WHO (2016) have established a 'Global action plan on antimicrobial resistance'. The action plan defines five critical objectives. The objectives are to improve awareness of antimicrobial resistance, increase the research and surveillance of both resistant and susceptible strains of bacteria, reduce the spread of infections, optimize the use of antimicrobials and to invest in future measures to counter the ever-growing problem of antimicrobial resistance (World Health Organisation 2016).

1.6.1 Introduction to nanoparticles

Nanoparticles are spherical or rod-shaped particles composed of natural or inorganic polymers, within a size range of 10-500nm, with applications in delivering drugs across biological barriers (Singla and Upadhyayula, 2022). Types of nanoparticles that can be used consists of three main categories: polymeric, inorganic and lipid based. Polymeric nanoparticles are subcategorised into polymersome, dendrimers, polymer micelle and nanosphere (Mitchell, Billingsley *et al.,* 2021). Advantages of the use of polymeric nanoparticles consists of precise control of particle characteristics, payload flexibility for hydrophilic and hydrophobic cargo and easy surface modification. However, disadvantages

include poor stability due to the possibility of aggregation and toxicity (Elmowafy, Shalaby *et al.,* 2023).

Similarly, inorganic nanoparticles can be subcategorised into silica nanoparticles, quantum dot, iron oxide nanoparticles and gold nanoparticles. Inorganic nanoparticles have unique electrical, magnetic and optical properties, can vary in size, structure and geometry and are well suited for theranostic applications but also have toxicity and solubility limitations (Laurent, Forge *et al.,* 2008).

Lipid based nanoparticles are subcategorised into liposomes, solid lipid nanoparticles (SLN), nanostructured lipid carriers (NLCs) and nanoemulsions. Lipid based nanoparticles have advantages of high bioavailability and payload flexibility especially with solid lipid nanoparticles (SLN) and nanostructured lipid carriers (NLC) (Dhiman, Awasthi *et al.,* 2021). Limitations to SLNs include low encapsulation efficiency due to the ridged crystalline lipid matrix, causing drug expulsion and burst release. However, these limitations have been overcome by the development of second-generation lipid based nanoparticles; NLCs allowing for increased drug payload in the amorphous lipid matrix consequently extending drug release (Dhiman, Awasthi *et al.,* 2021).

Nanoparticles can be used as a targeted treatment therapy by utilizing a controlled delivery and release of either organic or inorganic pharmaceutical compounds at a specific target site. For example, the use of protein ligands such as single domain antibodies can be used for active targeting in bacterial infections (Gao *et al.,* 2014). Both organic and synthetic drugs are often encapsulated to nanoparticles due to low solubility of the drug proposed in either water or nontoxic solutes (Patra *et al.,* 2018). Conjugating drugs to nanoparticles are determined by

several factors including physical structures, toxicity, chemical structure, and surface charge of the conjugated particles.

The uptake of nanoparticles within bacterial and eukaryotic can be either passive or active. Passive uptake is categorised as pinocytosis and is limited due to the limited permeability of the cell membrane, therefore limiting the passive diffusion to small particles with a neutral charge (Mitchell, Billingsley *et al.,* 2021). Active diffusion of molecules can be achieved via three possible pathways caveolin-mediated endocytosis, clathrin-mediated endocytosis and independent endocytosis. The endocytic pathways are influenced by the characteristics of the nanoparticles including rigidness and size. Rod shaped nanoparticles are most commonly diffused by caveolin-mediated endocytosis, which occur in molecules smaller than approximately 60 nanometres (Sousa de Almeida, Susnik *et al.,* 2021), whereas spherical nanoparticles are most commonly diffused using clathrin-mediated endocytosis, which is receptor mediated and which relies on the electrostatic or hydrophobic interactions of nanoparticles and the cell membrane in areas that have high expression of clathrin (Sousa de Almeida, Susnik *et al.,* 2021). Caveolin-mediated endocytosis and clathrin-mediated endocytosis occur in mammalian cells and bacteria.

Factors that can affect the uptake and dispersion of nanoparticles throughout the human body include size, shape, charge, surface coating and targeting ligands appended to the nanoparticles. Nanoparticles that are spherical compared to rod shaped are less likely to promote margination which is the migration of white blood cells to the endothelium in the inflammatory response (Mitchell, Billingsley *et al.,* 2021). The negatively charged are also less likely to be cleared by macrophages in phagocytosis than the nanoparticles which are positively charged (Mitchell, Billingsley *et al.,* 2021). However, rod shaped and negatively

charged nanoparticles are more able to penetrate tumours because of larger than normal intercellular gaps, example of this is the use of gold nanorods for biomedical imagining (Ashikbayeva, Tosi *et al.,* 2019). Negatively charged spherical nanoparticles are also able to pass through mucosal barriers. This can be seen in the study conducted by Lai (2023) investigating the use of lipid nanoparticles for therapeutic potential of *Helicobacter pylori*. This is important for individuals with CF due to increased viscous mucous layers. Additionally, the human body has a multitude of biological barriers that also impacts the distribution of nanoparticles. Nanoparticles can be administered by inhalation, injection or orally so circulation within the body is a barrier which affects biodistribution because blood flow, phagocytosis by white blood cells and excretion can all reduce the circulation time and delivery of the nanoparticles to the target site (Mitchell, Billingsley *et al.,* 2021). Despite this, nanoparticles can be tailored to overcome such limitations because physicochemical properties can be altered, such as PEGylation whereby nanoparticles are coated with suitable polyethylene glycol (PEG), or surface modifications such as platelet membrane cloaking. An example of this is Paclitaxel-loaded nanoparticles with platelet membranes (PM-lipid-PTX) used for chemotherapy (Han, Bártolo *et al.,* 2022). Platelet membrane cloaking is used in order to prevent the recognition and phagocytosis of the nanoparticle by immune response. Similarly, the distribution of nanoparticle is also directly linked to the administration route. The excretion of nanoparticles is affected by the characterisation of the nanoparticle, such as the size. For example, small nanoparticles are more readily able to cross the capillary walls (Mitchell, Billingsley *et al.,* 2021). This therefore allows for accumulation of larger nanoparticles in organs such as the liver and spleen. This can be overcome by the addition of targeting motifs such as antibodies or glucose on the nanoparticle surface. Along with this the physical barriers also impact the distribution of nanoparticles, including the tight junctions

of the epithelial and endothelial cells of the blood brain barrier or the gastrointestinal tract (Mitchell, Billingsley *et al.,* 2021). Furthermore, the microenvironment can also affect the circulation, stability and the physical characteristics of the nanoparticles. For example, in the gastrointestinal system, a low pH may induce the degradation of the nanoparticles, and therefore the overall stability decreases.

1.6.2 Nanostructured lipid carriers

Nanostructured lipid carriers (NLCs) are constructed of an outer surfactant layer and an inner matrix formed of amorphous liquid lipids and crystalline solid lipids (Figure 1.3) with the particle size varying from 10-1000nm (Mukherjee, Ray and Thakur, 2009). NLCs are comprised of solid and liquid lipids which in combination allows for enhanced drug loading and decreased amounts of drug leaching out of the NLCs during storage (Khosa, Reddi and Saha, 2018). Additionally, NLCs are considered nontoxic, as they are produced from organic monomers including triglycerides. The advantages of NLCs are their high versatility due to the enhanced drug loading capabilities, improved stability, and drug release flexibility (Khosa, Reddi and Saha, 2018). Similarly, the use of NLCs for encapsulating a beta-lactam antibiotic can aid in the drug efficacy by increasing interaction with the bacterial cell wall by using cationic NLCs to increase electrostatic interactions with the cell wall (Aflakian, Mirzavi *et al.,* 2023). Furthermore, the use of different components such as surfactants can allow for prolonged and controlled release of the conjugated drug and a greater half-life. For example, Alalaiwe *et al.,* (2018) used a formulation containing of squalene, hexadecyl palmitate, Phospholipon 80H®, deoxycholic acid, and Pluronic F68 to encapsulate oxacillin for treatment

of MRSA. Advantages of the nanostructured lipid carrier include improved bioavailability, controlled release characteristics and the protection of encapsulated drugs from degradation (Khan *et al.,* 2015). This is important for patients with CF as it would allow the antibiotic to reach the site of infection before degradation. An example of inhaled nanoparticles used for the treatment of lung cancer by Ahmad, Akhter *et al.,* 2015 indicates the feasibility of using nanoparticles as a feasible drug delivery system for treatment of bacterial infections in the respiratory tract of individuals with CF.

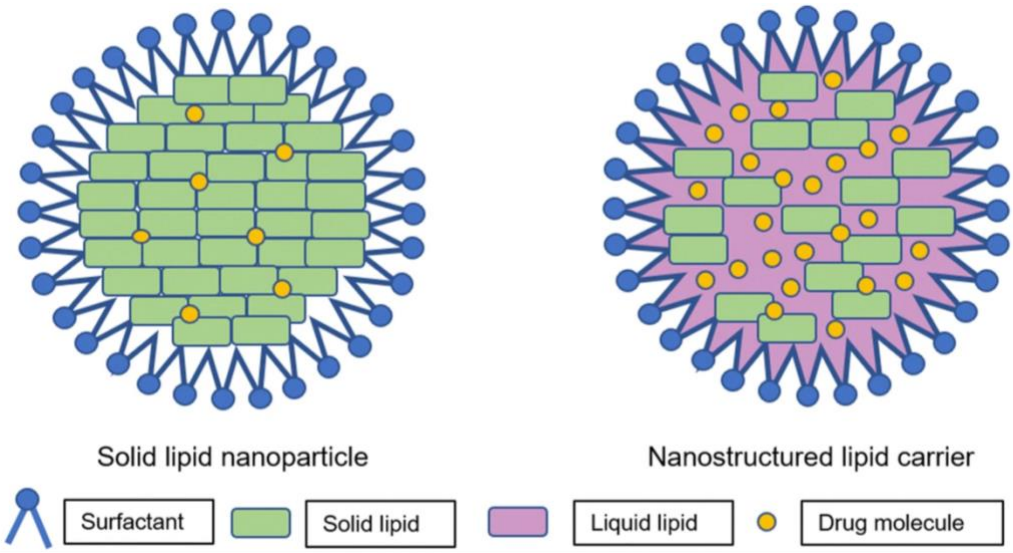

Figure 1. 3. Illustration to show the drug loading difference between Solid lipid nanoparticles and Nanostructured Lipid Carriers and its components (Subramaniam *et al.*, 2020).

1.6.3 Current therapeutic applications of nanoparticles

The use of nanoparticles within immune therapy, genome editing, and cancer therapy is being investigated due to their abilities to overcome biological barriers. Chemotherapeutic drugs for cancer therapy could be improved by encapsulation into nanoparticles to decrease the toxicity of the drug to non-diseased cells by the addition of the specific targeting surface modification (Mundekkad and Cho, 2022). Additionally, nanoparticles have also been used for diagnostic reasons as well for therapies. An example of this is the use of lipid nanoparticles with surface modifications of ^{64}Cu to detect metastatic breast cancer cells (Mitchell, Billingsley *et al.,* 2021).

The use of nanoparticles in the pharmaceutical industry in the United States of America was first introduced by the Food and Drug administration (FDA) by the approval of INFeD in 1992 for the application to iron deficiency anaemia (Mitchell, Billingsley *et al.,* 2021). In the subsequent decade the FDA approved a further twelve nanomedicines, including four lipid-based nanomedicines, five polymeric nanomedicines and three inorganic nanomedicines. From 1992-2018 the FDA has approved a total of twenty-three nanomedicines with applications varying from the treatment of fungal infections, metastatic pancreatic cancer and multiple sclerosis (Mitchell, Billingsley *et al.,* 2021). The nanomedicine AmBisome® is a liposomal product encapsulating the antifungal drug amphotericin B used for antimicrobial treatment for fungal infections such as aspergillus or candida, and is administered via intravenous injection (Mitchell, Billingsley *et al.,* 2021). However, there is an opportunity for

the development and approval of nanomedicines for sensitive and increasingly resistant bacterial infections.

There are five mechanisms of action of nanomaterials against bacteria: membrane fusion, induction of oxidative stress, electrolyte imbalance, binding of intracellular components and physical impairment (He, Hong *et al.,* 2022).

Additionally, it has been reported by Yeh *et al* (2020) that lipid based nanoparticles including liposomes, solid lipid carriers, nanostructured lipid carriers and nanoemulsions can be applied as an alternative antimicrobial delivery pathway for bacteria by direct interaction with the bacterial membrane.

1.6.4. The use of NLCs as precision medicines in other microorganisms

Novel research into the use of NLCs for treatment of bacterial infections is empirical to antimicrobial resistance as NLCs could provide an alternative drug delivery pathway for treatment of both sensitive and resistant strains of bacteria, consequently, improving pharmacokinetic outcomes and decreasing the toxicity and decrease elimination of antibiotics in the body. A study conducted by Muraca in 2021 investigated the use of ciprofloxacin encapsulated NLCs for antimicrobial activity for treatment of *P. aeruginosa* biofilm infections. The efficacy for the NLCs was determined by the characteristics including particle size, PDI, ZP and entrapment efficiency. The antimicrobial activity of the NLCs was determined by the minimum inhibitory concentration (MIC), which found that the encapsulated ciprofloxacin, had the same MIC values as the MIC for free drug (Muraca, Soler-Arango *et al.,* 2021). Similarly, Alalaiwe *et al.,* (2018) investigated the use of oxacillin-loaded

NLCs as a topical treatment of sensitive and resistant strains of *Staphylococcus aureus* infections. The antimicrobial effect of the NLCs was determined by the calculation of encapsulation efficiency and the minimum bactericidal concentration (MBC) value. The research showed that the encapsulation of oxacillin did not reduce the MBC value of the sensitive strain but for the resistant strain the MBC value for oxacillin was 250 μg/ml whereas oxacillin encapsulated NLC produced an MBC value of 62.5 μg/ml (Alalaiwe, Wang *et al.,* 2018). Alalaiwe suggested the four-fold reduction is due to the synergistic effect of the cationic NLC and oxacillin.

1.6.5. The use of NLCs to encapsulate meropenem for use as an antimicrobial treatment for *Pseudomonas aeruginosa.*

Meropenem is commonly used as a treatment for *P. aeruginosa* infections. However, can only be administered to patients intravenously due to the instability of the molecule in aqueous solution, in a clinical setting is limited due to the current prescribing information that a three-hour infusion must be completed within four hours upon reconstitution as meropenem is stable for ~4-6 hours when stored at 25° C (Fawaz, Barton *et al.,* 2019). Along with this meropenem also has a high elimination, with 70% being excreted unchanged in the urine after 12 hours (Thalhammer, Schenk *et al.,* 1998). Therefore, encapsulating the meropenem molecule into a NLC could provide increased stability to the molecule, this has also been suggested by Nguyen *et al.,* (2022). Additionally providing a potential decrease in elimination due to controlled release and alter the administration type of the antibiotic.

1.7. Aims and objectives of the project.

1.7.1 Aims

The aim of the investigation was to optimise and develop meropenem encapsulated nanostructured lipid carriers (ME-NLCs) and to evaluate the use of ME-NLCs as an antimicrobial treatment for *Pseudomonas aeruginosa* infection. Additionally, to evaluate the drug release characteristic of ME-NLCs.

1.7.2. Specific objectives

- To develop meropenem-encapsulated nanostructured lipid carriers and optimise for product and process parameters.
- To optimise NLCs with high drug content and entrapment efficiency of meropenem
- To characterise the physicochemical properties of the ME-NLCs
- To develop and validate a high-performance liquid chromatography method for quantification of meropenem in NLCs.
- To analyse a high-performance liquid chromatography method for quantification of meropenem in pH 6.8 dissolution medium for drug release study for ME-NLCs.
- To evaluate and compare the antimicrobial properties of the ME-NLCs to free meropenem as treatment of *Pseudomonas aeruginosa*.

Chapter 2: Material and methods

2.1. Chemicals and Reagents

Pseudomonas aeruginosa strain (ATCC 27853) was purchased from Bioconnections (Staffordshire, United Kingdom). *P. aeruginosa* was cultured on both Cystine-Lactose-Electrolyte Deficient agar (CLED) purchased from Neogen (Michigan, USA) and incubated at 37 °C for 24 h. All bacterial growth media and containers were sterilised by autoclaving at 121 °C for 15 minutes.

Meropenem was purchased from Activate Scientific GmbH (Prien am Chiemsee, Germany). Sodium cholate and Oleic acid were purchased from Sigma Aldrich (Gillingham, United Kingdom). Capryol 90 and Transcutol were purchased from Gattefosse (Neuilly-sur-Seine, France), Kolliphor HS15 purchased from BASF (Ludwigshafen, Germany), Phospholipon 90 H, lipoid E80 and S75 purchased from Lipoid (Ludwigshafen, Germany). Dynasan 114 was purchased from Emery Oleochemicals (Hampshire, UK).

2.1.1 Solubility studies of liquid lipids

Solubility of meropenem in two liquid lipids, Capryol 90 and Transcutol, and one solubiliser, Kolliphor HS15, was determined. Fifty milligrams of meropenem were added to 1ml of solvent and mixed well by rotating in circular motion three times and repeated until meropenem had completely dissolved.

2.2.1 Preparation and formulation of Nanostructured Lipid Carriers

Blank NLCs and meropenem loaded NLCs (ME-NLCs) were prepared by a hot homogenisation method. Briefly the aqueous phase was prepared with sodium cholate and Milli-q water (Sigma-Aldrich, UK). Similarly, the lipid phase was prepared with Capryol 90, Kolliphor HS15, Phospholipon 90 H, Lipoid E80, Lipoid S 75, Dynasan 114 and oleic acid (Table 2.1 and 2.2). Both phases were melted separately at 80 °C in water baths until completely molten. Both phases were maintained at 80 °C before mixing for the formation of pre-emulsion, necessary for the formation of nanoparticles. The hot aqueous phase was added to the lipid phase and dispersed for 30 minutes with constant mixing using a magnetic stirrer to get a coarse emulsion (Duong, Nguyen *et al.,* 2020). The emulsion was then homogenized using a Sonic vibra-cell probe sonicator (Sonics & materials Inc, USA) for 3 minutes at 40% intensity to increase dispersion and to decrease the particle size (Lasoń, Sikora *et al.,* 2013). The three minutes of sonication was determined by the optimisation of sonication time by observing the change in particle size, poly dispersity index (PDI) and zeta potential (ZP) after intervals of five minutes of sonication for a period of ten minutes. Further to this the sonication time was then optimised through observing changes in one minute intervals. The homogenised product was then allowed to cool to obtain NLCs.

Table 2. 1. Blank formulations used for optimisation of particle size, PDI and zeta potential before encapsulating meropenem.

Oleic acid was added in the final blank (Blank 13 and 14) formulation after initial drug encapsulation to increase encapsulation efficiency and to decrease particle size.

Formulation No	Aqueous Phase			Lipid Phase						
	Milli-Q water (ml)	Sodium Cholate (mg)	Kolliphor P188 (mg)	Capryol (mg)	Kolliphor HS 15 (mg)	Phospholipon 90H (mg)	Lipoid E80 (mg)	Lipoid S75 (mg)	Dynasan 114 (mg)	Oleic acid (mg)
Blank 1	25	150	N/A	100	200	80	300	300	1000	NA
Blank 2	25	150	N/A	200	200	80	300	300	1000	NA
Blank 3	25	200	N/A	200	200	80	300	300	1000	NA
Blank 4	25	250	N/A	200	200	80	300	300	1000	NA
Blank 5	25	200	N/A	200	200	80	300	300	1000	NA
Blank 6	25	250	N/A	200	200	80	300	300	1000	NA
Blank 7	25	150	N/A	200	200	80	300	300	1000	NA
Blank 8	25	150	N/A	200	300	80	300	300	1000	NA
Blank 9	25	125	125	200	300	80	300	300	1000	NA
Blank 10	25	150	N/A	200	300	100	300	300	1000	NA
Blank 11	25	150	N/A	200	200	100	300	300	1000	NA
Blank 12	15	90	N/A	120	180	48	180	180	600	NA
Blank 13	15	90	N/A	120	180	48	180	180	600	100
Blank 14	15	90	N/A	120	250	48	180	180	600	100

Table 2. 2.Compositions of Meropenem loaded NLC formulations (0.5mg/ml) used for optimisation of particle size, PDI, zeta potential and encapsulation efficiency.

Formulation No	Aqueous Phase			Lipid Phase							
	Milli-Q water (ml)	Sodium Cholate (mg)	Meropenem (mg)	Capryol (mg)	Kolliphor HS 15 (mg)	Phospholipon 90H (mg)	Lipoid E80 (mg)	Lipoid S75 (mg)	Dynasan 114 (mg)	Oleic acid (mg)	Meropenem (mg)
ME 1	15	90	7.5	120	180	48	180	180	600	N/A	N/A
ME 2	15	90	N/A	120	180	48	180	180	600	N/A	7.5
ME 3	15	90	N/A	120	180	48	180	180	600	100	7.5
ME 4	15	90	N/A	120	180	48	180	180	600	100	7.5
ME 5	15	90	N/A	120	180	48	180	180	600	150	7.5
ME 6	15	90	N/A	120	180	48	180	180	600	200	7.5
ME 7*	15	90	N/A	120	250	48	180	180	600	100	7.5
ME 8	15	90	N/A	200	250	48	180	180	600	100	7.5

2.2.2 Optimisation of blank and drug loaded NLCs.

Initially nanostructured lipid carriers were optimised without meropenem to study the effect of the product parameter and process parameters on the critical quality attributes.

The effect of the product parameter was investigated by increasing surfactant concentration of sodium cholate (100-250mg) and liquid lipids concentrations Capryol 90 (120mg and 200mg), oleic acid (100-200mg) and solubiliser Kolliphor HS15 (200mg and 300mg) individually. The effects of product parameters were studied by observing the changes in particle size, poly dispersity index (PDI) and zeta potential (ZP).

The effect of the process parameter, sonication time was also studied by observing the change in particle size, poly dispersity index (PDI) and zeta potential (ZP) after intervals of five minutes of sonication for a period of ten minutes. The optimised nondrug loaded formulation was taken for loading with meropenem, and further optimisation was to determine the amount of drug to be added and the selection of liquid lipid.

The drug loaded formulation was optimised by observing the change in particle size, poly dispersity index (PDI) and zeta potential (ZP) when the drug was added within the aqueous phase and then the lipid phase and compared using encapsulation efficiency and was discovered that within the aqueous phase encapsulation was lower therefore formulations ME 2- ME 8 (Table 2.2) meropenem was added to the lipid phase.

2.2.3. NLCs characterisation

The particle size, poly dispersion index (PDI) and zeta potential (ZP) of both the blank NLCs and ME-NLCs were measured by dynamic light scattering (DLS) at 90^0 and 173^0 with a wavelength of 633nm using a Malvern Zetasizer (Zetasizer Nano ZS, Malvern Instruments, UK)

at 25 ^{0}C (Mhango, Kalhapure *et al.,* 2017). The physical stability of the blank and ME-NLCs particles regarding particle size, PDI and ZP was measured for 48 hours. The samples were kept at ambient room temperature. All samples tested were not diluted and each test was done in triplicate.

2.2.4. Lyophilisation of NLCs

Lyophilisation was conducted by adding 1ml of a cryoprotectant sucrose solution at concentrations of 5%, 7% and 10% to 1ml of ME-NLCs dispersion.

This product was then frozen at -70 °C for 24 hours. Once frozen, the samples were placed into the Christ Alpha 2-4 LDplus freeze dryer (Martin Christ Gefriertrocknungsanlagen GmbH, Germany). Samples were then put under the conditions of -90°C for 48 hours (Khan, Mudassir *et al.,* 2019). Once completely lyophilised the samples were sealed and placed in -20^{0}C freezer. The lyophilised nanoparticles which were stored for five weeks in a -20°C freezer was then analysed by observing the change of particle size, poly dispersion index (PDI) and zeta potential (ZP) after reconstitution using 2ml of Milli-Q water.

Table 2. 3 Compositions of Meropenem loaded NLCs formulated using four different percentages of cryoprotectant for lyophilisation.

Formulation No	Aqueous Phase		Lipid Phase								Cryoprotectant
	Milli-Q water (ml)	Sodium Cholate (mg)	Capryol (mg)	Kolliphor HS 15 (mg)	Phospholipon 90H (mg)	Lipoid E80 (mg)	Lipoid S75 (mg)	Dynasan 114 (mg)	Oleic acid (mg)	Meropenem (mg)	Sucrose (%)
ME 7	15	90	120	250	48	180	180	600	100	7.5	0
ME 7- 5%	15	90	120	250	48	180	180	600	100	7.5	5
ME 7 - 7%	15	90	120	250	48	180	180	600	100	7.5	7
ME 7 - 10%	15	90	120	250	48	180	180	600	100	7.5	10

2.3. Differential Scanning Calorimetry of meropenem, blank NLC and ME-NLC

Differential scanning calorimetry (DSC) analysis of meropenem, Dynasan 114, the physical mixture of the lipid phase containing meropenem, and blank NLCs were performed using the DSC Q2000 TA (Thermal Analysis Instruments, Delaware, USA). The instrument was calibrated with an empty reference pan. Samples (3-7mg) were heated in hermetic aluminium pans purchased from TA instruments (Thermal Analysis Instruments, Delaware, USA) under a dry nitrogen environment. The analysis was performed at a heating rate of 10 °C per minute to 300 °C (Mhango, Kalhapure *et al.,* 2017).

2.4. Fourier transform infrared spectroscopy (FTIR) of meropenem, blank NLC and ME-NLC

The interaction between the materials was measured using FTIR (Nicolet iS 10 FTIR, Thermo Scientific, UK). Meropenem in aqueous solution was investigated against ME-NLCs and Blank NLCs. Samples were measured in the range of 500–4000 cm^{-1} using a crystal and a resolution of 0.5 cm^{-1} (Zwain, Alder *et al.,* 2021). The data were analysed using the OMNIC software (Thermo Scientific, UK).

2.5. High-Performance Liquid Chromatography of meropenem

A HPLC method was developed to quantify meropenem in NLCs and determine the drug loading and drug release from NLCs.

2.5.1 Preparation of pH 2.7 Orthophosphate buffer

Monobasic potassium phosphate (0.68g) and triethanolamine (1.13g) were dissolved in 400ml of Milli-Q water. The volume was then made up to 500ml in a volumetric flask with Milli-Q water. The pH was adjusted using orthophosphoric acid.

2.5.2 Preparation of pH 6.8 orthophosphate buffer

Monobasic potassium phosphate (5.7 grams) and disodium hydrogen phosphate (14.1 grams) were dissolved in 400ml of Milli-Q water. The volume was then made up to 500ml in a volumetric flask with Milli-Q water. The pH was adjusted using orthophosphoric acid.

2.5.3. Preparation of standard solution in water

Ten milligrams of meropenem were accurately weighed and transferred to a 10 ml volumetric flask. The volume was made up with Milli-Q water and mixed thoroughly using a vortex. Five hundred microlitres of aliquot was withdrawn and transferred into 1.5ml centrifuge tubes and frozen at -20°C to prevent drug degradation.

2.5.4. Preparation of standard solution in pH 6.8 buffer

Ten milligrams of meropenem were accurately weighed and transferred to a 10 ml volumetric flask. The volume was made up with pH 6.8 orthophosphate buffer and mixed thoroughly using a vortex. Each standard solution was made up on the day of use.

2.5.5. Optimisation of chromatographic conditions for validation of meropenem in water

The system comprised of an Agilent technologies (Agilent HPLC 1260 Infinity, Agilent Technologies, USA) HPLC Pump equipped with Agilent technologies UV/VIS detector. The column used for chromatography was Kinetex 5 µ C18 100 Å, 150x4, 6 mm (Phenomenex, Castelmaggiore, Bologna, Italy). The column temperature was maintained at 25°C. The data were observed using Agilent's software OpenLAB CDS CS Workstation (Agilent Technologies, USA). The wavelength for detection of meropenem, mobile phase ratio and peak symmetry were optimised individually to obtain a well separated peak of meropenem with a retention time within 5 to 10 minutes. The mobile phase, composed of orthophosphate buffer and methanol: (84:16%); adjusted to a pH of 2.7, was used for the validation study. The mobile phase was degassed ultrasonically for five minutes after mixing. A standard solution of meropenem at 10µg/ml concentration was used for optimisation of chromatographic conditions. Twenty microliters of the test solution were injected. The flow rate was maintained at 0.77 ml/min. The detection was carried out at a wavelength of 308 nm. The run time for the analysis was 18 min.

2.5.6. Chromatographic conditions for analysis of meropenem concentration in orthophosphate buffer pH 6.8

An orthophosphate buffer of pH6.8 was used in the analysis of meropenem concentration released from the NLC as the buffer mimics that of an *in vitro* release.

The system comprised of an Agilent technologies (Agilent HPLC 1260 Infinity, Agilent Technologies, USA) HPLC Pump equipped with Agilent technologies UV/VIS detector. The column used for chromatography was Kinetex 5 µ C18 100 Å, 150x4, 6 mm (Phenomenex, Castelmaggiore, Bologna, Italy). The column temperature was maintained at 25°C. The data were observed using Agilent's software OpenLAB CDS CS Workstation (Agilent Technologies, USA). Wavelength for detection, mobile phase ratio and peak symmetry were optimised individually to obtain a well separated peak of meropenem with a retention time within 5 to 10 minutes. The mobile phase, composed of orthophosphate buffer and methanol: (80:20%); adjusted to a pH of 6.8, was used for the study. The mobile phase was degassed ultrasonically for five minutes after mixing. Twenty microliters of the sample were injected. The flow rate was maintained at 0.9 ml/min. The detection was carried out at a wavelength of 308 nm. The run time for the analysis was 10 min. The difference between the run times for pH 6.8 and pH2.7 were due to the flow rate, pH and the ratio of the mobile phase.

2.5.7. HPLC method validation

The HPLC methods were validated in accordance with the International Conference on Harmonisation (ICH) guidelines for validation of analytical procedures (European Medicines Agency, 1995).

2.5.7.1 Linearity of HPLC method

A stock solution of meropenem (100μg/ml) was prepared in water. The stock solution was suitably diluted to obtain working standards at concentrations of 2, 4, 8, 10, 16, 20 μg/ml. At each concentration level, HPLC analysis was carried out in triplicate. The peak areas versus concentration data were evaluated by linear regression analysis. Data sets corresponding to three sets of triplicates were analysed by mean and standard deviation, and a calibration curve was constructed.

2.5.7.2 Precision of HPLC method

The precision of the assay method was evaluated by performing six independent assays (intra-day) of meropenem at two concentration levels using the validated chromatographic conditions as mentioned in section 2.5.6. The intermediate precision of the method was checked by performing the same procedure on three consecutive days (inter-day). Two concentrations of meropenem solution in water, 4 μg/ml and 20 μg/ml were used for intermediate precision.

2.5.7.3 Accuracy of HPLC method

The accuracy was evaluated in terms of repeatability. At each concentration level (4,8,16μg/ml), analysis was carried out in triplicate and calculated by percentage accuracy compared to the target concentration using the same chromatographic conditions as were used for validation studies.

2.5.8. Preparation of sample solution for analysis of drug loading

The entrapment efficiency (EE) of the ME-NLCs was determined by quantifying free drug in the supernatant fluid (FD), which was separated by filtering NLCs (0.5 ml) using Amicon™ 30 kDa molecular centrifuge filters purchased from Merck Millipore (UK) centrifuged at 2500 x *g* for 15 minutes. The supernatant was then removed using a pipette, diluted 1:100 and analysed immediately. The linearity curve was used to calculate the concentration of free drug. Equation 1 was then used to determine the %EE.

$$\%EE = \left\{\frac{Free\ Drug}{Total\ amount\ of\ meropenem\ added}\right\} x100$$

Equation 1. Percentage Encapsulation efficiency

2.6. *In vitro* drug release study of ME-NLCs

Dissolution study of ME-NLCs was conducted in triplicate at 37 °C, over a 24-hour period. Spectra/Porâ3, 3.5kD dialysis membranes (Thermofisher, Altrincham, UK) were soaked for 24

hours prior to use. A sample of 2ml ME-NLCs was added to the dialysis membranes tube which was secured at both ends. The dialysis tube containing the sample was placed in the dissolution vessels containing 400ml of pH 6.8 orthophosphate buffer as the release medium. A sample (1 ml) of dissolution medium was withdrawn every hour until hour eight and then samples were taken at the 24th hour. After withdrawal of every sample the dissolution medium was replaced by a fresh 1ml of the orthophosphate buffer (Nagaich and Gulati, 2016) to maintain the same conditions throughout. Samples were analysed using a HPLC and chromatographic conditions validated as described in chapter 2.5.7. The concentration of meropenem in each sample was calculated by the use of a spreadsheet produced by K. Singh.

2.7. Bacterial investigations of *P. aeruginosa*

2.7.1 Bacterial growth on solid media and overnight cultures

Colonies of *Pseudomonas aeruginosa* ATCC 27853 were grown in 90 mm diameter Petri-dishes containing approximately 20 mL of either Nutrient agar or Mueller Hinton agar purchased from Oxoid (Thermo-scientific, Altrincham UK) or CLED agar (Neogen, Bury UK) and incubated aerobically at 37 °C overnight. CLED agar was used to restrict colony sizes to allow for accurate counting. Stock cultures were prepared in 20% glycerol and Brain Heart Infusion broth (BHI) purchased from Oxoid (Thermo-scientific, Altrincham UK) and were frozen at −80 °C in 2ml plastic vials. Alternatively stock cultures were also prepared on Nutrient agar slopes in 30ml glass universal tubes and kept sealed and refrigerated at 2-8 °C for up to four weeks. When culturing cells from frozen stocks, cells were defrosted at ambient temperature. A sterile inoculation loop was used to spread the cells across the agar using the streaking method to produce single colonies.

Overnight cultures were produced by taking a single bacterial colony and inoculating a 9 mL Nutrient or Mueller Hinton broth in 30mL glass universal tube. The culture was grown at 37°C for approximately 18 hours.

2.7.2 Antibiotic preparation for bacterial susceptibility testing

Meropenem solution was prepared in accordance with section 2.5.3. The stock was diluted with sterile Milli Q water to prepare the working stock.

2.7.3. Characterisation of *Pseudomonas aeruginosa*

Characterisation of six reference strains of *Pseudomonas aeruginosa* were determined by morphological and biochemical tests. Bacterial cell morphology testing was confirmed by Gram stain. The strain exhibited two distinct colony morphologies, and these were checked for purity using Gram stain (Public Health England, 2019). In addition to this the biochemical testing: oxidase (Public Health England, 2019) and catalase (Public Health England, 2019) tests were carried out. The pigment production of *P. aeruginosa* on CLED was observed. The ability to grow aerobically and at 37 °C is also used to characterise *P. aeruginosa.*

Characterisation of all *Pseudomonas aeruginosa* strains was also determined by conducting an antibiogram using the EUCAST disc susceptibility method (EUCAST, 2023) to determine susceptibility to the following antibiotics: trimethoprim 5μg (W), ampicillin 10μg (AMP),

ceftazidime 10μg (CAZ), tetracycline 30μg (TE), gentamicin 10μg (CN), ciprofloxacin 5μg (CIP), vancomycin 30μg (VA) and meropenem 10μg (ME).

2.7.4. Growth curve of *P. aeruginosa* ATCC 27853

A growth curve of *P. aeruginosa* ATCC 27853 was determined by adding 5ml of a bacterial overnight culture to a conical flask containing a 250ml of autoclaved Mueller Hinton broth and incubated at 37 °C for 24 hours taking optical density readings every hour using a Jenway 7135 spectrophotometer at a wavelength of 600nm. In addition, bacterial counts were also estimated by taking serial 10-fold dilutions with autoclaved Mueller Hinton broth and pipetting 10ul of four dilutions (10^7 - 10^1 cfu/ml) onto a CLED agar plate using the Miles and Misra method (Miles, *et al.,* 1938). CLED agar was used to restrict the colony size for counting as described above.

2.7.5. Minimal inhibitory concentration

Bacterial overnight cultures were suspended in a 9ml Mueller Hinton broth to a density equivalent to a 0.5 MacFarland standard inoculum (A) using a Densilameter purchased from ERBA Mannheim (Mannheim, Germany). From inoculum A, a bacterial suspension of approximately 5 x10^5 cfu/ml was prepared (inoculum B). The inoculum B was then pipetted in a quantity of 100μl into each well of a sterile 96 well flat-bottomed plate purchased from Thermo-fisher (UK). Subsequently 100μl of the highest concentration of antibiotic (64μg/ml)

was added to the first well and serially diluted. Each well had a total of 100μl before incubation. Minimal inhibitory concentrations (MIC) were performed in triplicate. A Positive control was prepared by adding 100μl of inoculum to an empty well within the 96-well plate. A negative growth control was prepared by adding 100μl of sterile Mueller-Hinton broth to an empty well within the 96-well plate. The 96 well plate was then incubated at 37 °C for 24 hours before readings were taken.

2.7.6. Minimum bactericidal concentration

Once the MIC had been determined by examining each well for turbidity, 10μl from each well without turbidity was pipetted onto a CLED agar and incubated for 24 hours at 37 °C. The MBC was determined by the lowest concentration of antibiotic with no viable colonies on CLED agar after incubation.

2.7.7. Kill time assay

A kill time curve of *P. aeruginosa* ATCC 27853 was determined by adding 2ml of a bacterial overnight culture and 2ml of ME-NLCs at either a concentration of 2μg/ml or 32μg/ml. Broths were incubated at 37 °C for 24 hours and sampled every hour for seven hours and again at twenty-four hours. Bacterial counts were made by taking serial 10 fold dilutions in Mueller Hinton broth and pipetting 10μl of each dilution (10^7 - 10^1 cfu/ml) onto a CLED agar plate. A growth control without ME-NLCs was included. All samples were performed in triplicate.

2.8. Visualisation of P. aeruginosa after treatment of ME-NLCs using fluorescent microscopy

The internalisation of fluorescently labelled NLCs was studied in planktonic culture suspensions under glass coverslips. For in suspension studies, the inoculum prepared consisted of 2ml of *Pseudomonas aeruginosa* ATCC 27853 suspended in Mueller Hinton broth and adjusted to a density equivalent to 0.5 MacFarland standard and with 2ml of ME-NLCs suspension. The ME-NLCs were labelled with rhodamine 123 (ThermoFisher, Altrincham, UK) The mixture was incubated for 24 hours at 37 °C. Samples of 0.5ml were taken and centrifuged for one minute at 13,000rpm, the supernatant was removed, and the pellet was washed with 0.5ml of PBS. Sample was resuspended and centrifuged again, and PBS decanted, and the pellet was then stained using BacLight Kit L7007 (Thermofisher, UK) for 15 minutes in the dark. The sample was washed twice with PBS using the method described above.

Samples were then fixed using 10% formalin solution and incubated in the dark for 15 minutes. Once incubated the samples were washed with PBS twice and then resuspended for visualisation using Zeiss cell observer™ (Jena, Germany).

2.9. Statistical Analysis

The statistical analysis was conducted using Microsoft excel to determine the mean, standard deviation, relative standard deviation for HPLC analysis, particle size, PDI, Zeta potential, bacterial counts, MIC, MBC. SPSS version 27 was used to conduct T-Tests with a P value of 0.05 to determine the significance of the results regarding particle size, PDI, Zeta potential.

Chapter 3: Results

3.1 Solubility studies of crystalline meropenem in lipids

A preliminary investigation into the solubility of meropenem in different liquid lipids to be incorporated into the NLCs was conducted to select the appropriate liquid lipid to enhance drug loading capability of NLCs. The study found that meropenem was more soluble in Capryol 90 and insoluble in Transcutol (Table 3.1). Therefore, Transcutol was considered not suitable for preparing meropenem loaded NLCs because of its limited solubility for meropenem, and Caproyl 90 was selected as the liquid lipid for formulation of NLCs. Furthermore, the solubility of meropenem was found to be high in Kolliphor HS 15 which was used as the solubiliser in the NLC formulations. Kolliphor HS 15 is known for its solubilising properties and also acts as surfactant to stabilise the NLCs (Zwain, Alder *et al.,* 2021). The liquid lipid oleic acid was added after the optimisation of the blank formulation to increase drug encapsulation and solubility was not tested as research conducted by Rajpoot *et al.,* (2022) showed that oleic acid does solubilize meropenem.

Table 3. 1. Solubility of meropenem in lipids.

Lipid	**Solubility of meropenem per ml of liquid lipid and solubiliser**
Capryol 90	1.6 mg/ml
Transcutol	0 mg/ml (insoluble)
Kolliphor HS 15	2.3 mg/ml

3.2.1 Optimisation of Blank NLC formulation.

Initial investigations were carried out with non-drug loaded NLCs to optimize the process and product parameters. In order to produce NLCs with desired particle size <200nm and PDI <0.3.

The product parameters optimised were surfactant and solubiliser concentration and the process.

The sodium cholate concentration was varied at four levels (100mg, 150mg, 200mg and 250mg), and it was observed that though 100mg of sodium cholate resulted in the lowest particle size (nm), the PDI was highest (0.28) at this concentration. A sodium cholate concentration of 150 mg resulted in the lowest particle size of 138.9 nm and a PDI of 0.139 providing the best values (Figure 3.1). The size difference between 100mg and 150mg is significant as the p-value is less than 0.05. However, the difference in DI results of 100mg and 150mg is not significant as the p-value is greater than 0.05. Sodium cholate at concentrations above 150mg led to an increase in particle size as well as resulting in high PDI values. Excessive surfactant concentration can lead to micelle formation leading to polydispersed sample and thus resulting in a PDI value higher than desired for the NLCs (Pezeshki et al. 2014).

It was shown that 5 minutes of sonication time was sufficient to obtain a particle size less than 200nm and PDI less than 0.3 in formulation 'Blank 6' (Table 2.1). Particle size distribution profile showed a narrow single peak with uniform distribution (Figure 3.2). Particle size and PDI of NLCs was found to increase beyond 5 minutes of sonication time with particle distribution profiles showing two peaks demonstrating polydispersion and a wide distribution as can be seen in figure 3.2. Particle size increased beyond 5 minutes of sonication due to excess energy provided by ultrasound waves leading to the aggregation of particles (Ali et al. 2014). Sonication for 10 minutes also led to an increase in particle size. Sodium cholate, the hydrophilic surfactant, had a critical impact on the particle size and PDI of the NLCs.

Kolliphor HS. 15 was used as solubilising agent and its effect on particle size and PDI was investigated at two concentrations, 200mg and 300mg. Though the higher concentration of

Kolliphor HS 15 led to lower the particle size initially, on 5 minutes ultra-sonication the 200mg concentration resulted in the lower particle size of 139.5nm, and a PDI of 0.256 providing the best values. The size difference between 200mg and 300mg is significant as the p-value is less than 0.05. The difference in PDI results of 200mg and 300mg is significant as the p-value is less than 0.05. At both the concentration levels, 5 minutes of sonication time was sufficient to obtain particle size <200nm and PDI <0.3 at all concentrations of hydrophilic surfactant (Figure 3.3).

The optimised non-drug loaded NLCs, formulation Blank 12 (Table 2.2) were taken for loading with meropenem.

3.2.2 Optimisation of meropenem loaded NLC formulation.

Investigations were carried out to determine the optimum drug concentrations that can be loaded in the NLCs before saturation concentration is achieved with have negative impact on particle size or PDI. Meropenem concentrations 0.5mg/ml and 0.75mg/ml produce desired particle size <200nm and PDI <0.3 after three minutes of sonication. (Figure 3.4). Increasing meropenem concentration to 1mg/ml and 1.5mg/ml resulted in a PDI of >0.3 although the particles size was <200nm (Figure 3.4). The concentration of the drug selected for further testing in the NLCs was 0.5mg/ml which resulted in the lowest particle size of 152.7nm and a PDI of 0.297 providing best values. Additionally, the zeta potential of NLCs for each concentration was investigated and showed that all concentrations show a negative charge, with the 0.5mg/ml ME-NLCs producing a zeta potential of -22.7mV (Figure 3.4).

Also, it was observed that on drug loading three minutes of sonication time was sufficient to obtain particle size <200nm and PDI <0.3 as compared to five minutes which was required for non-drug loaded NLCs (Figure 3.5). The size difference between 3 minutes sonication and 4 minutes is significant as the p-value is less than 0.05. The difference in PDI results of 3 minutes and 4 minutes is also significant as the p-value is greater than 0.05.

Capryol 90 was used as liquid lipid in the NLCs as it had good solubility for meropenem. Effect of Capryol 90 was investigated and it was revealed that increasing the Capryol 90 concentration from 120mg to 200mg decrease the particle size, but the PDI value increase beyond 0.3 to 0.308, which is not desirable (because it indicates a polydispersed sample with wide variation in particle size of the NLCs). The zeta potential was also more favourable in the formulation containing 200mg of Capryol 90 (-32.2mV). The size difference between 120mg and 200mg of Capryol 90 is significant as the p-value is less than 0.05. Similarly, the difference in PDI between 120mg and 200mg of Capryol 90 is significant as the p-value is less than 0.05. Also, the difference in the zeta potential between 120mg and 200mg of Capryol 90 is significant as the p-value is less than 0.05. The concentration selected was 120mg of Capryol 90 due to providing the overall best values (particle size of 169.7nm and 0.29 PDI) (Fig 3.6).

A

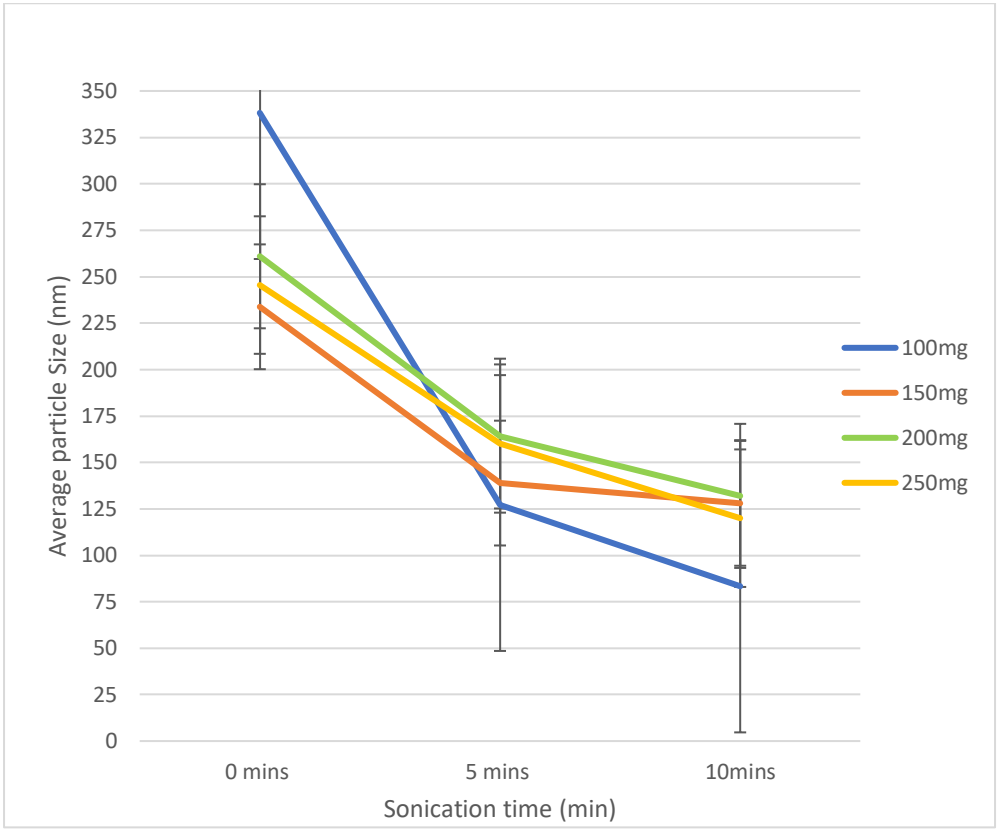

B

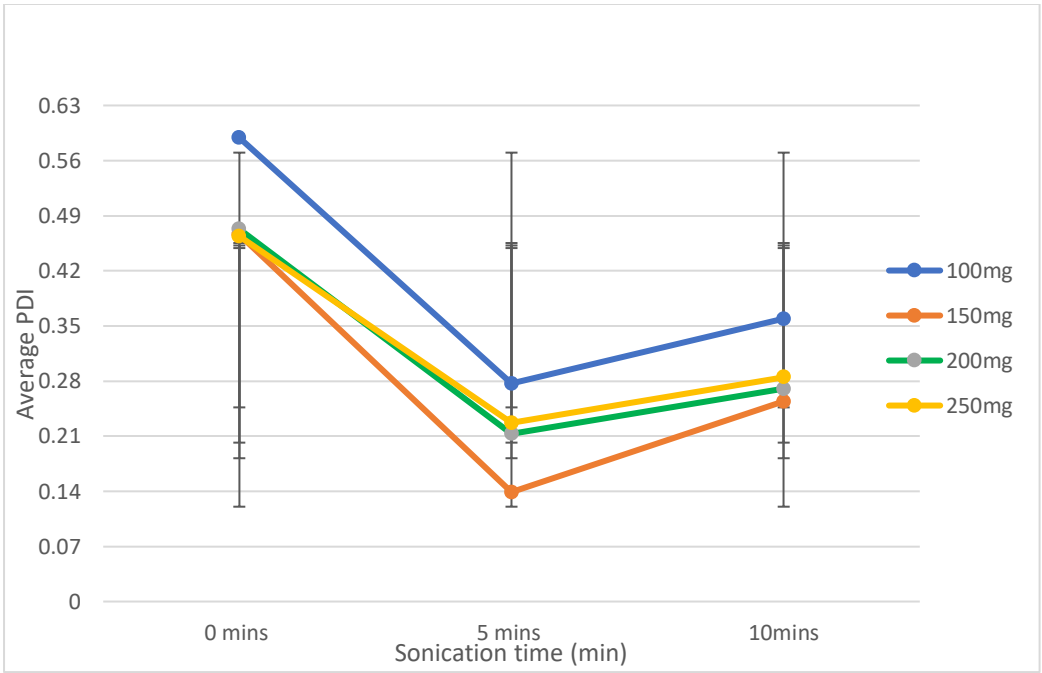

Figure 3. 1. Compositions of Blank NLCs formulated using four different concentrations of hydrophilic surfactant (Sodium Cholate) to study the effect of sonication on particle size (A) and polydispersity index (B) Data is presented as mean ± SD, n = 3. (A) *** p < 0.05, refers to a significant difference when formulations 100mg and 150 mg were compared.

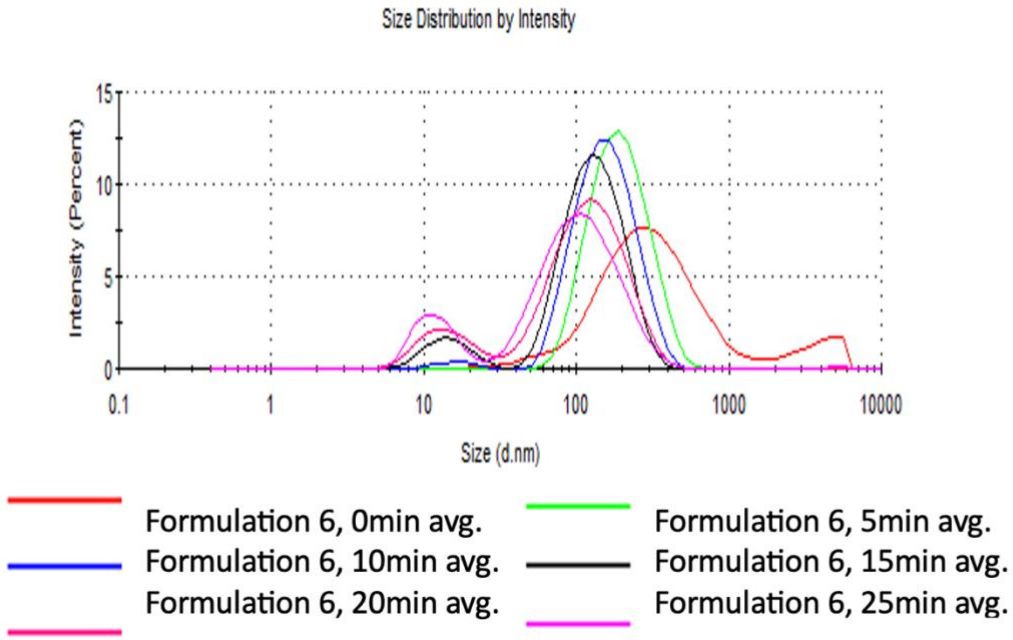

Figure 3. 2.Particle size profiles showing the effect of sonication time on particle size and PDI of formulation Blank 6. Data is presented as mean, n=3. The solid coloured lines identify the PDI of each sample, with the green line showing one uniformed peak, whereas the other five have multiple peaks showing a higher polydispersion in the sample.

A

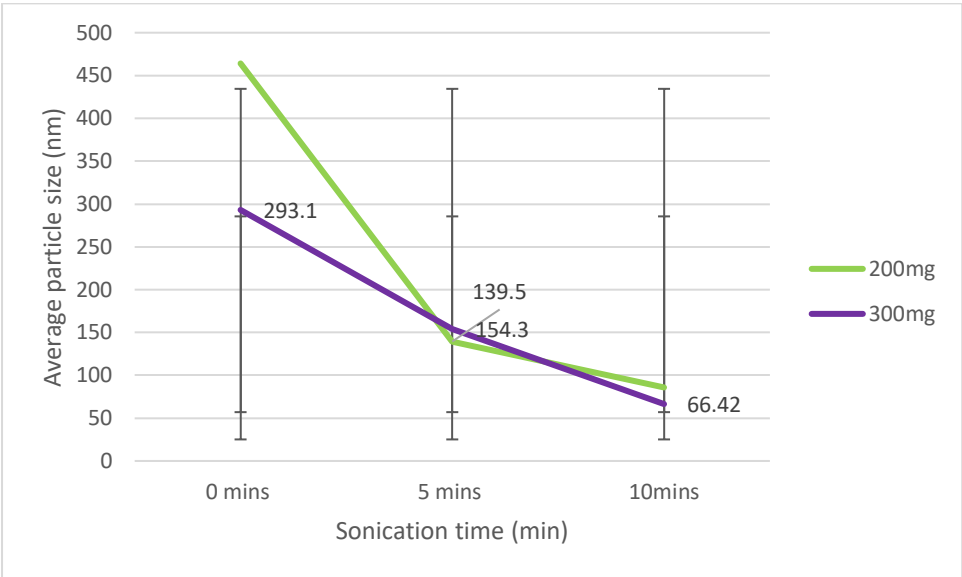

B

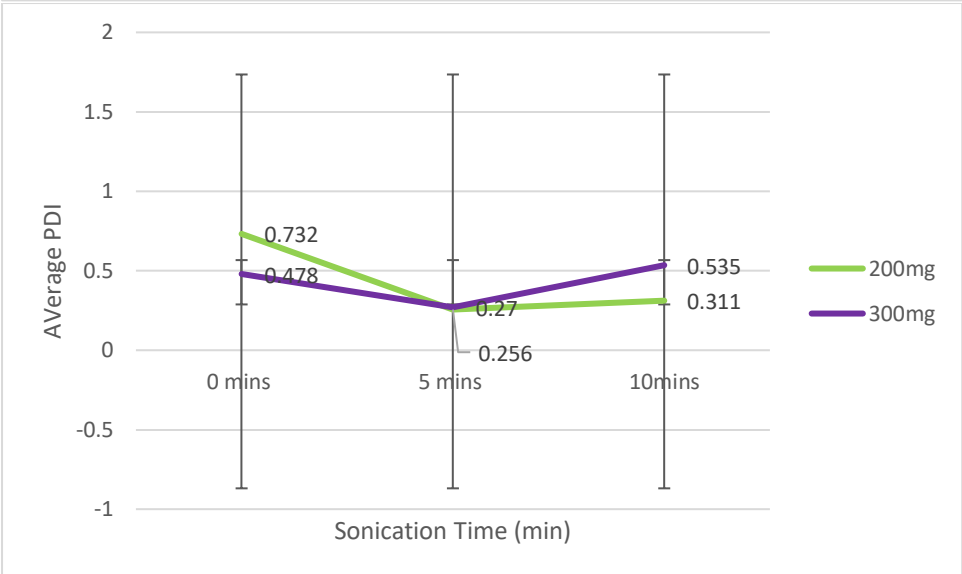

Figure 3. 3. Compositions of Blank NLCs (Formulations Blank 7 and Blank 8) formulated using two different concentrations of Kolliphor HS 15 to study the effect of sonication on particle size (A) and polydispersity index (B) Data is presented as mean ± SD, n = 3. (A) *** $p < 0.05$, refers to a significant difference when formulations 200mg and 300mg were compared. (B) *** $p < 0.05$, refers to a significant difference when formulations 200mg and 300 mg were compared.

A

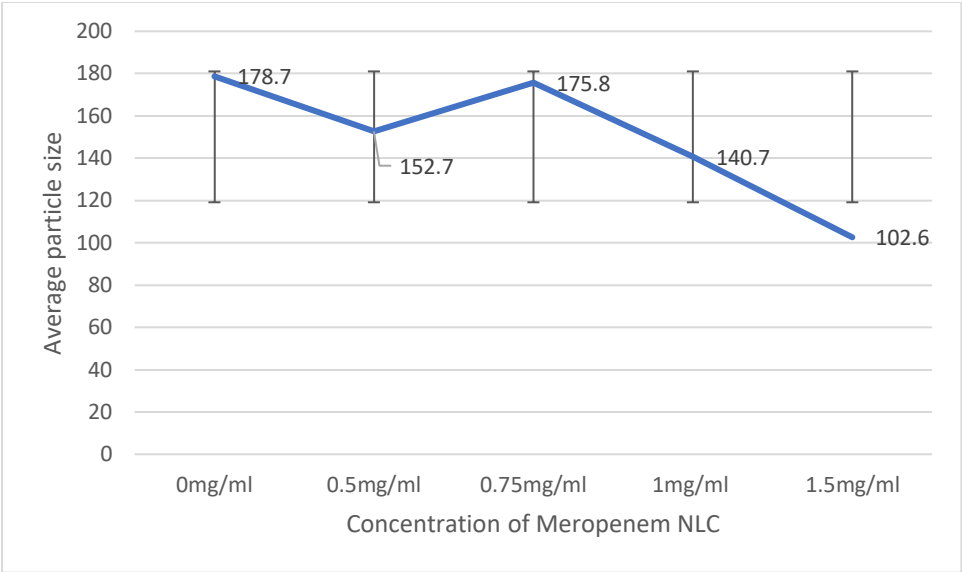

B

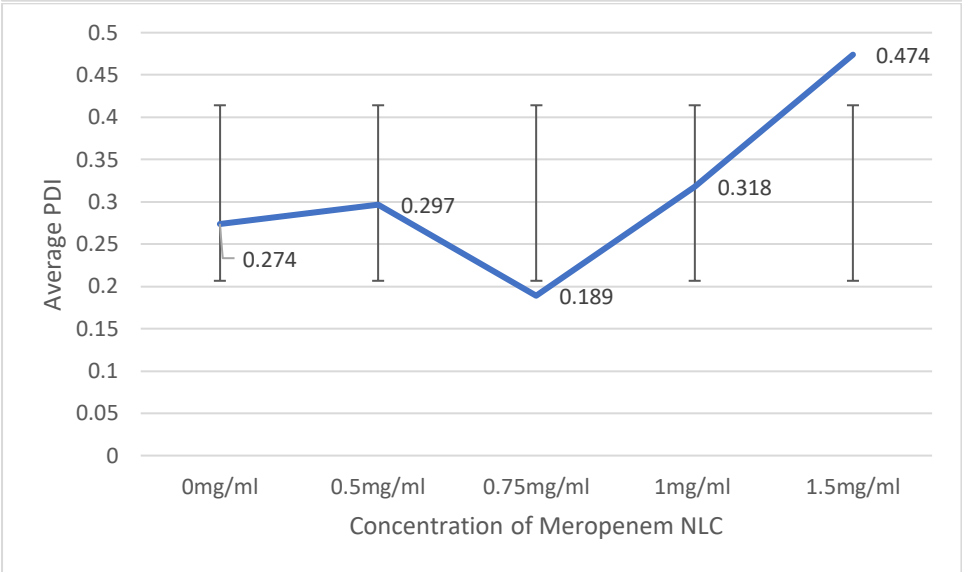

C

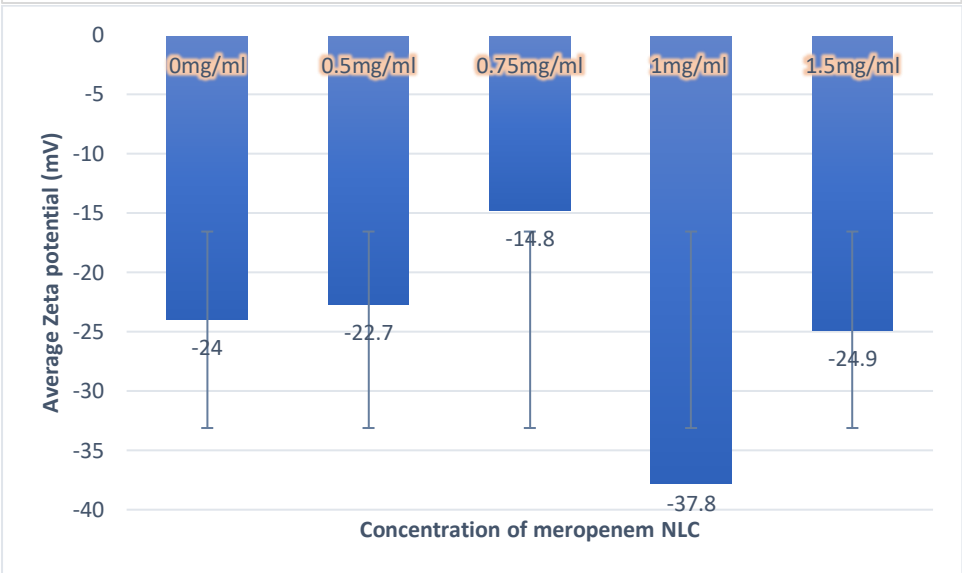

Figure 3. 4.Compositions of ME-NLCs formulated using four different concentrations of meropenem to study the effect of drug concentration on particle size (A) and polydispersity index (B) zeta potential (C). Data is presented as mean ± SD, n = 3. (A) **** p < 0.05, refers to a significant difference when formulations 0.5mg/ml and 0.75mg/ml

were compared. (B) ** p < 0.05, refers to a significant difference when formulations 0.5mg/ml and 0.75mg/ml were compared. (C) **** p < 0.05, refers to a significant difference when formulations 0.5mg/ml and 0.75mg/ml were compared.

A

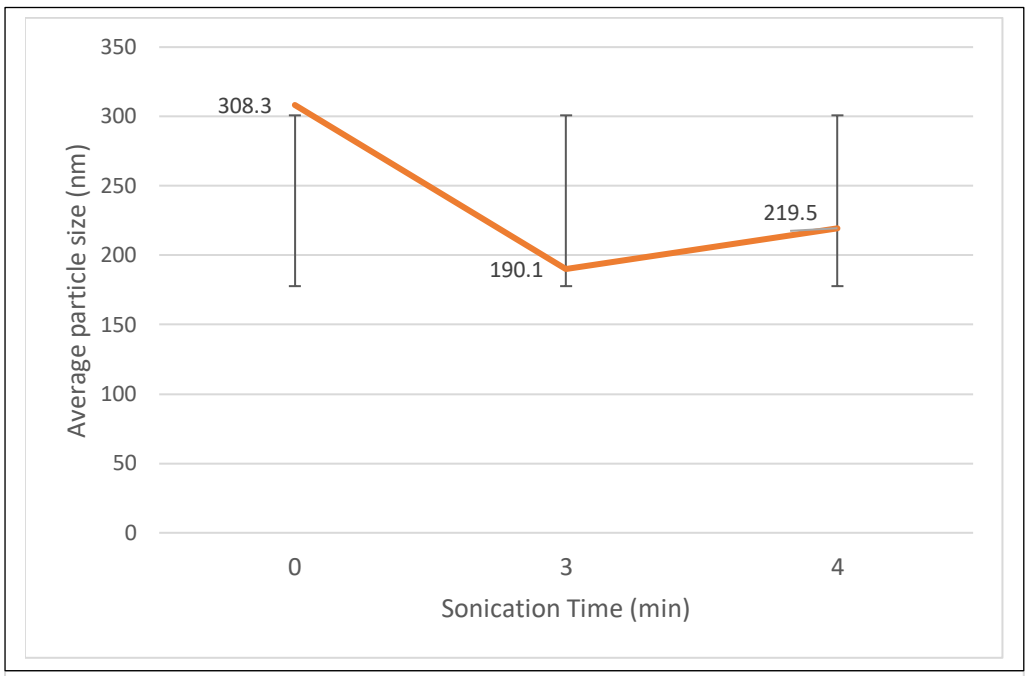

B

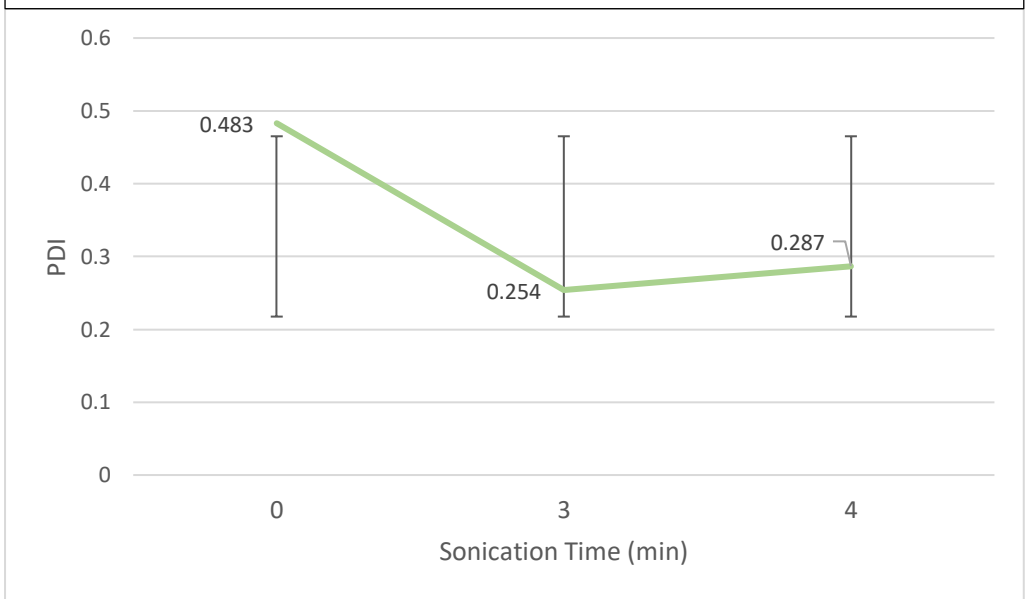

Figure 3. 5. Compositions of meropenem-loaded NLCs (Formulation ME 1)) to study the effect of sonication time on particle size (A) and polydispersity index (B) Data is presented as mean ± SD, n = 3. (A) ** p < 0.05, refers to a significant difference when sonication time 3 minutes and 4 minutes were compared. (B) * p < 0.05, refers to a significant difference when sonication time 3 minutes and 4 minutes were compared.

A

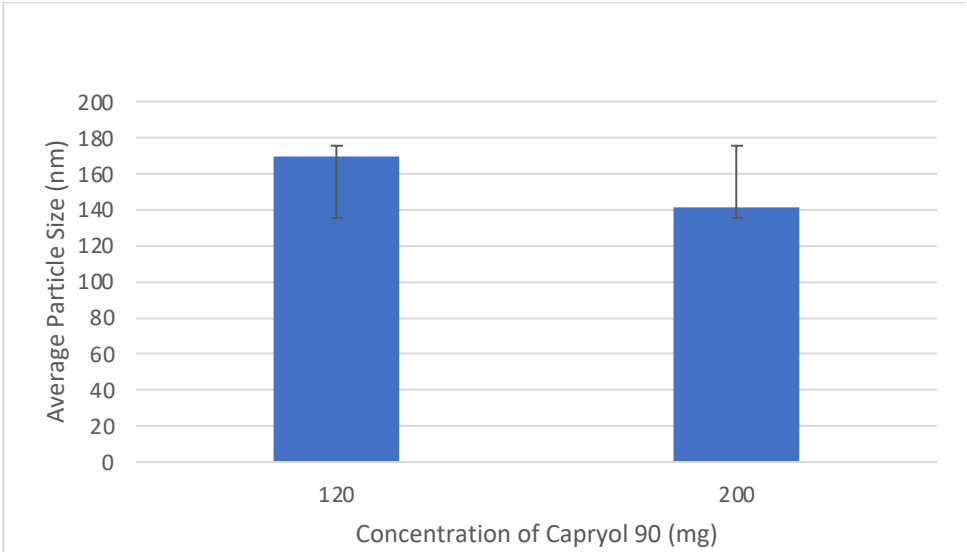

B

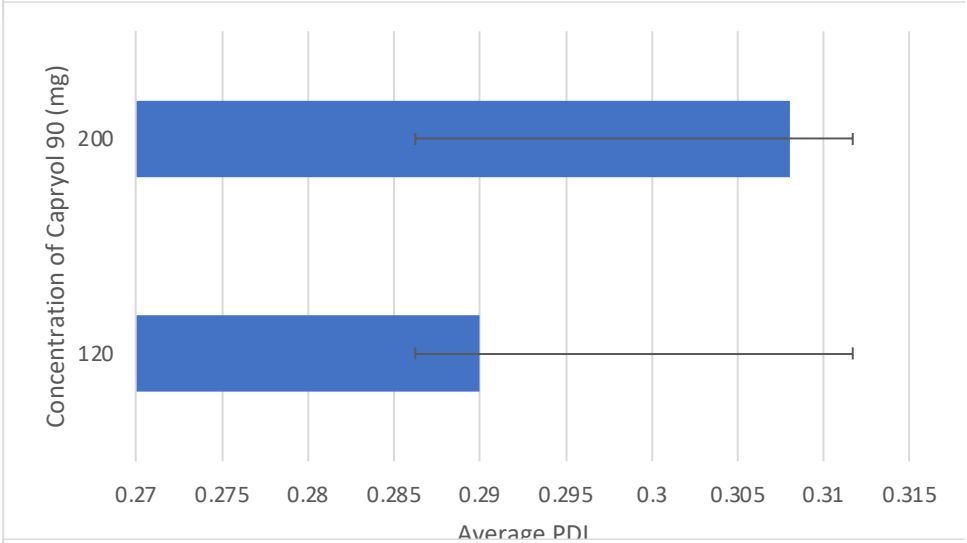

C

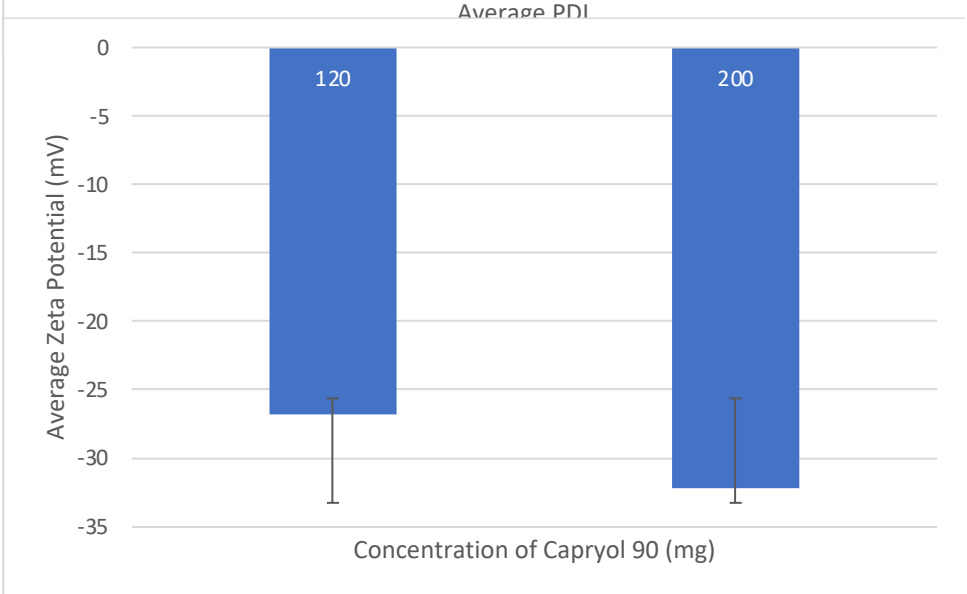

Figure 3. 6. Compositions of ME-NLCs formulated using two different concentrations of Capryol 90 to study the effect Capryol 90 concentration on particle size (A) and polydispersity index (B) zeta potential (C). Data is presented as mean ± SD, n = 3. (A) **** $p < 0.05$, refers to a significant difference when 120mg and 200mg were compared. (B) ** $p < 0.05$, refers to a significant difference when 120mg and 200mg were compared. (C) * $p < 0.05$, refers to a significant difference when 120mg and 200mg were compared.

3.2.3 Short term stability studies of blank and meropenem loaded NLCs.

The effect of storage time and temperature on the stability of blank and ME-NLCs (formulation ME 7, Table 2.2) was assessed by the change in particle size, PDI, and zeta potential over the period of forty eight hours (Figure 3.7).

The blank NLCs, showed in an increase of particle size from 165.9nm on the day of preparation to 182.4nm after 24 hours of storage at 20° C and then increased to 182.9nm after forty-eight hours. However, the PDI of the blank NLCs decreased over the investigated time point from 0.281 on the day of preparation to 0.263 after 48 hours. The change in zeta potential started at -36.7mV and then decreased to -27.6 after twenty-four hours, but then further increased to -53.6mV after forty-eight hours. The change in particle size and PDI during the investigated remained within the optimal ranges of (particle size <200nm and PDI <0.3) indicating that the NLCs were stable over the period of 48 hours.

The effect of time on the ME-NLCs stored at 20 °C, resulted in an increase of average particle size from 178.8 nm on the day of preparation to 185.4nm after 24 hours of storage. The particle size from twenty-four hours to forty-eight then decreased to 179.3nm. The PDI of the ME-NLCs stored at 20 °C decreased over the first twenty-four hours by 2% (0.283 on the day of preparation to 0.276). The PDI then increased by 27.5% from 0.276 to 0.352 after forty-eight hours with the PDI increasing over the optimal value (<0.3).

Furthermore, the effect of time on the ME-NLCs zeta potential stored at 20 °C, resulted in an increase from the time of preparation from -31mV to -39.9mV. The zeta potential then decreased to -30.3mV after forty-eight hours. The difference in size from the day of

preparation and 24 hours storage is not significant as the p-value is greater than 0.05. The difference in PDI from the day of preparation and 24 hours storage is not significant as the p-value is greater than 0.05. The difference in zeta potential from the day of preparation and 24 hours storage is significant as the p-value is less than 0.05.

The ME-NLCs stored at 37 °C, resulted in an increase of average particle size from 178.8nm on the day of preparation to 187nm after 24 hours and increased again by 2.6nm (189.6nm) after forty-eight hours.

In addition, the PDI of the ME-NLCs stored at 37 °C decreased over the first twenty-four hours from 0.283 on the day of preparation to 0.273. The PDI then increased from 0.276 to 0.29 after forty-eight hours.

The effect of time on the ME-NLCs zeta potential stored at 37 °C, also followed the same trend as that of the ME-NLCSS stored at 20 °C with the zeta potential increasing from -31mV to -41mV and then decreased again to -36.3mV at forty-eight hours. The difference in size from the day of preparation and 24 hours storage is significant as the p-value is less than 0.05. The difference in PDI from the day of preparation and 24 hours storage is significant as the p-value is less than 0.05. The difference in zeta potential from the day of preparation and 24 hours storage is not significant as the p-value is greater than 0.05.

A

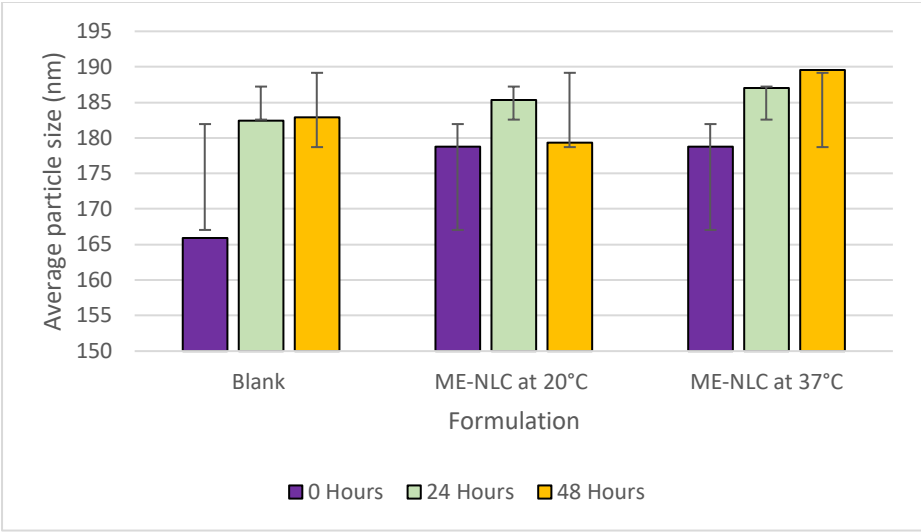

B

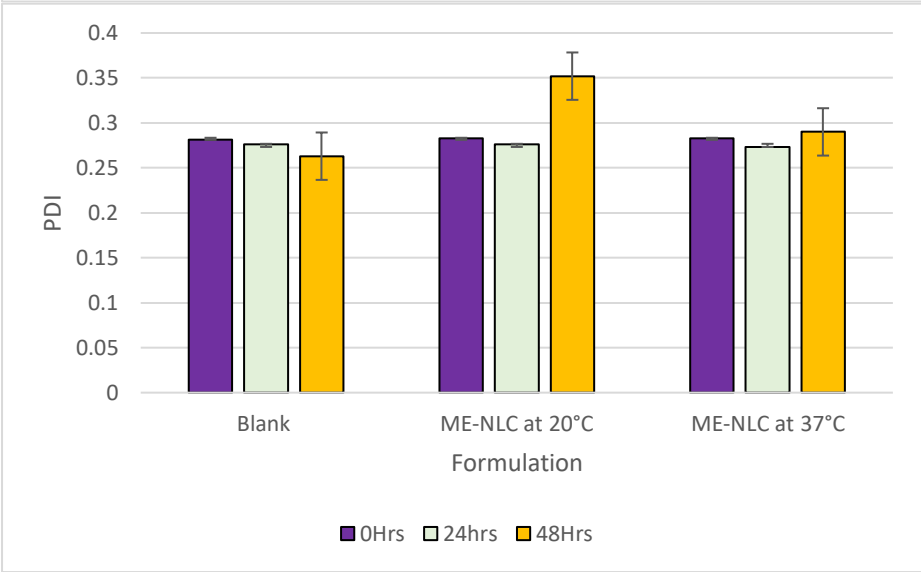

C

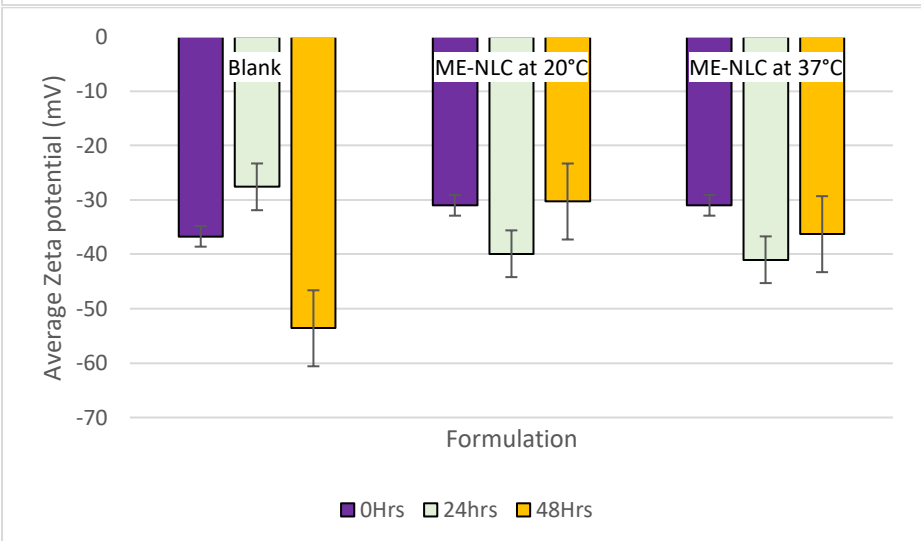

Figure 3. 7. Compositions of ME-NLCs formulated were stored at two different temperatures to study the effect of time and storage temperature on particle size (A) and polydispersity index (B) zeta potential (C). Data is presented as mean ± SD, n = 3.(A) **p < 0.05, refers to a significant difference when formulations stored at 37°C, on the day of preparation and 24 hours storage were compared. (C) ** p < 0.05, refers to a significant difference when formulations formulations stored at 20° C, on the day of preparation and 24 hours storage were compared.

3.2.4. Lyophilisation of meropenem loaded NLCs.

As meropenem degrades in aqueous solutions an attempt was made to lyophilise ME-NLCs. Sucrose which is a widely accepted cryoprotectant and was used during the lyophilisation process and it was investigated at three different concentrations. The effect of cryoprotectant concentration was evaluated on particle size, PDI, and zeta potential of ME-NLCs (Figure 3.8). The particle size of the ME-NLCs aqueous dispersions was 178.8nm, PDI of 0.283 and a zeta potential of -31mV. The lyophilized ME-NLCs with 5% sucrose resulted in an increase of particle size from the 178.8nm to 262.1nm. The PDI of the lyophilized ME-NLCs with 5% sucrose increased from 0.283 to 0.49, the zeta potential of lyophilised ME-NLCs decreased to -20.6mV as compared to at -31mV of the aqueous dispersion. The difference in size from the day of preparation and lyophilised ME-NLCs after five weeks storage is significant as the p-value is less than 0.05. The difference in PDI from the day of preparation and lyophilised ME-NLCs after five weeks storage is significant as the p-value is less than 0.05. The difference in zeta potential from the day of preparation and lyophilised ME-NLCs after five weeks storage is significant as the p-value is less than 0.05.

The lyophilized ME-NLCs with 7% sucrose resulted in an increase of particle size from 178.8nm to 299.5nm. The PDI of the lyophilized ME-NLCs with 7% sucrose also increased from 0.283 to 0.647 indicating that the formulation was polydispersed. A change in zeta potential was observed, being decreased to -21.6mV after lyophilisation. The difference in size from the day of preparation and lyophilised ME-NLCs after five weeks storage is significant as the p-value is less than 0.05. The difference in PDI from the day of preparation and lyophilised ME-NLCs

after five weeks storage is significant as the p-value is less than 0.05. The difference in zeta potential from the day of preparation and lyophilised ME-NLCs after five weeks storage is significant as the p-value is less than 0.05.

The lyophilized ME-NLCs with 10% sucrose resulted in an increase of particle size from 178.8nm to 319.1nm after two months of storage. However, the PDI of the lyophilized ME-NLCs with 10% sucrose also increased from 0.283 to 0.456 indicating the lyophilised formulation was polydisperse. The zeta potential started at -31mV on the day of preparation and then decreased to -21.9mV. The difference in size from the day of preparation and lyophilised ME-NLCs after five weeks storage is significant as the p-value is less than 0.05. The difference in PDI from the day of preparation and lyophilised ME-NLCs after five weeks storage is significant as the p-value is less than 0.05. The difference in zeta potential from the day of preparation and lyophilised ME-NLCs after five weeks storage is significant as the p-value is less than 0.05.

Therefore, showing that the lyophilization of ME-NLCs with varying concentrations of sucrose as a cryoprotectant did not enhance the stability of the NLCs as the size, PDI and zeta potential did not remain within the optimal ranges of particle size being <200nm and PDI being to <0.3, indicating that the NLCs was not stable over the period and further investigations with different cryoprotectants are required for lyophilisation.

A

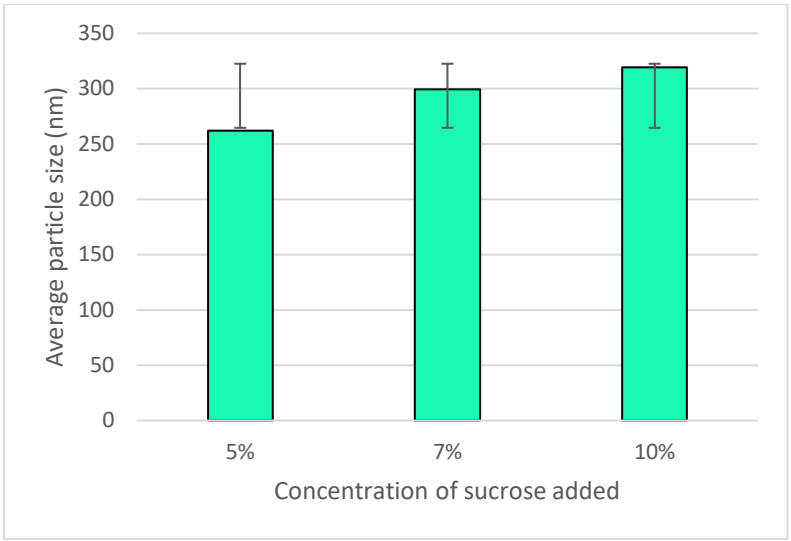

B

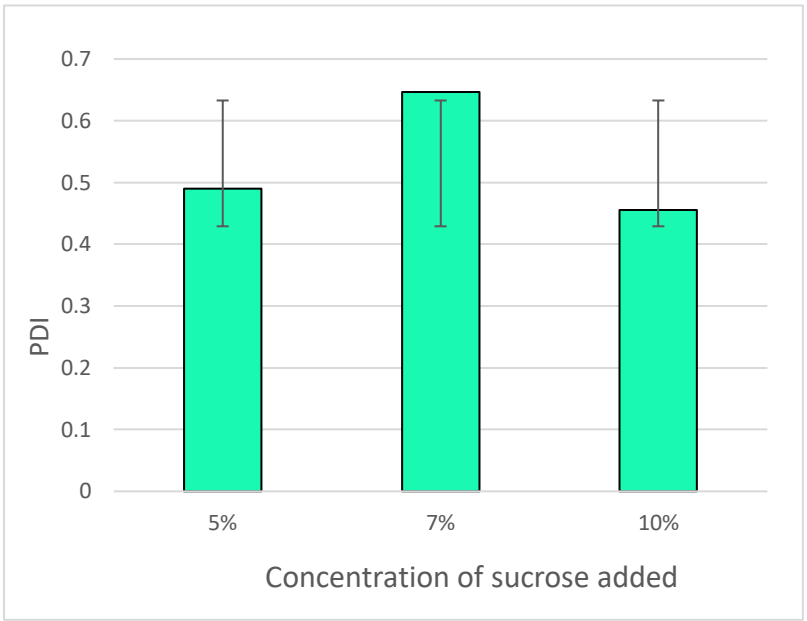

C

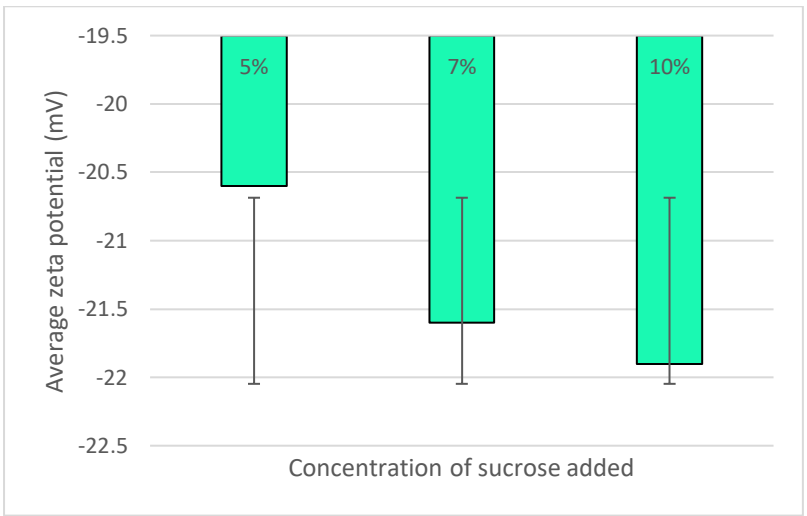

Figure 3. 8. Compositions of ME-NLCs formulated using three different concentrations of cyroprotectant to study the effect of lyophilistaion of ME-NLCs after 5 weeks of storage on particle size (A) and polydispersity index (B) zeta

potential (C). Data is presented as mean ± SD, n = 3.(A) ****p < 0.05, refers to a significant difference when formulations with 0% and 5% of cyroprotectant storage were compared. ****p < 0.05, refers to a significant difference when formulations with 0% and 7% of cyroprotectant storage were compared. ****p < 0.05, refers to a significant difference when formulations with 0% and 10% of cyroprotectant storage were compared.(B) ****p < 0.05, refers to a significant difference when formulations with 0% and 5% of cyroprotectant storage were compared. ***p < 0.05, refers to a significant difference when formulations with 0% and 7% of cyroprotectant storage were compared. **p < 0.05, refers to a significant difference when formulations with 0% and 10% of cyroprotectant storage were compared.(C) (B) ****p < 0.05, refers to a significant difference when formulations with 0% and 5% of cyroprotectant storage were compared. ****p < 0.05, refers to a significant difference when formulations with 0% and 7% of cyroprotectant storage were compared. ****p < 0.05, refers to a significant difference when formulations with 0% and 10% of cyroprotectant storage were compared.

3.3. Fourier transform infrared spectroscopy (FTIR) of meropenem, blank NLC and ME-NLC

The FTIR absorbance spectra of meropenem (Figure 3.9A) shows the absorbance peaks for the functional groups. The broad peak at around 3323.4 cm-1 suggests the stretching of the oxygen-hydrogen bonds within the water molecules as all the samples were in aqueous solution, whereas the second and third peaks at 2168.13cm-1 indicates stretching of N=N=N bonds and 2114.21 and indicates weak stretching of alkyne groups. The final peak at 1635.45cm-1 correlates with the stretching of alkene groups within the molecule. These correspond to the FTIR fingerprint of meropenem (Muneer, Wang *et al.,* 2020).

Once the meropenem has been encapsulated into the NLCs (Figure 3.9B) the absorbance fingerprint changes exhibiting the same peaks as meropenem and ME-NLCs spectra show additional peaks corresponding to meropenem (figure 3.9B). These additional peaks are at 2925.19, 2114.62 and 1376.66cm-1. The increased number of peaks due to presence of lipids present in the NLCs. However, the peaks from figure A; 2168.13cm-1 shifted to 2182.67 and 2114.21 to 2151.63cm-1 and have shifted to the right. Additional four peaks can be seen in the absorbance spectra in figure 3.9B compared to 3.9A. The peak at 2835.14 indicates the stretching in C-H bonds within aldehyde groups. The small peak at 1462.39 suggests the bending of the bonds between saturated alkane molecules. Similarly, the two peaks at 1178.38 and 1081.67 both suggest the stretching of carbon and oxygen bonds in alcohol groups which can be explained due to the excipients of the NLCs, suggesting the encapsulation of meropenem in the NLCs.

Further, the FTIR spectra of blank NLCs (figure 3.9C) shows the peaks due to lipid excipients in the NLCs. ME-NLCs spectra show additional peaks corresponding to meropenem (figure 3.9B). These additional peaks are at 2925.19, 2114.62 and 1376.66cm-1.

A

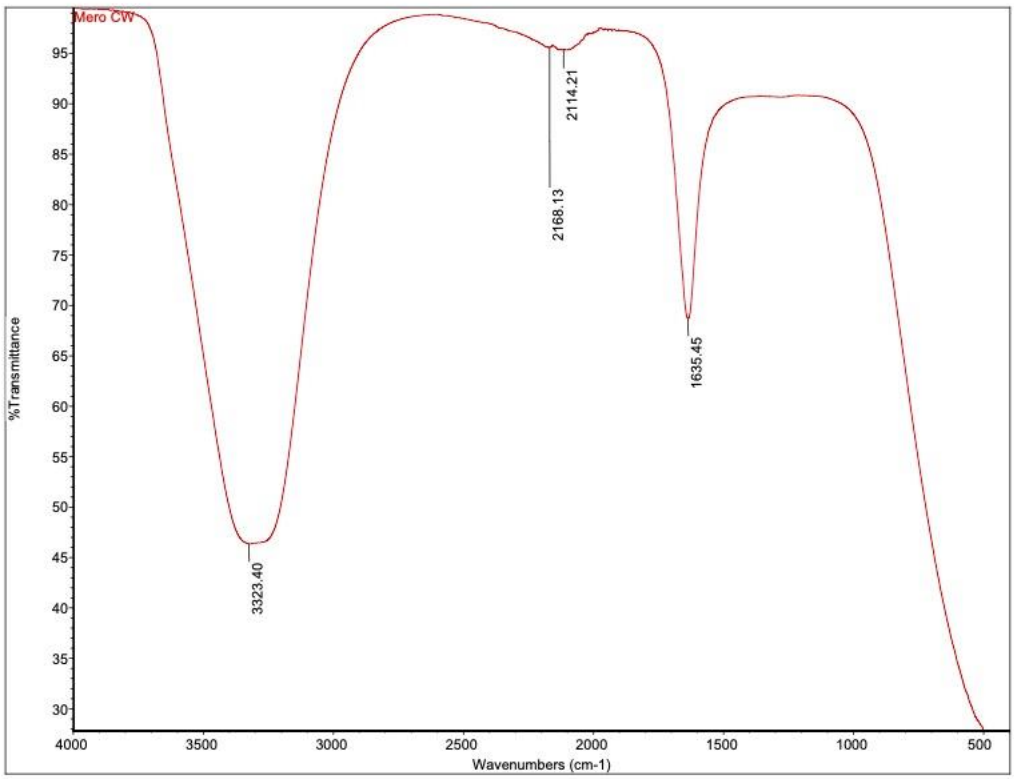

B

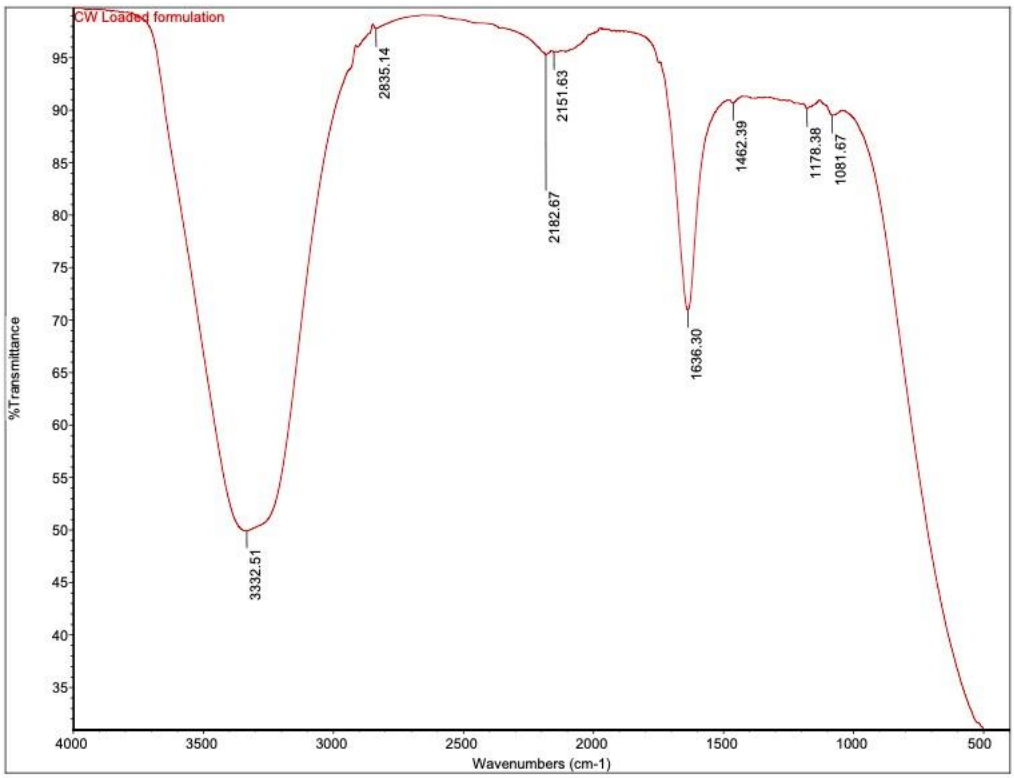

C

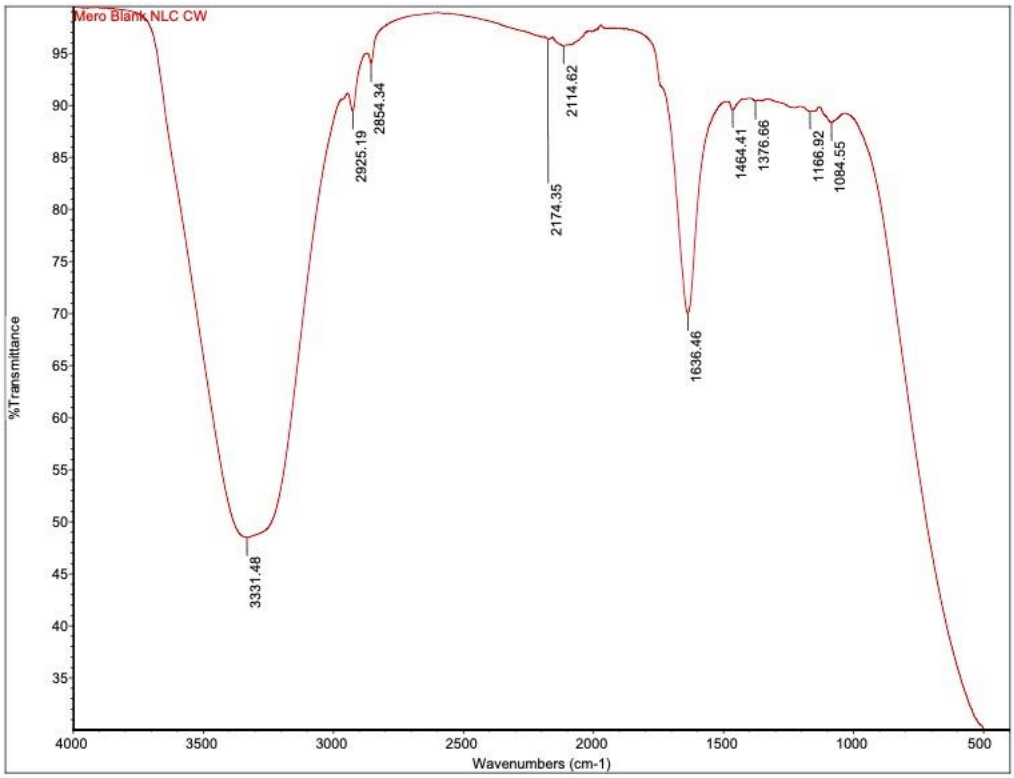

Figure 3. 9. FTIR spectra for meropenem (A), ME-NLCs (B) and blank NLCs (C)

3.4. Differential Scanning Calorimetry of meropenem, blank NLC and ME-NLC

Differential scanning calorimetry analysis was performed to study the effect of the incorporation of meropenem on the crystallinity of the NLCs and its melting behaviour (Figure 3.10 A-E). The DSC thermogram for meropenem shows a broad endothermic peak at approximately 137.5 °C. Once incorporated into the physical mixture of the lipids of the NLCs the endothermic peak becomes sharper, and shifts left to a decreased temperature of approximately 60 °C. However, there is also a sharp exothermic peak before this at 50 °C. The thermogram for Dynasan 114, which is the solid lipid in the NLCs also shows a sharp endothermic peak at approximately 50 °C. The blank NLCs thermogram has a broad endothermic peak at approximately 100 °C . The thermogram for ME-NLCs (D) shows an endothermic peak around 118 °C, due to the absence of the meropenem peak due to encapsulation and the increase in melting temperature compared to the blank NLCs suggests the incorporation of the meropenem into the NLCs.

A

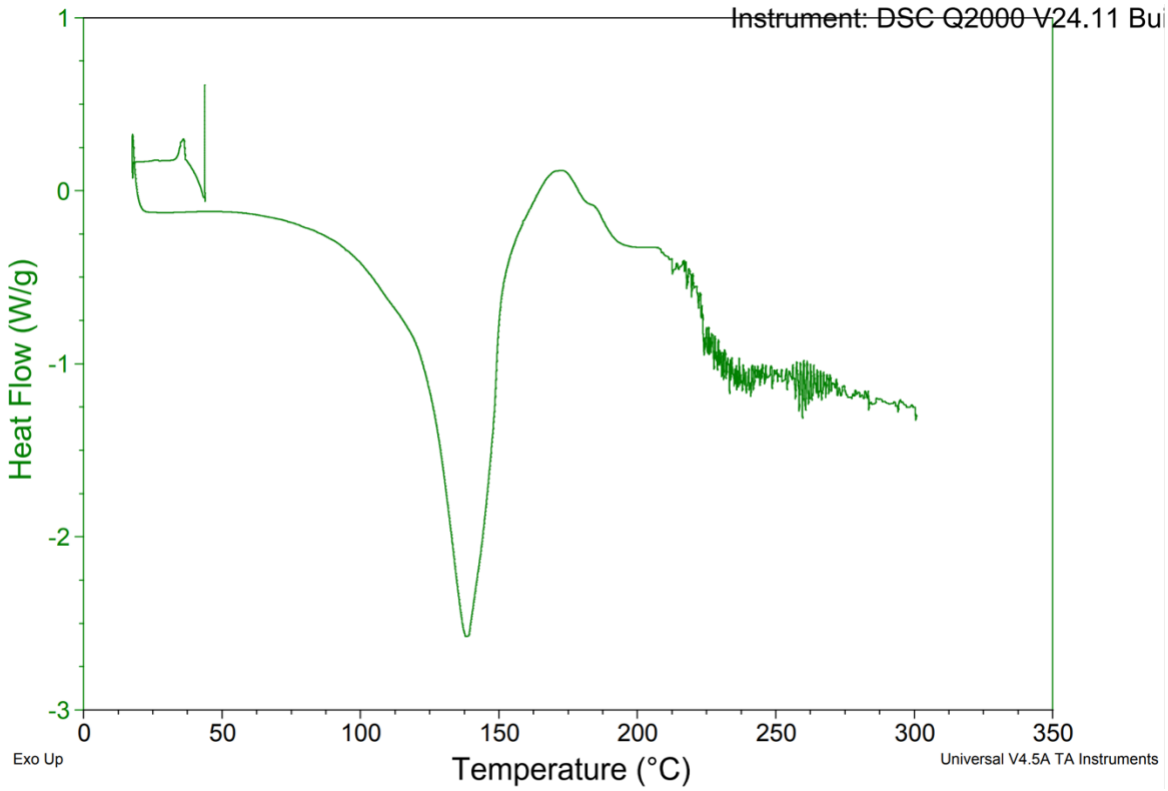
Instrument: DSC Q2000 V24.11 Bu
Heat Flow (W/g)
1
0
-1
-2
-3
0
50
100
150
200
250
300
350
Exo Up
Temperature (°C)
Universal V4.5A TA Instruments

B

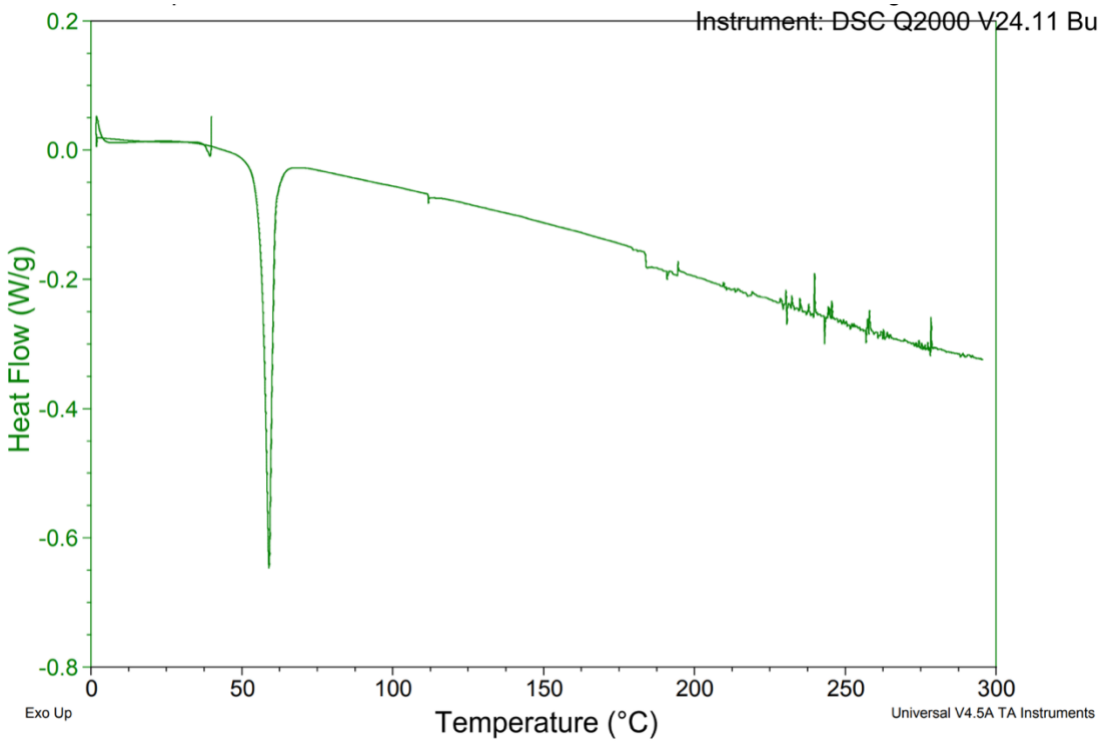
Instrument: DSC Q2000 V24.11 Bu
Heat Flow (W/g)
0.2
0.0
-0.2
-0.4
-0.6
-0.8
0
50
100
150
200
250
300
Exo Up
Temperature (°C)
Universal V4.5A TA Instruments

C

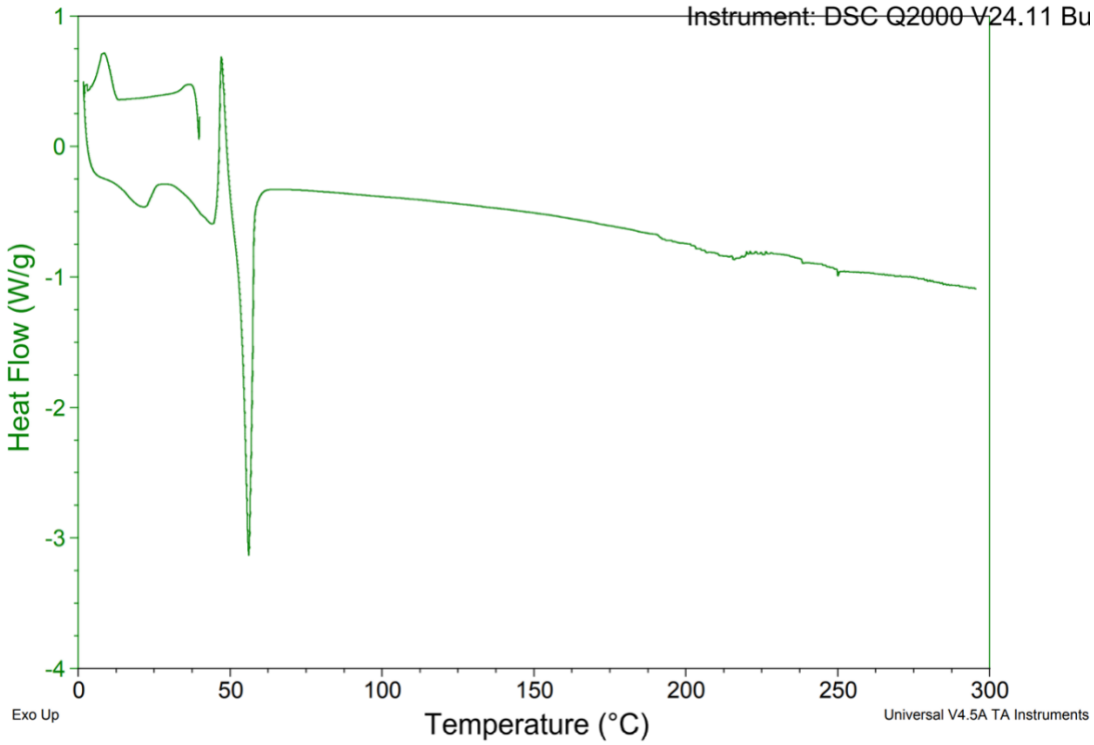
Instrument: DSC Q2000 V24.11 Bu
Heat Flow (W/g)
1
0
-1
-2
-3
-4
0
50
100
150
200
250
300
Exo Up
Temperature (°C)
Universal V4.5A TA Instruments

D

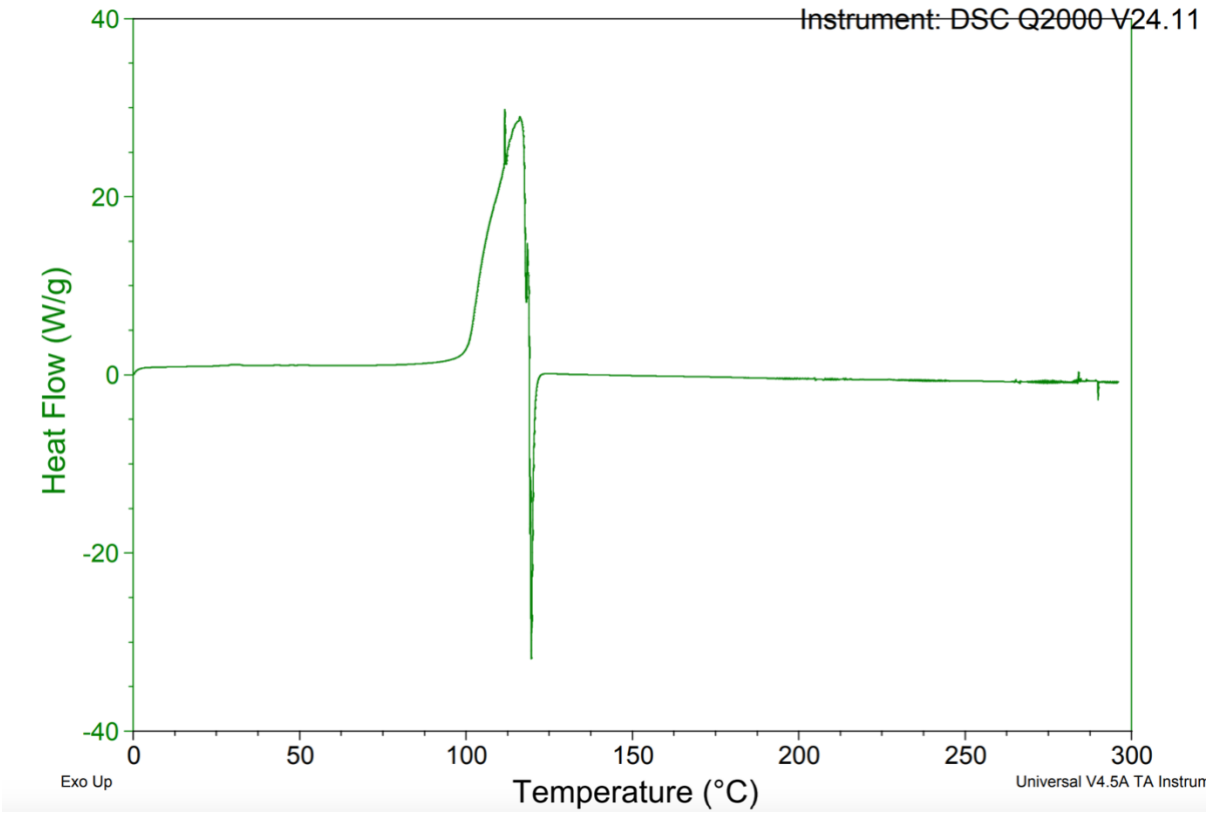
Instrument: DSC Q2000 V24.11
Heat Flow (W/g)
40
20
0
-20
-40
0
50
100
150
200
250
300
Exo Up
Temperature (°C)
Universal V4.5A TA Instrum

E

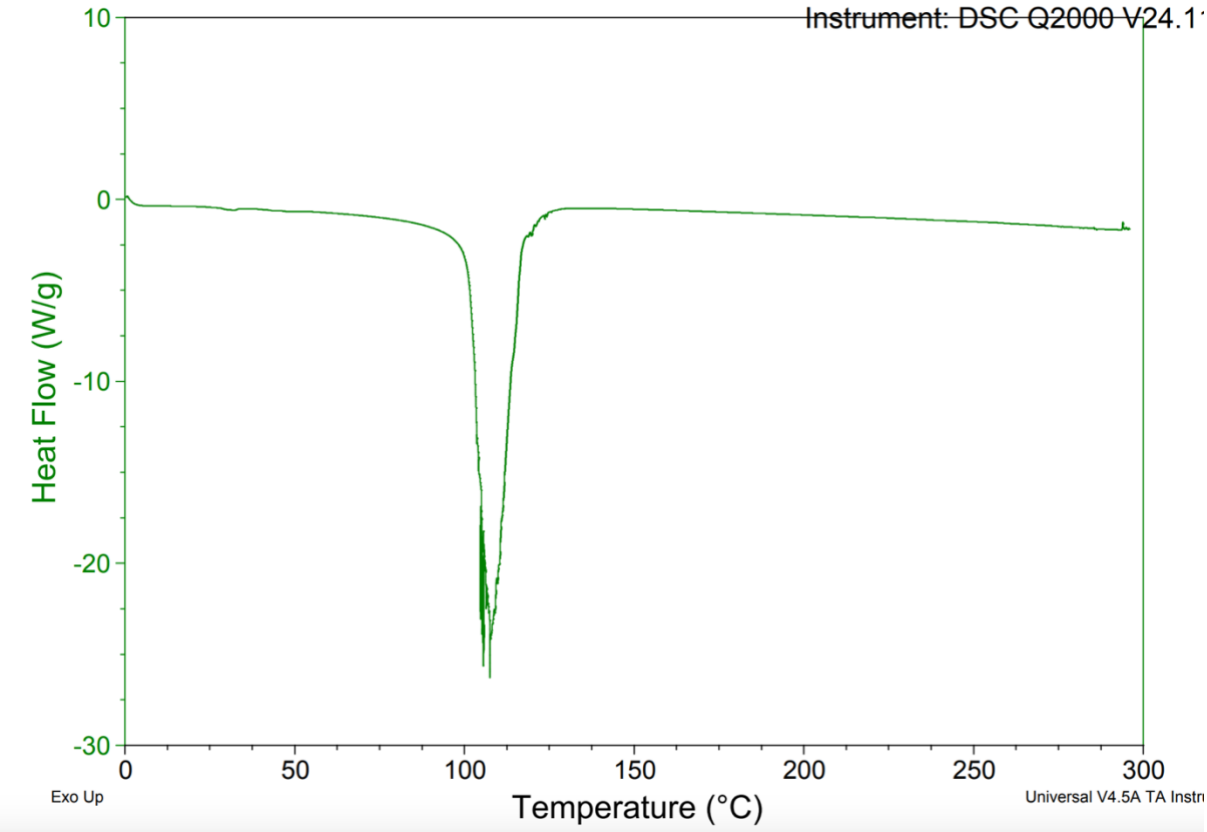

Figure 3. 10. Differential scanning calorimetry (DSC) thermograms for meropenem (A), Dynasan 114 (B), physical mixture (C), ME-NLCs (D)and blank NLCs (E).

3.5.1. Development and optimisation of HPLC method for analysis of meropenem

Various chromatographic conditions for HPLC analysis of meropenem were optimised.

3.5.1.1 Optimisation of detection wavelength

Effect of detection wavelength was observed on the peak area of meropenem. The trend observed was that as the wavelength increased the peak area increased. However, a wavelength of 260nm or less produced a negative peak (Table 3.2). The wavelength selected was 308nm as it gave the largest peak area of 186.6, whereas the wavelengths such as 270nm resulted in a much smaller peak area of 31.1 (Table 3.2).

3.5.1.2 Optimisation of mobile phase ratio

Orthophosphate buffer: methanol was used as mobile phase for HPLC quantification of meropenem as per the previous report by (Milla, Ferrari *et al.,* 2020). Ratio of the two components of the mobile phase was optimised by evaluating the retention time (RT), peak area and peak symmetry (Table 3.3). Mobile phase composition of 70% Orthophosphate buffer: 30% methanol resulted in meropenem eluting at RT of 2.21 minutes with an acceptable peak area (270.3) and symmetry (0.723) while the solvent peak was shown at 2 minutes . As the RT of the peak was close to the solvent peak and therefore would be difficult to distinguish when testing low concentrations of meropenem (Table 3.3) decreasing the methanol concentration with a mobile phase ratio of 84% orthophosphate buffer: 16% methanol provided the analysis of meropenem with a sharp well separated peak eluting at RT of 8. 031 minutes, with acceptable peak area (194.65) and good symmetry (0.788) along with no peak interference with the solvent peak. Hence this mobile ratio was selected for

chromatographic analysis (Table 3.3). The chromatogram of meropenem (10μg/ml) is shown in figure 3.11. A further two meropenem concentrations were injected at 4 μg/ml and 20 μg/ml (Figure 3.11).

During the HPLC analysis of meropenem it was observed that the RT varied in the range of 8-9 minutes. This could be due to the use of orthophosphate buffer in the mobile phase which was prepared fresh on each day on the on the day of analysis. Minor variations in the pH of the orthophosphate could have resulted in the day to day variation of the RT. However, it must be highlighted that there was no change in the RT between the chromatographic runs on a given day of analysis.

3.5.2. Calibration Curve of meropenem in aqueous solution

Linearity of the HPLC method was determined by the use of six concentration points from 0-20μg/ml and repeated in triplicate. A representative of the calibration curve is depicted in Figure 3.12. The representative linear equation was $y = 16.01x + 30.444$ with $R^2 = 0.994$ (Figure 3.12). The repeatability studies were carried out by repeating seven injections of 4μg/ml. The results showed a percentage relative standard deviation (%RSD) of 3.97 between the injections (Table 3.4).

Precision studies showed that there was decrease in the peak area of meropenem of the samples injected in the afternoon compared to freshly prepared meropenem solution in the morning (Table 3.5). This could be due to the degradation of meropenem in the methanol phosphate buffer mixture. Meropenem is well known to degrade in aqueous buffers (Jamieson, Allwood *et al.,* 2020). In view of these results meropenem standard solutions were

prepared fresh daily in the morning and afternoon and a standard solution was injected for every HPLC analysis. The accuracy studies at carried out three concentration (4, 8, 16 μg/ml) showed good recovery with %RSD in the range of 1.48-6.23 (Table 3.6).

Table 3. 2. The effect of wavelength on the peak area of a standard sample of 10μg/ml of meropenem. Data is presented as mean ± SD, n = 3. * is the wavelength selected.

Wavelength (nm)	Peak Area
240	Negative peak
250	Negative peak
260	Negative peak
270	31.1
280	72.6
285	107.9
290	143.2
295	159.5
298	160.3
300	168.5
302	175.4
304	180.7
306	184.2
308**	186.6

Table 3. 3. The effect of mobile phase ratio on the peak area, retention time and peak symmetry of a standard drug solution of 10μg/ml of meropenem. Data is presented as mean ± SD, n = 3. * is the mobile phase ratio selected.

Mobile Phase ratio	Retention time (min)	Peak Area	Symmetry
70% Orthophosphate buffer: 30% methanol	2.21	270.3	0.723
83% Orthophosphate buffer: 17% methanol	5.32	288.8	0.536
84% Orthophosphate buffer: 16% methanol *	8.068	265.9	0.773
85% Orthophosphate buffer: 15% methanol	9	258.6	0.769

A

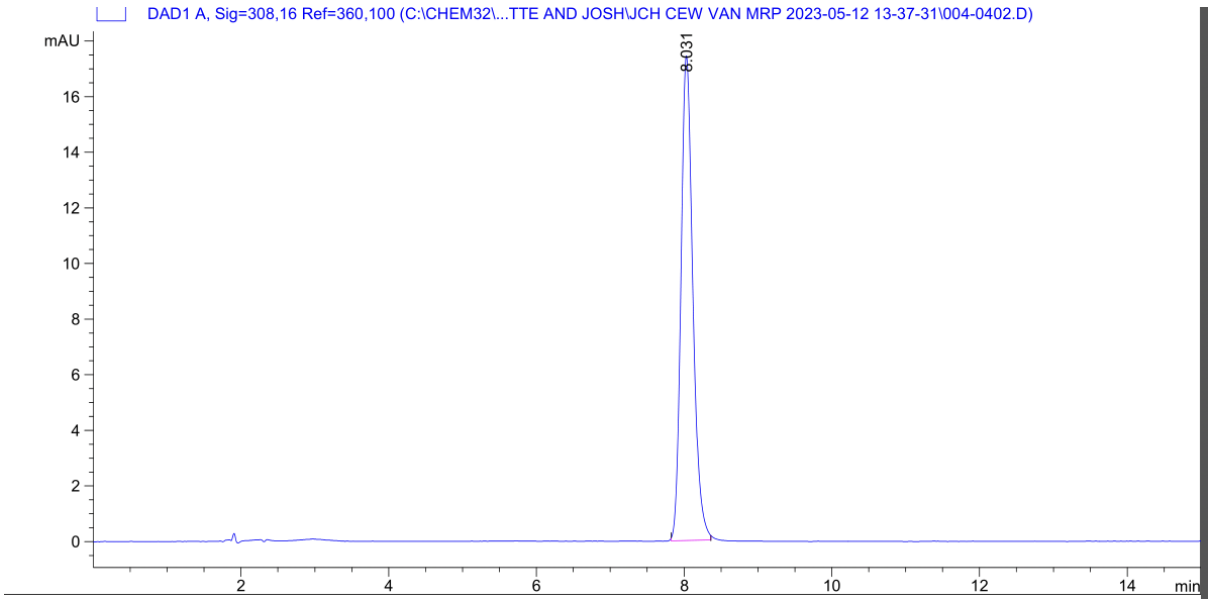
DAD1 A, Sig=308,16 Ref=360,100 (C:\CHEM32\...TTE AND JOSH\JCH CEW VAN MRP 2023-05-12 13-37-31\004-0402.D)
mAU
8.031
min

B

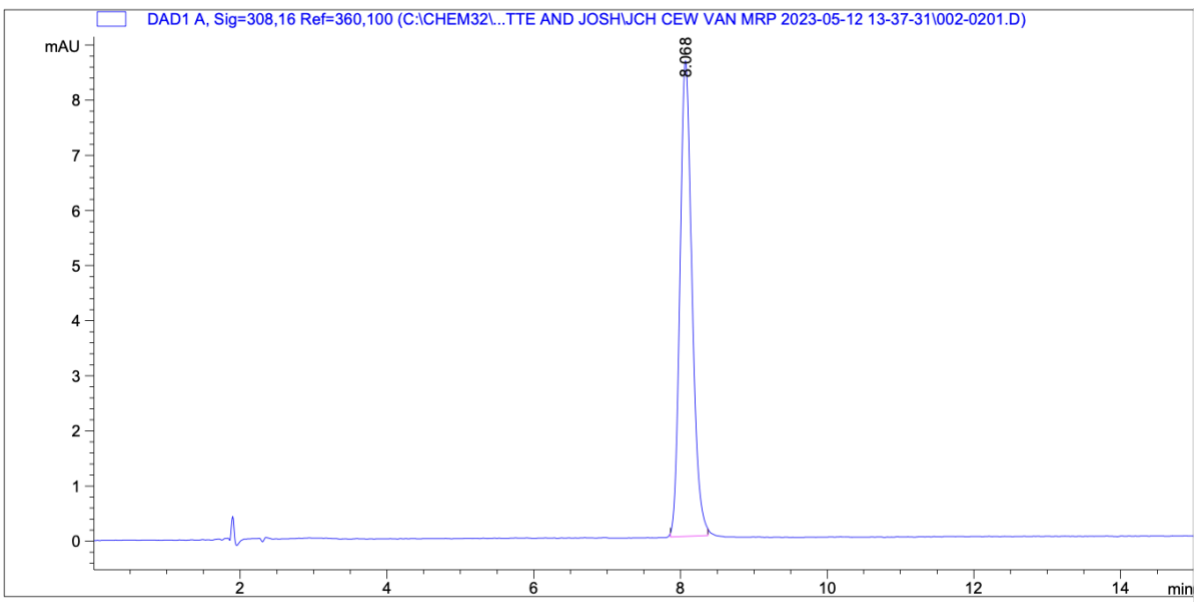
DAD1 A, Sig=308,16 Ref=360,100 (C:\CHEM32\...TTE AND JOSH\JCH CEW VAN MRP 2023-05-12 13-37-31\002-0201.D)
mAU
8.068
min

C

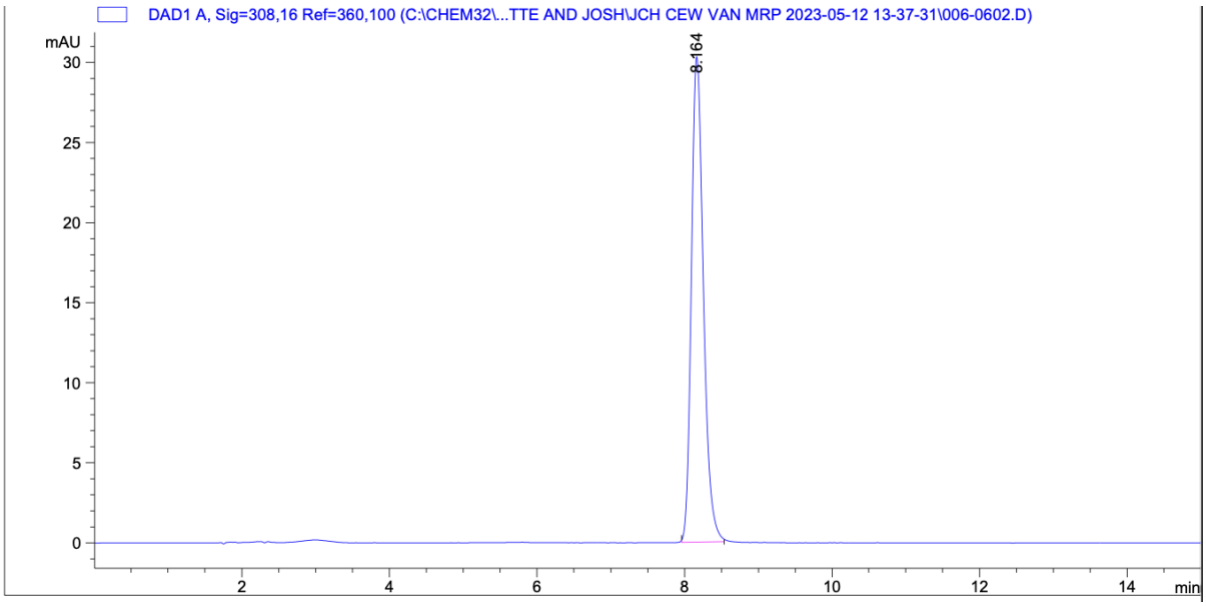

Figure 3. 11. HPLC chromatograms of meropenem reference standards 10 µg/ml (A), 4 µg/ml (B) and 20 µg/ml (C).

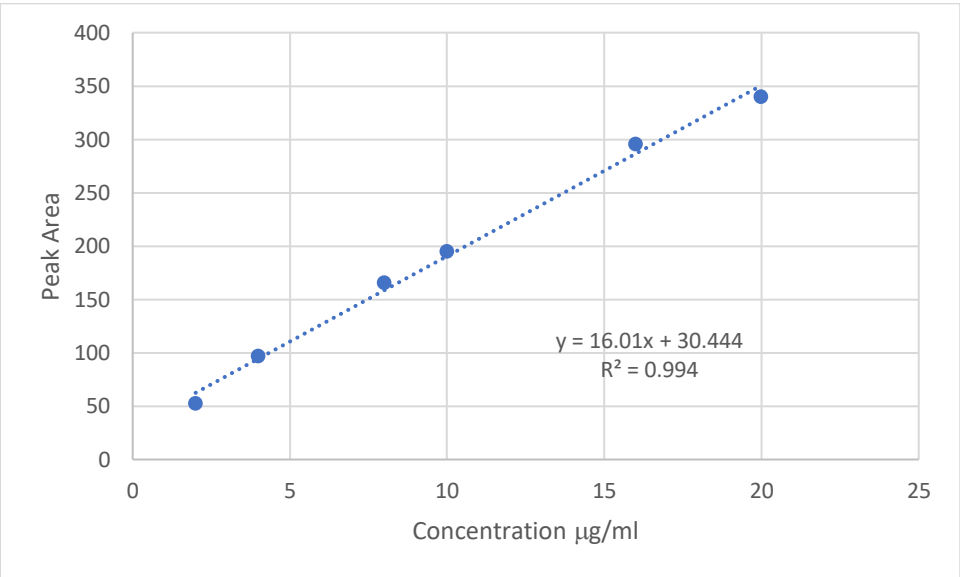

Figure 3. 12. Calibration curve of meropenem concentrations (2-20 µg/ml) Data is presented as mean, n = 3.

Table 3. 4. . Results for repeatability assay, of 10 injections of one concentration. N= 10.

Meropenem labelled concentration (μg/ml)	Calculated concentration of Meropenem (μg/ml)
4	4.28
	4.20
	4.06
	4.11
	4.00
	3.98
	4.14
	3.74
Average	4.06
SD	0.16
RSD %	3.97

Table 3. 5. Results of Intra and inter day assay for validation. Data is presented as mean ± SD, n = 3.

Day	Time	Concentration (μg/ml)	Average Peak Area	Calculated Concentration (μg/ml)	Standard deviation	%RSD
Day 1	AM	4	90.60	3.76	0.19	5.16
		20	412.37	23.86	0.84	3.54
	PM	4	71.83	2.59	0.17	6.64
		20	317.37	17.92	0.77	4.29
Day 2	AM	4	97.73	4.20	0.19	4.53
		20	384.5	22.12	0.73	3.31
	PM	4	77.87	2.96	0.18	5.91
		20	302.33	16.98	0.68	3.98
Day 3	AM	4	95.73	4.08	0.19	4.68
		20	384.9	22.14	0.81	3.66
	PM	4	117	5.41	0.19	3.64
		20	479.37	28.04	0.86	3.06

Table 3. 6. Results of accuracy assay of three concentrations. Data is presented as mean ± SD, n = 3.

Meropenem concentration (μg/ml)	Recovered meropenem concentration (m μg/ml)	% Recovery	% RSD
4	4.18	104.50	4.53
8	8.35	104.40	1.48
16	16.16	101	6.23

3.5.3. Entrapment efficiency of ME-NLCs

A

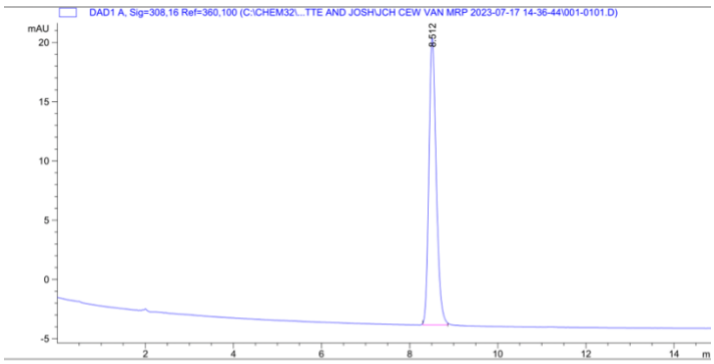


```
=====================================================================
                    Area Percent Report
=====================================================================

Sorted By             :      Signal
Multiplier:                   :      1.0000
Dilution:                     :      1.0000
Use Multiplier & Dilution Factor with ISTDs


Signal 1: DAD1 A, Sig=308,16 Ref=360,100

Peak RetTime Type  Width     Area      Height     Area
  #   [min]        [min]   [mAU*s]     [mAU]       %
----|-------|----|-------|----------|----------|--------|
   1   8.512 BB    0.1792  281.11386   24.25812 100.0000
```

B

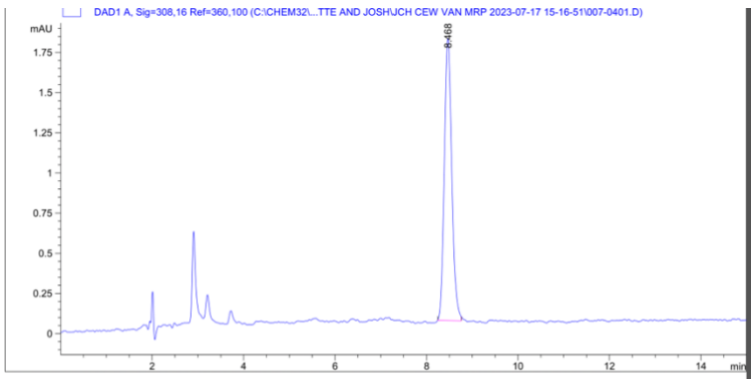


```
=====================================================================
                    Area Percent Report
=====================================================================

Sorted By             :      Signal
Multiplier:                   :      1.0000
Dilution:                     :      1.0000
Use Multiplier & Dilution Factor with ISTDs


Signal 1: DAD1 A, Sig=308,16 Ref=360,100

Peak RetTime Type  Width     Area      Height     Area
  #   [min]        [min]   [mAU*s]     [mAU]       %
----|-------|----|-------|----------|----------|--------|
   1   8.468 BB    0.1767   19.99576   1.75755 100.0000
```

Figure 3. 13. HPLC chromatograms of meropenem reference standard 10 µg/ml (A) and free drug from ME-NLCs (B).

Table 3. 7. Calculated encapsulation efficiency for ME-NLCs formulations.

	Concentration of free drug mg/ml	Calculated encapsulation efficiency (%)
Formulation ME 2	0.600	40.00
Formulation ME 7	0.071	85.72

The free drug concentration was calculated by comparing the peak area of a standard solution to the sample injected, in which resulted in 0.6mg/ml free drug in ME-NLCs therefore using the equation 1 in chapter 2.6.8, the calculated encapsulation efficiency indicated a 40% encapsulation.

In attempt to increase the encapsulation efficiency oleic acid was added to the ME-NLCs formulation ME 7 (Table 2.2) The effect of the oleic acid was investigated on particle size, PDI at three concentration levels.

Increasing the concentration of oleic acid resulted in an increase in particle size, the results between 100mg and 150mg are statistically significant as the p value is less than 0.05. However, the results between 150mg and 200mg is not statistically significant as the p value is greater than 0.05. 100mg of oleic acid concentration was selected as it resulted in the lowest particle size of 170.7nm and a PDI of 0.245 providing best values. Interestingly PDI was found be quite stable over the range of various oleic acid concentrations studied (Figure 3.14) and the results between 100mg and 150mg are statistically significant as the p value is less than 0.05. However, the results between 150mg and 200mg is not statistically significant as the p value is greater than 0.05.

Entrapment efficiency was found to significantly increase to 85.72% on addition of oleic acid (Table 3.7).

A

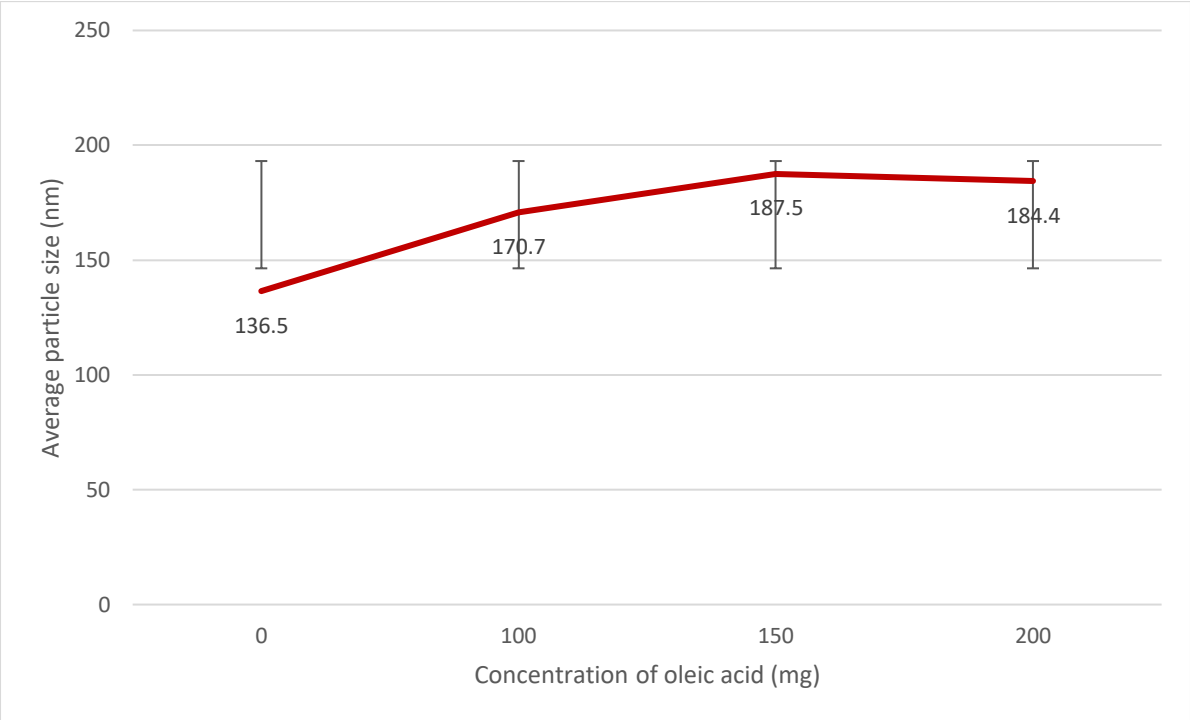

B

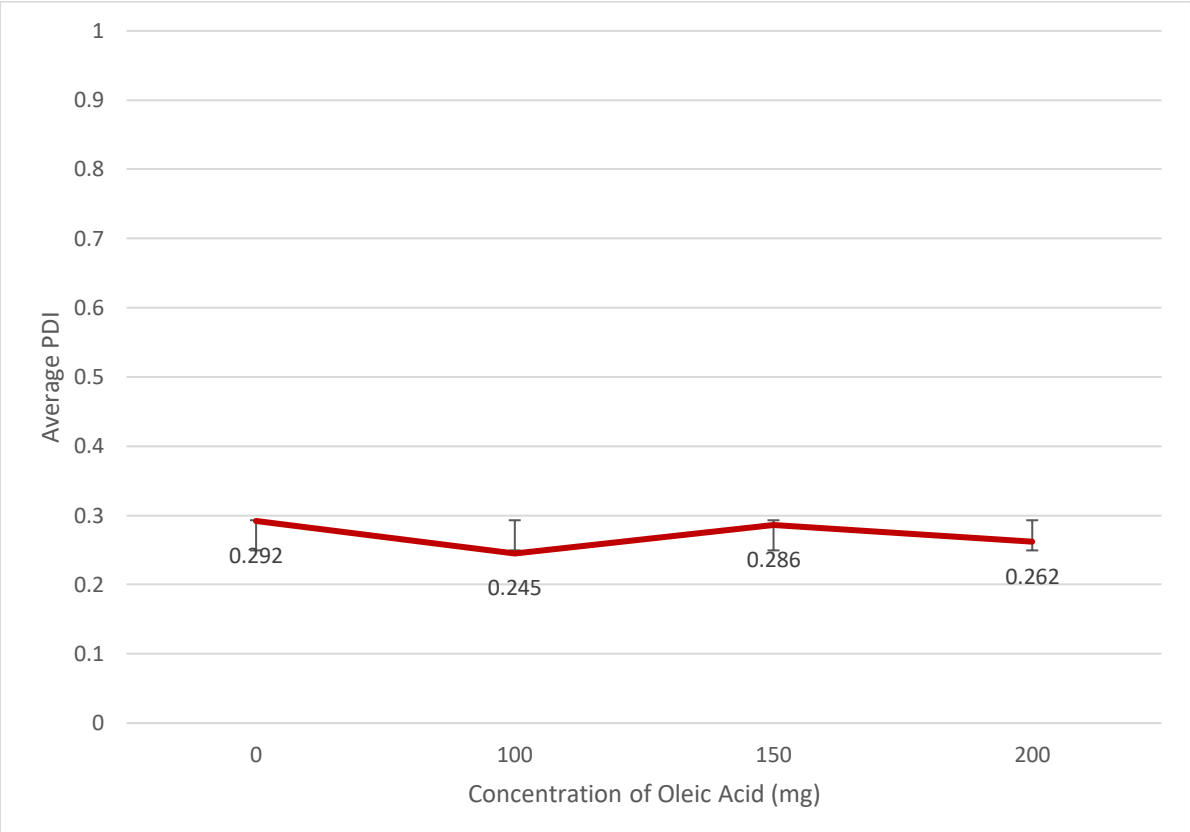

Figure 3. 14. Compositions of ME-NLCs formulated using four different concentrations of oleic acid to study the effect on particle size (A) and polydispersity index (B). Data is presented as mean ± SD, n = 3.(A) *p < 0.05, refers to a significant difference when formulations with 100mg and 150mg of oleic acid were compared. *p < 0.05, refers to a significant difference when formulations with 100mg and 200mg of oleic acid were compared. (B) *p < 0.05, refers to a significant difference when formulations with 100mg and 150mg of oleic acid were compared. **p < 0.05, refers to a significant difference when formulations with 100mg and 200mg of oleic acid were compared.

3.6. Calibration curve of Meropenem in pH 6.8 orthophosphate buffer using HPLC

The in vitro drug release studies of meropenem from ME-NLCs was conducted in phosphate buffer pH 6.8. To quantify the drug in the release medium the, HPLC method of meropenem detection in phosphate pH6.8 was validated. The meropenem peak produced by the validated method (Figure 3.15) showed a narrow tall peak with limited peak tailing and fronting, with peak symmetry within the range of 0.7-0.85 and RT of 4.09 minutes. The chromatogram showed a solvent peak at 1.6 minutes which was well separated from the meropenem peak and there was no interference. The chromatograms of meropenem reference standard of 8μg/ml and 16μg/ml are shown in figure 3.15.

It was observed that meropenem eluted much earlier at 4.09 minutes in pH 6.8 orthophosphate buffer as compared to meropenem being dissolved in the mobile phase (methanol and orthophosphate buffer pH 2.7), with a RT of 8 minutes (Figure 3.11). This could be due to the increase of pH (Studzińska, Buszewski 2013). Linearity of the HPLC method was determined by the use of six concentration points from 2 - 20μg/ml and repeated in triplicate. A representative of the linearity can be seen in Figure 3.16 The representative linear equation was $y = 20.412x$ and $R^2 = 0.9994$. the calculated concentration as compared to the injected concentrations are given in table 3.8. The repeatability studies were carried out by repeating seven injections of 4μg/ml, the results showed a percentage relative standard deviation (%RSD) of 5.84 between the injections (Table 3.9). The accuracy studies at carried out three concentration (4, 8, 16 μg/ml) showed good recovery with %RSD in the range of 0.31-2.33 (Table 3.10).

A

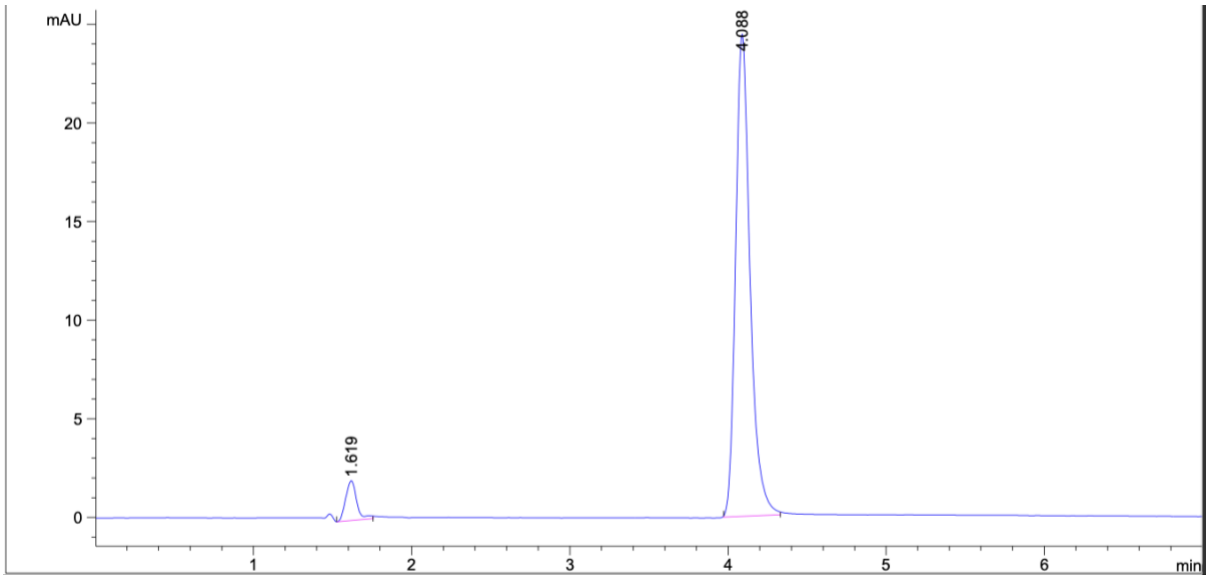

B

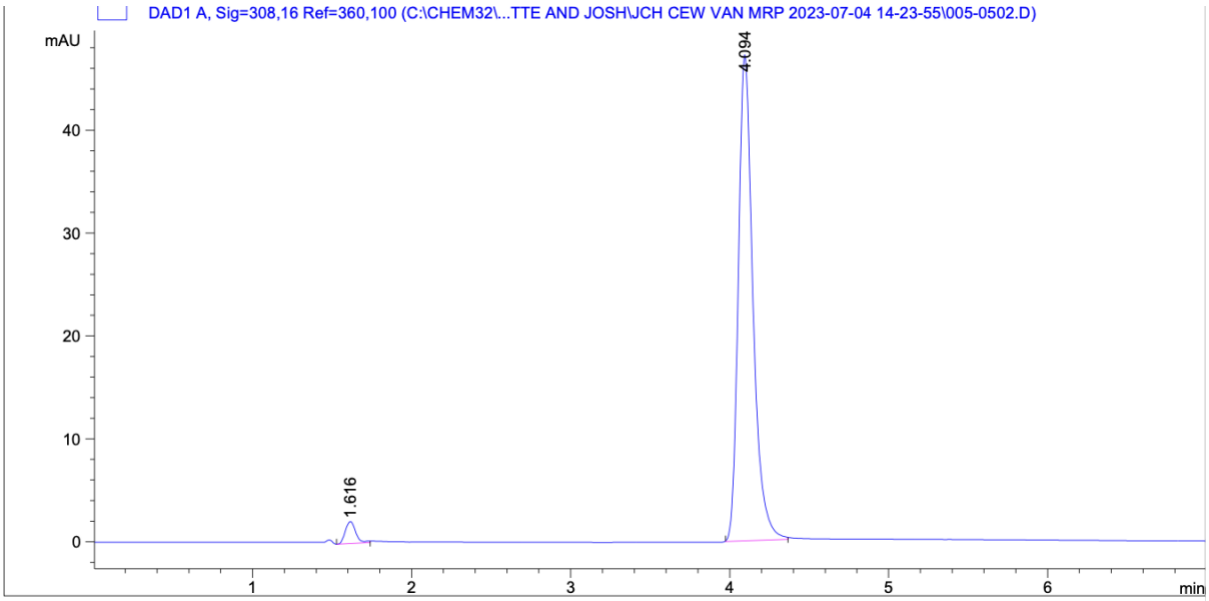

Figure 3. 15. HPLC chromatograms of meropenem reference standard 8 µg/ml (A) and 16 µg/ml (B).

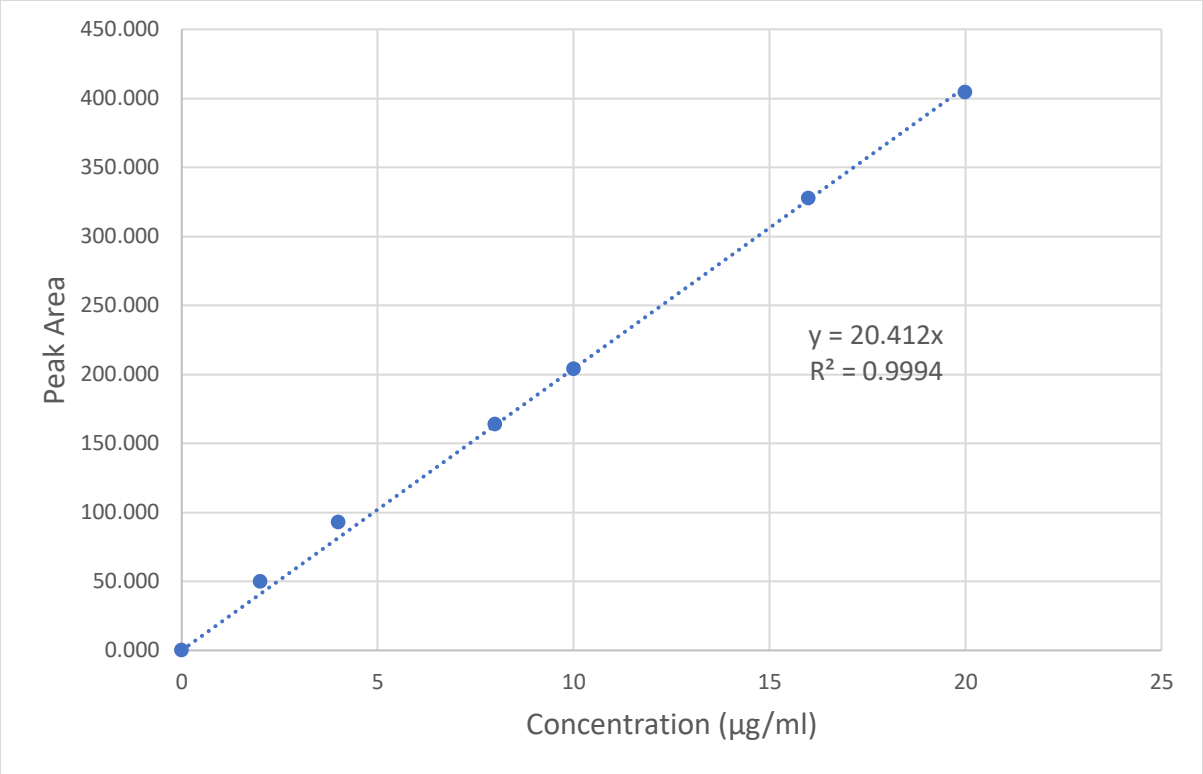

Figure 3. 16. Graph to show the linearity of with concentrations 2-20µg/ml of meropenem.

Table 3. 8. Calculated concentrations of meropenem for standards used for linearity (2-20µg/ml). N=3.

Concentration (µg/ml)	Average peak area	Calculated Concentration (µg/ml)
0	0.000	0
2	49.73	2.44
4	92.87	4.55
8	164.03	8.04
10	204.03	9.99
16	327.43	16.04
20	404.20	19.80

Table 3. 9. Results from repeatability assay of ten injections of one concentration of meropenem. N=10.

Meropenem labelled concentration (μg/ml)	Calculated concentration of Meropenem (μg/ml)
4	4.00
	3.99
	4.57
	4.55
	4.56
	4.55
	4.20
	4.18
	4.18
	4.01
Average	4.28
SD	0.25
RSD %	5.84

Table 3. 10. Results from accuracy assay of three concentrations of meropenem. Data are mean ± SD, N=3.

Meropenem concentration (μg/ml)	Recovered meropenem concentration (μg/ml)	% Recovery	% RSD
4	4.12	103.1	2.33
8	8.04	100.5	0.31
16	16.05	100.3	0.49

3.7. *In vitro* drug release study of ME-NLCs

As can be observed from the drug release profile (figure 3.17.) the ME-NLCs when in a controlled environment of 37 °C, 30% of the drug was released in the first thirty minutes which could be due to the burst release from the meropenem present on the surface of NLCs. This was followed by a sustained release with 70% of the drug being released at eight hours. The sample withdrawn at twenty-four hours showed that only 30% of meropenem was present. This could be due to the degradation of meropenem in the buffer at 37°C . To understand the degradation profile of meropenem, degradation studies were carried out at 37 °C . It can be seen in figure 3.18 that meropenem degrades over the period of time in aqueous environment. The results from on the day of preparation to twenty-four hours is significant as the p-value is less than 0.05. Similarly, the results between twenty-four hours to forty-eight hours and the results for forty-eight hours and seven days are also significant as the p-value is less than 0.05. Furthermore, when comparing the results of the day of preparation to seven days is also statistically significant as the p-value is less than 0.05.

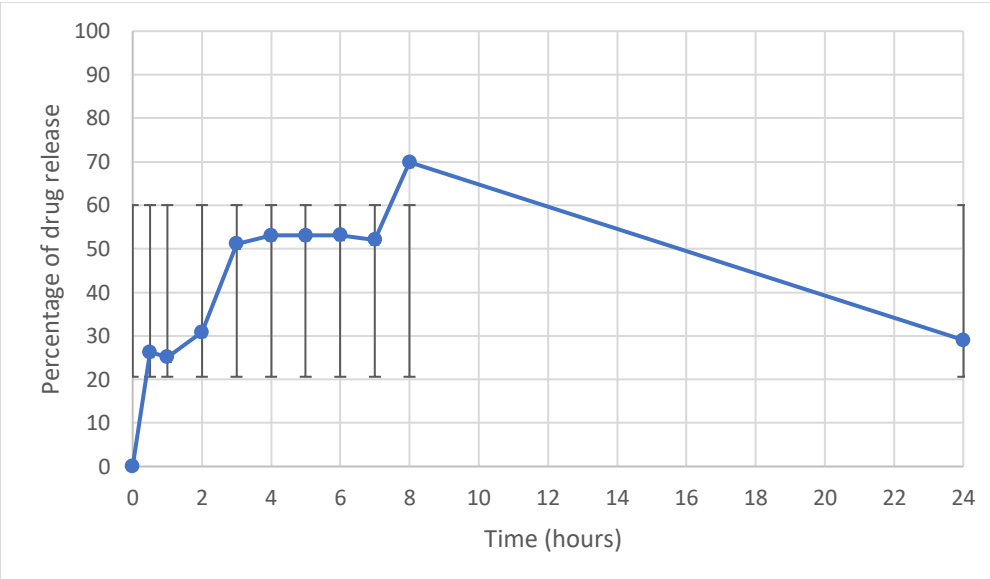

Figure 3. 17. *In vitro* drug release study ME-NLC vs. time, conducted at 37 °C in pH 6.8 dissolution media for 24 hours. N=3

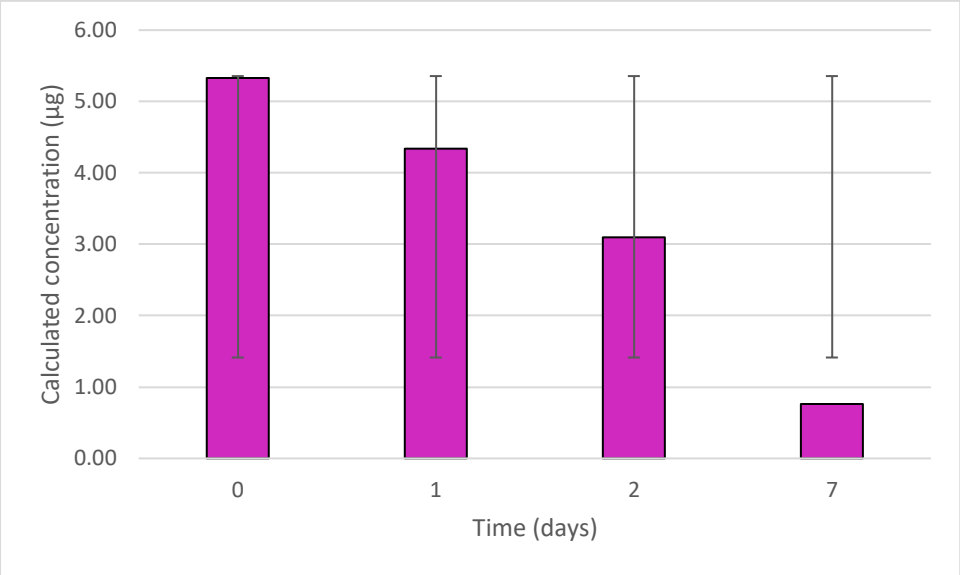

Figure 3. 18. Degradation of meropenem (5µg/ml) in aqueous solution at 37°C over seven days. N=3. ***** $p < 0.05$, refers to a significant difference when the calculated concentration on the day of preparation and after seven days were compared.

3.8.1. Bacterial characterisation of *Pseudomonas aeruginosa*

The antibiogram analysis of six reference strains of *P. aeruginosa* showed that all test strains were not susceptible to the antibiotics trimethoprim (5µg), ampicillin (10µg), and vancomycin(30µg). All strains were susceptible to ceftazidime (10µg), tetracycline (30µg), gentamicin (10µg), and meropenem (10µg)(Table 3.11). All strains of *P. aeruginosa* were positive in the biochemical tests oxidase and catalase . The pigment production for all strains of *P. aeruginosa* on CLED agar was blue/green indicating the presence of the pigment pyocyanin. Additionally, none of the *P. aeruginosa* strains fermented lactose on CLED agar.

Screening of the reference strains resulted in the selection of the meropenem susceptible strain, *Pseudomonas aeruginosa* ATCC 27853. Pseudomonas aeruginosa ATCC 27853 was selected for testing with ME-NLC because it is the EUCAST quality control strain and could be considered representative as it was shown to share many common characteristics with other *P. aeruginosa* reference isolates (Figure 3.19).

The growth curve for ATCC 27853 over a 24-hour period showed a lag phase of approximately 5 hours after which the bacteria entered the log phase and remained in log phase for the rest of the investigation (Figure 3.20).

Table 3. 11. Table to show results of disc diffusion to antibiotic susceptibility testing of six strains of *Pseudomonas aeruginosa*.

	Zone of inhibition of individual strains (mm)					
Antibiotic	NCIMB 10848	**ATCC 27853	NCIMB 10548	NCIMB 8295	NCTC 10662	NCIMB 11835
(W)5mg Trimethoprim	No Zone	No Zone	No Zone	No Zone	No Zone	No Zone
(AMP)10mg Ampicillin	No Zone	No Zone	No Zone	No Zone	No Zone	No Zone
(CAZ)10mg Ceftazidime	25	25	26	25	27	25
(TE)30 μg Tetracycline	9	12.5	9	9	11	12
(CN)10μg Gentamicin	21	19	19	18	17	19
(CIP) 5μg Ciprofloxacin	35	32	36	33	30	34
(VA) 30μg Vancomycin	No Zone	No Zone	No Zone	No Zone	No Zone	No Zone
(ME)10μg Meropenem	40	36.5	37	34	25	33

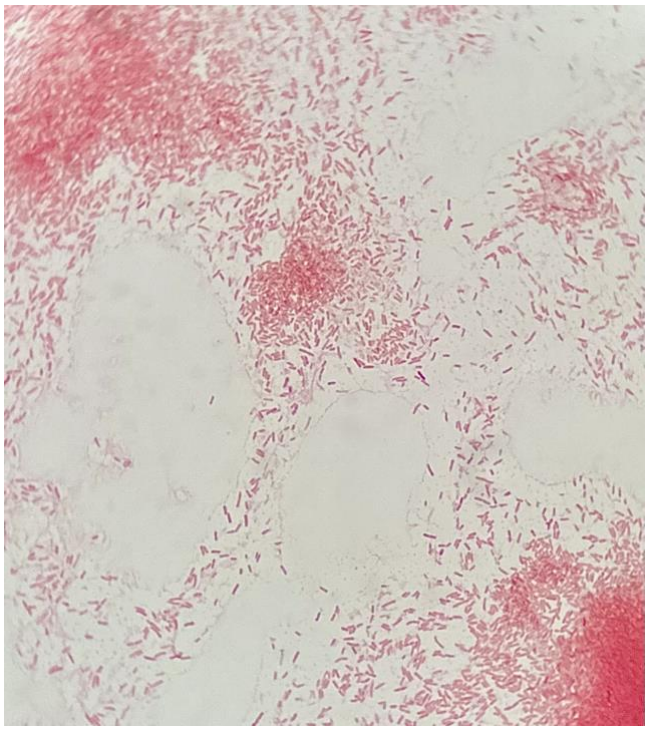

Figure 3. 19. Gram stain of *P. aeruginosa* ATCC 27853

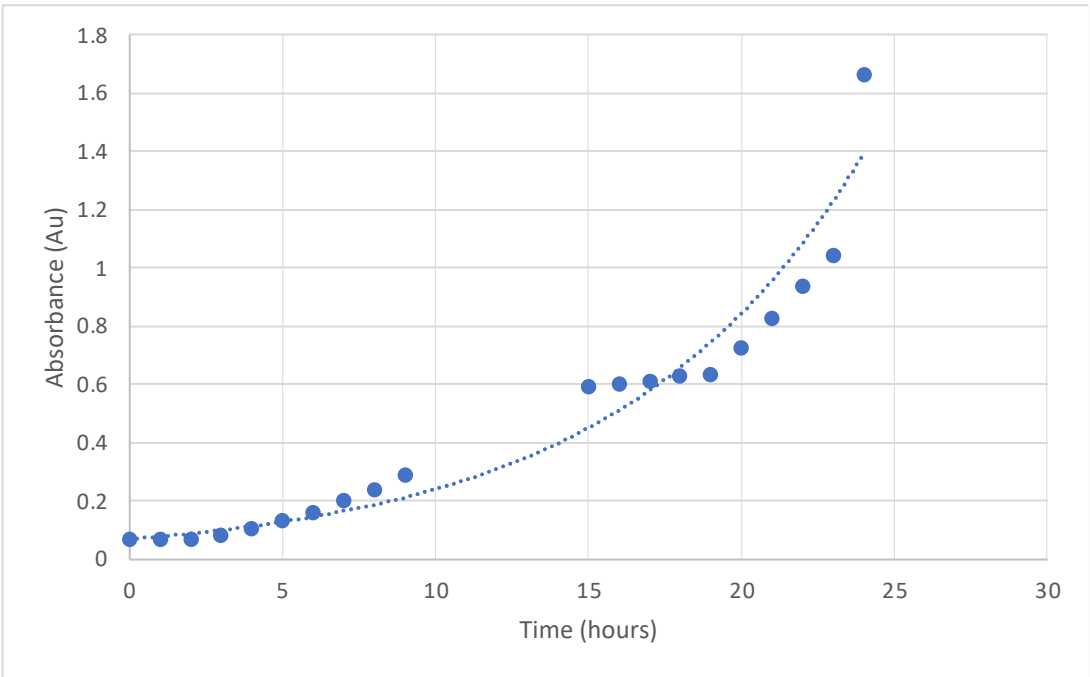

Figure 3. 20. Growth curve for *P. aeruginosa* ATCC 27853 taken over 24 hours with 1 hour time intervals. N= 3.

3.8.2. Minimum inhibitory concentration and Minimum bactericidal concentration of *Pseudomonas aeruginosa*

There was no antimicrobial effect observed with blank NLCs on *Pseudomonas aeruginosa* strain ATCC 27853.

The MIC value for *P. aeruginosa* ATCC 27853 with meropenem was 0.5 μg/ml and the MBC value was 4μg/ml. However, when the meropenem was encapsulated into a NLCs the MIC values were 2 μg/ml and MBC value of 8 μg/ml (Table 3.12).

3.8.3 Kill time assay

Kill time analysis showed that when a healthy culture of *P. aeruginosa* ATCC 27853 was challenged with a concentration of meropenem that was sixteen times (32μg/ml) greater than that of the MBC value, the time required for complete bactericidal effect was approximately two hours. When challenged with a concentration between the MIC and MBC of meropenem (1 μg/ml), growth was inhibited for two hours before the bacteria continued to a level of growth equivalent to that of the growth control. After seven hours of treatment with ME-NLCs below the MBC level (1 μg/ml) the organisms recovered , and the viable count was equivalent to that of the growth control.(Figure 3.21).

Table 3. 12. MIC and MBC values for *P. aeruginosa* ATCC 27853 when treated with meropenem, blank NLCs and ME-NLCs. N=3.

Compound	MIC value (μg/ml)	MBC value (μg /ml)
Meropenem	0.5	4
Blank NLC	-	-
Meropenem loaded ME-NLCs	2	8

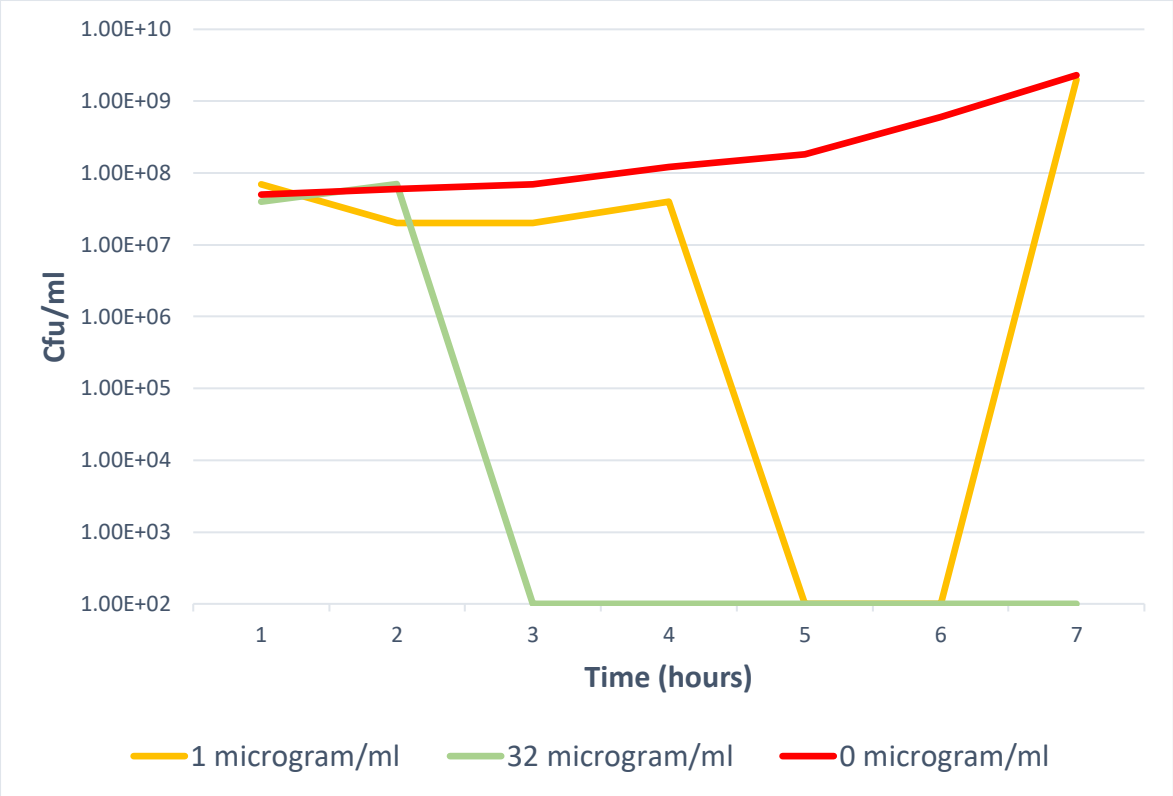

Figure 3. 21. . Kill time assay for *P. aeruginosa* ATCC27853 at two concentrations of meropenem. N=3.

3.9. Fluorescence microscopy of *Pseudomonas aeruginosa* ATCC 27853 after treatment with ME-NLCs

A

B

C

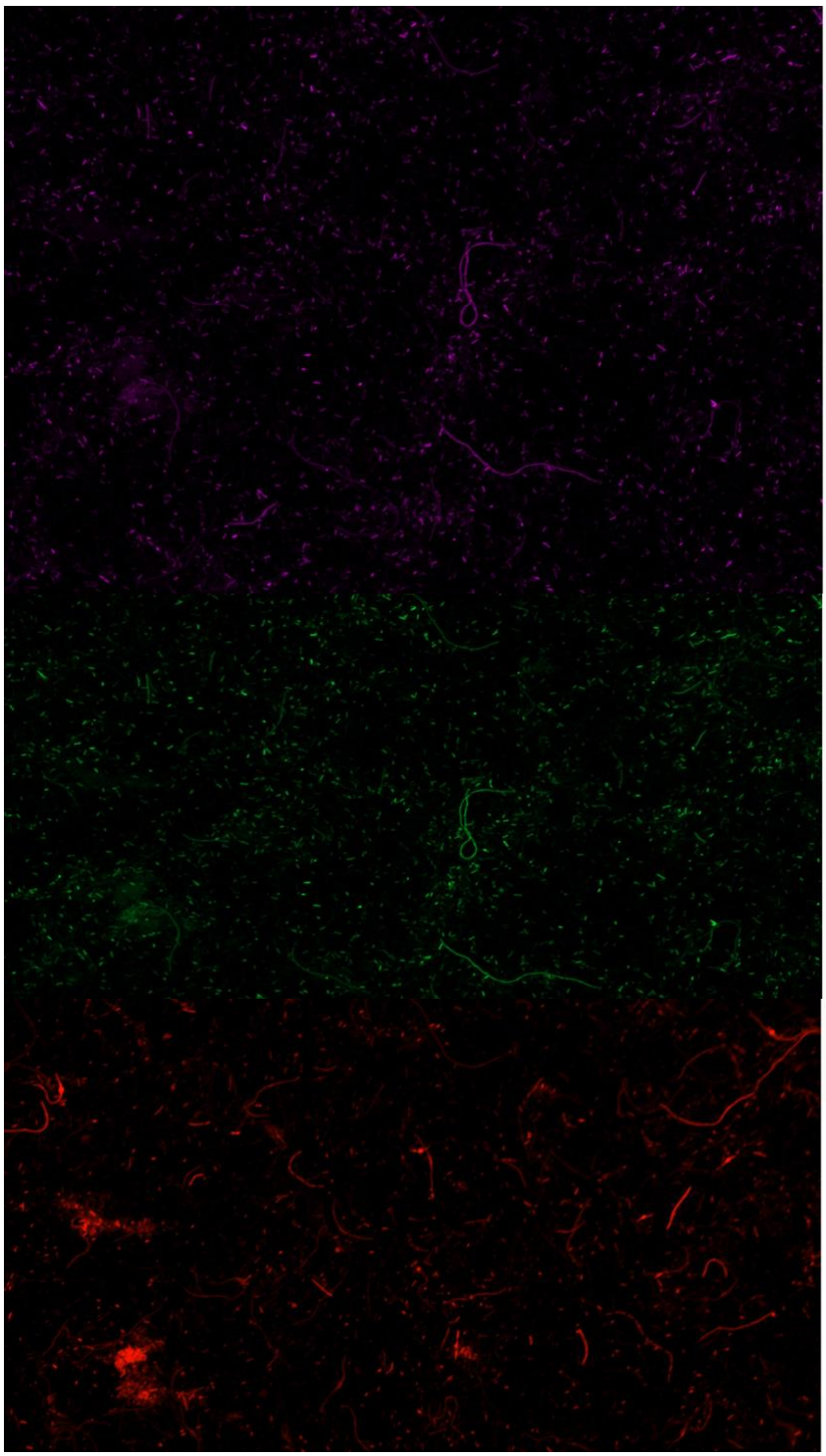

Figure 3. 22. *P. aeruginosa* after treatment of 1µg/ml ME-NLCs for 17 hours. Rhodamine (A) Live (B) Dead (C)

A

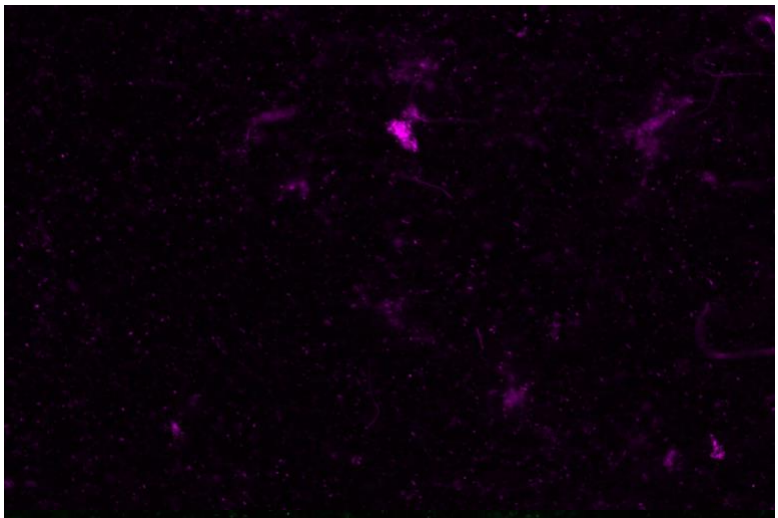

B

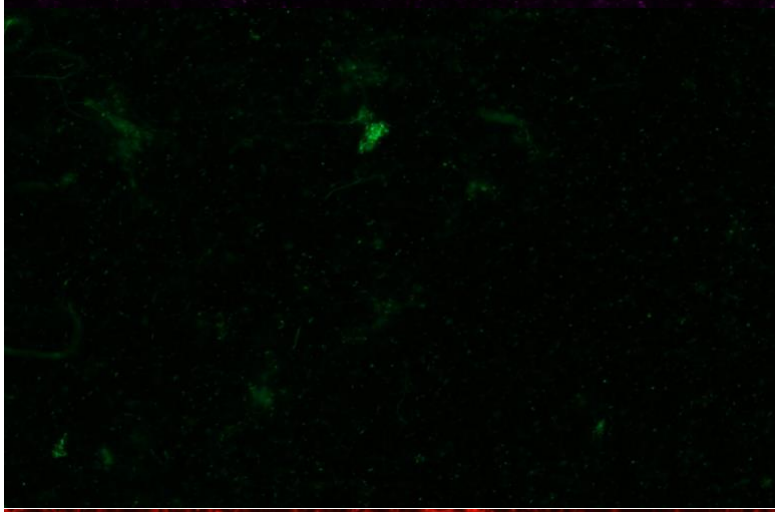

C

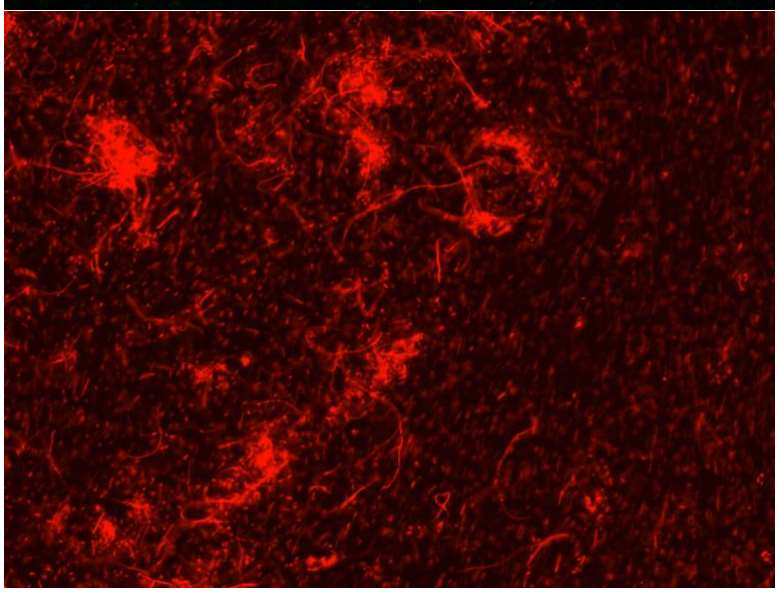

Figure 3. 23. *P. aeruginosa* after treatment of 1μg/ml ME-NLCs for 24 hours. Rhodamine (A) Live (B) Dead (C)

Fluorescence microscopy of *P. aeruginosa* using the BacLight (Thermo-fisher Scientific, Altrincham, UK) live/dead assay after treatment with ME-NLCs for 17 hours shows a change in morphology from short individual rod-shaped bacteria to a mixed population including elongated rod-shaped cells, with an estimated 1% being elongated (Figure 3.22 C). The sample from twenty-four hours presented with an estimated 5-10% of cells being abnormal in morphology (Figure 3.23 C)

Similarly, compared to the seventeen hours sample, the 24 hour sample shows an increase in the visible intensity of the fluorescence from figure 3.22 compared to figure 3.23 suggesting further loss of viability of the bacteria.

3.10. Bacterial studies of the stability of ME-NLCs

Table 3. 13. MIC and MBC values for *P. aeruginosa* ATCC 27853 when treated with ME-NLCs that had been stored at 20 °C (A), 37 °C (B)

A

Compounds	Compounds kept at 20° C					
	0hrs		24hrs		48hrs	
	MIC value (μg/ml)	MBC Value (μg/ml)	MIC value (μg/ml)	MBC Value (μg/ml)	MIC value (μg/ml)	MBC Value (μg/ml)
Meropenem	0.5	4	1	16	2	16
ME-NLCs	2	8	2	2	1	8

B

Compounds	Compounds kept at 37° C					
	0hrs		24hrs		48hrs	
	MIC value (μg/ml)	MBC Value (μg/ml)	MIC value (μg/ml)	MBC Value (μg/ml)	MIC value (μg/ml)	MBC Value (μg/ml)
Meropenem	0.5	4	1	4	2	4
ME-NLCs	2	8	2	8	2	4

The stability of ME-NLCs and meropenem was also investigated by MIC and MBC (Table 3.13 A &B)

The MIC value for *P. aeruginosa* ATCC 27853 when treated with meropenem on the day of preparation was 0.5μg /ml and the MBC value was 4μg /ml.

However, when the meropenem stored at 20 °C the MIC value increases after twenty-four hours. After forty-eight hours the MIC value also increases. Similar to this the MBC value increases after twenty-four hours but remains the same for forty-eight hours (Table 3.13 A).

The meropenem stored at 37 °C followed the same trend, with the MIC increasing after twenty-four hours and again after forty-eight hours. But the MBC values however remained the same over the investigation period (Table 3.13 B).

The MIC value for *P. aeruginosa* when treated with ME-NLCs (which were prepared on the day of testing) was 2μg/ml and the MBC value was 8μg /ml. However, when the ME-NLCs were stored at 20 °C the MIC value remained the same after twenty-four hours but decreased lower than the MIC value after forty-eight hours. The MBC value also decreased after twenty-four hours and then increased to the initial MBC after forty-eight hours, therefore suggesting that the results from the ME-NLCs samples at twenty-four hours may be outliers (Table 3.13 A).

Additionally, the ME-NLCs stored at 37 °C did not follow the same trend for the as the ME-NLCs stored at 20 °C. The MIC value remained the same for whole time period of the investigation (Table 3.13 B).

But the MBC values remained the same after twenty-four hours and then decreased lower than the MBC value.

These results suggest that due to the result of the ME-NLCs at both temperatures remaining the same as the MIC value and the MIC value increasing for meropenem the overall stability of ME-NLCs is greater than that of meropenem.

Chapter 4: Discussion

4.1. NLC optimisation and characterisation

The increase in antibiotic resistance poses a significant challenge to the treatment of bacterial infections. The increased use of antibiotics is selecting for antibiotic resistance in bacteria. This is particularly important in immunocompromised individuals, for example a *P. aeruginosa* infection in an individual with cystic fibrosis, can result in an infection with antibiotic resistant bacteria which could be life threatening. The present research aimed to develop and evaluate meropenem-encapsulated nanostructured lipid carriers (ME-NLCs) as an alternative drug delivery method for treatment of sensitive strains of *P. aeruginosa.*

The drug encapsulation capacity of the NLCs is directly impacted by the solubility of the drug in the lipid matrix (Elkateb, Cauldbeck *et al.,* 2023) , therefore liquid lipids with higher solubility for meropenem were selected to achieve the maximum encapsulation. However, the solubility of meropenem in liquid lipids has not previously been described . Solubility studies of meropenem confirmed that the liquid lipids Capryol 90 and solubiliser Kolliphor HS15 were appropriate for drug encapsulation, due to the non-ionic properties of the solubiliser Kolliphor HS15, which allows for the formation of the micelles that provide encapsulation for hydrophilic drugs including meropenem (Hou, Zhang *et al.,* 2019). Transcutol did not solubilise meropenem. A possible explanation for this might be because the solubility of meropenem in ethanol is <1mg/ml and Transcutol (2-(2-Ethoxyethoxy) ethanol) has properties similar to ethanol.

An ME-NLCs formulation was optimised by changing the product and process parameters (surfactant, solubilizer concentration and sonication time) on the critical quality attributes, In

order to produce NLCs with the desired particle size, poly dispersion index, zeta potential and entrapment efficiency.

The ideal size for a nanostructured lipid carrier has a large range of 50-1000nm (Mukherjee, Ray and Thakur, 2009). However, a smaller particle size is preferred as this increases the surface area to volume ratio, resulting in a higher cellular uptake and interaction (Yagublu, Karimova *et al.,* 2022). The PDI is an indication of the distribution range of particle size of the NLCs population in the formulation. Therefore, a lower PDI is required as it indicates a uniform distribution of the particles, this is also supported by research conducted by Danaei *et al.,* (2018). In addition, the zeta potential is also a significant physical characterisation test as it indicates the stability of the formulation in suspension. The parameters which indicate stability is particles that are more positive than 30mV or more negative than -30mv (Malvern Company, 2018). If the particles exhibit low zeta potential e.g., -2mV or 7mV it would suggest low electrostatic repulsion leading to the aggregation of particles (Uskoković, Castiglione *et al.,* 2010).

NLCs incorporate surfactants to maintain colloidal repulsion between other NLCs particles. The ME-NLCs in this study incorporated sodium cholate as the aqueous surfactant. The self-assembly properties of the cholate ions aid the stability of the aqueous dispersion (Liu 2007). Increasing sodium cholate concentration from 100-250mg was found to increase particle size The trend has also been observed in a study by Talele, Sahu *et al.,* (2018) on the physicochemical characterization of solid lipid nanoparticles using sodium cholate. Similarly, Lipoid S 75 has been suggested to decrease particle size when used as a lipid surfactant (Upadhyay *et al.,* 2012). Kolliphor HS 15 was selected as a solubiliser to aid the generation of thermodynamically stable NLCs with enhanced bioavailability and increased absorption abilities (Chaudhuri, Kumar *et al.,* 2022). The liquid lipid Capryol 90 was selected

due to the data showing an increase in thermodynamic stability (Ukai *et al.,* 2020). In this thesis the increase of Capryol 90 showed a desirable decrease in particle size and a decrease in zeta potential, indicating increase in stability. This is due to the lipid's miscibility with solid lipids and the ability to increase the efficacy of encapsulated drug entrapment within the NLCs (Ukai *et al.,* 2020).

Dynasan 114 was selected as the solid lipid component as it allows for higher bioavailability of the conjugated drug (Olbrich, Kayser and Müller, 2002). Additionally, oleic acid was added to the formulation to increase the drug loading of meropenem. The ME-NLCs encapsulation increased from 40% without oleic acid to 85.72% after incorporation (Table 3.7). This trend was also observed by Patel (2012) where the drug encapsulation of aceclofenac increased by 8.2% from 69.3% to 77.5%.

The encapsulation of meropenem in NLCs, increases both the particle size and PDI with the blank NLC having an average size of 165.9nm and the ME-NLCs having an average size of 178.8nm. Similarly, the incorporation of meropenem also did not appear to increase poly dispersion index because the blank NLCs had a PDI of 0.281 and ME-NLCs had a PDI of 0.283. This minimal increase is likely due to more particles being present in the suspension, disrupting uniform dispersion. These results reflect those of (Elkateb, Cauldbeck *et al.,* 2023) who also found that drug loading of HIV drugs darunavir and ritonavir increased particle size and PDI in NLCs.

FTIR results for meropenem showed a spectrum with four peaks (Figure 3.9 A). The peaks produced mirrored those published by Muneer, Wang *et al.,* (2020). However, the spectra produced by Muneer, Wang *et al.,* 2020 also had more peaks. The differences could be as a result of the physical state in which samples were tested. Muneer, Wang *et al.,* (2020) tested

meropenem in a powdered state compared to this investigation testing in aqueous suspension.

FTIR showed that meropenem had been encapsulated due to the disappearance of the meropenem fingerprint within the ME-NLCs absorbance spectra (Figure 3.9 B). This data has not been previously described.

DSC data suggested that the meropenem had been encapsulated into the amorphous state of the NLCs due to the absence of the broad endothermic peak at approximately 137.5 °C (Figure 3.10 A). The DSC data for the meropenem peak was confirmed to be meropenem due to the consistency of the result with that of the research conducted by Zhou, Du *et al.,* 2017 who showed that meropenem trihydrate produces an endothermic peak at 130 °C.

4.2. Optimisation and validation of HPLC for detection of meropenem

An isocratic method was developed for this study, as the meropenem was solubilised in an aqueous solution. Preliminary studies were carried out based on previous findings of suitable chromatographic conditions for the quantification of meropenem. The quantification of meropenem by HPLC is done using gradient methods. An explanation for this, is that quantification of meropenem is typically conducted from serum or plasma samples, such as the work conducted by Dincel, Sagirli *et al.,* 2020. Previous investigations showed various solvents and concentrations being used for the mobile phase, for example Mendez, Steppe *et al.,* (2003) investigated the use of monobasic phosphate buffer and acetonitrile (90:10; v/v), adjusted to pH 3.0 with orthophosphoric acid, for the quantification of meropenem in a pharmaceutical dosage form. However, in this study the mobile phase used was

orthophosphate buffer and methanol (84; 16v/v), adjusted to pH 2.7 with orthophosphoric acid due to the solubility of meropenem in potassium phosphate solution being 5% (Kamalinder Singh, personal communication, 2023).

Investigations into appropriate wavelength for peak area of meropenem detection found that 308nm gave the best detection, although previously described results (Milla, Ferrari *et al.,* 2020) suggest that 298nm was the optimum wavelength. Investigations showed that there was an increase of 16.4% in detection when using 308nm compared to 298nm.

The method was then validated for linearity using a standard concentration range from 2-20μg/ml, which demonstrated a linearity of R^2 = 0.994. This linearity was considered acceptable according to ICH guidelines (European Medicines Agency, 1995) which stipulates a R^2 value close to 1 is desired.

The repeatability assay produced a %RSD of 3.97, although the ICH guidelines (European Medicines Agency, 1995) suggest a % RSD ≤ 1%. Additionally, the precision assay provided a %RSD ranging from 1.48-6.23, which is greater than the ICH accepted range of % RSD ≤ 2 (European Medicines Agency, 1995). The accuracy assay however provided a %RSD of 1.48-6.23 which was acceptable compared to the ICH guidelines of 100 ± 2 % (European Medicines Agency, 1995). So, the method developed was appropriate for accurate quantification of meropenem in NLCs.

4.3 Encapsulation Efficiency of ME-NLCs

Encapsulation efficiency was calculated from the total drug in the ME-NLCs minus the free drug detected in aqueous phase after separation from the ME-NLC by filtration. Using the

calibrated HPLC method, the concentration of meropenem in the free drug was calculated and subtracted from the total added showing a calculated encapsulation efficiency of approximately 85.72%. The high encapsulation is a direct consequence of the drug solubility in the lipid matrix of the NLCs. This trend can also be seen in the study conducted by Zoubari, Staufenbiel *et al.,* (2017), who found that the highest encapsulation of diclofenac sodium was directly linked to the liquid lipid's affinity to the drug.

4.4.Validation of HPLC for detection of meropenem in pH6.8 orthophosphate buffer for *in vitro* drug release

A new isocratic method was developed for this study, as the meropenem was solubilised in an aqueous solution and based on the previously optimised chromatographic conditions in chapter 3.5.1.1-3.5.1.2. The method was then validated for linearity using a range standard concentration from 2-20μg/ml, which demonstrated a linearity of $R^2 = 0.9994$. This linearity was considered acceptable according to ICH guidelines which stipulates a R^2 value close to 1 is desired (European Medicines Agency, 1995) .

The repeatability assay produced a %RSD of 5.84, although the ICH guidelines suggest a % RSD ≤ 1% (European Medicines Agency, 1995) . The accuracy assay however provided a %RSD of 0.31-2.33 which was acceptable compared to the ICH guidelines of 100 ± 2 % (European Medicines Agency, 1995) .

4.5. *In vitro* drug release study

The ME-NLCs drug release studies at 37 °C, revealed that 30% of the drug was released in the first thirty minutes, which could be due to the burst release of the drug present on the surface of NLCs. Burst release was followed by a sustained release with 70% of the drug being released within eight hours. This is possibly due to the fast diffusion of meropenem molecules along the high concentration gradient. It has also been suggested that the initial fast release is caused by the presence of free drug on the surface of the NLC (Khan, Baboota *et al.,* 2015), whereas the sustained release is caused by the leaching of drug from the lipid matrix (Khan, Baboota *et al.,* 2015).

These results reflect those of Almousallam (2015) who also found that release studies of NLCs encapsulating dacarbazine have an initial fast release of 48.18% for the first two hours, followed by a sustained release.

4.6.1. Stability of ME-NLCs

Since a potential use for ME-NLCs is for the treatment of *P. aeruginosa* in cystic fibrosis patients, with the administration by nebuliser or intravenously it was important to study the colloidal stability of the ME-NLCs (Zwain, Alder *et al.,* 2021). The stability of the ME-NLCs is indicated by the change in particle size, and PDI.

The ME-NLCs when stored at 20 °C presents in an increase in particle size to 185nm (3.7%) after 24 hours of storage. The particle size then decreased to 179.3nm after forty-eight hours but remained in the optimal range <200nm. The PDI also decreased within the first twenty-

four hours by 2.4% but remained within the optimal range.< 0.3 The PDI then increase to over the optimal value after forty-eight hours. The zeta potential increase from the time of preparation from -31mV to -39.9mV. The zeta potential decreased to -30.3mV after forty-eight hours but remained optimal. This suggests the nanoparticles are stable for the first twenty-four hours at 20 °C.

The ME-NLCs stored at 37 °C, presented in an increase of average particle size from 178.8nm on the day of preparation to 187nm after 24 hours and increased again by 2.6nm (189.6nm) after forty-eight hours. but remained in the optimum value of <200nm. The PDI decreased within the first twenty-four hours from 0.283 on the day of preparation to 0.273. The PDI then increased from 0.276 to 0.29 after forty-eight hours but remained within the optimal range. The zeta potential increased from -31mV to -41mV and then decreased again to -36.3mV at forty-eight hours.

This suggests that the storage temperature did not affect the stability of the nanoparticles and that they are stable for the first twenty-four hours and subsequently may be used for treatment *in vitro* within this time period. The decrease in stability after 48 hours can be associated with particle aggregation, which led to an increase in the poly dispersity index of the formulation. The decrease in stability could also be due to the leaching of the entrapped drug from the NLCs as research by Khosa, Reddi and Saha, (2018) suggests that high drug encapsulation if beneficial to stability. The zeta potential of the nanoparticles also indicates the stability of the NLCs as the surface charge of the nanoparticle prevents aggregation.

4.6.2 Lyophilisation of ME-NLCs

Lyophilisation of the formulations with a cryoprotectant generally results in better long-term stability. Results from an investigation by Khan (2019) into the lyophilisation of Lopinavir-Loaded Nanostructured Lipid Carriers showed that trehalose was the most effective cryoprotectant. Additionally, Khan (2019) found that the use of sucrose as a cryoprotectant resulted with particle size and PDI increasing above the optimal range set in the investigation of particle size ≤ 150 nm, PDI ≤ 0.54 and ZP > −30 mV.

Findings from results presented in this thesis align with this latter trend because the particle size and PDI increased after lyophilisation using sucrose as a cryoprotectant (Figure 3.8). At a concentration of 5% the particle size increased by 46.6%, PDI by 73.1% and ZP by 30.3%. The concentration of 7% resulted in an increase of 67.5% in particle size, 128.6% PDI and 30.3% ZP. Furthermore 10% showed an increase of 78.3% in particle size, 61.1% PDI and 29.4%. Therefore, the concentrations of sucrose tested for lyophilisation was not an effective cryoprotectant for ME-NLCs but other cryoprotectants such as trehalose may be more effective.

4.7. Bacterial studies of the efficacy of ME-NLCs

Bacterial studies were aimed at evaluating the potential use of ME-NLCs as an antimicrobial treatment for *P. aeruginosa* infections.

Six reference strains of *Pseudomonas aeruginosa* were characterised by the EUCAST disc diffusion breakpoint method and all were found to be susceptible to ceftazidime, tetracycline,

gentamicin, ciprofloxacin and most importantly meropenem. These strains were also found to be resistant to trimethoprim, ampicillin and vancomycin.

The strain selected for evaluating the antimicrobial properties of the ME-NLCs was a EUCAST quality control reference strain of *Pseudomonas aeruginosa* (ATCC 27583). This allowed for comparison of MIC values for free drug and ME-NLCs.

For enumeration, the strain used was cultured using an adapted Miles, Misra method (Miles, *et al.,* 1938) in order to allow 10µl spots of serial dilutions for estimating total viable count. CLED agar was used to restrict the colony sizes for accurate counting. When cultured on Nutrient or Mueller Hinton agar the organism produced flat slightly spreading colonies. This limited the number of colonies that could be counted in each 10µl spot. Additionally, when cultured on CLED agar the cultures produce isolated non-lactose fermenting colonies with a blue pigment due to the presence of pyocyanin. When the blank NLCs was used as a treatment for *P. aeruginosa* no antimicrobial effect was observed, therefore showing no antimicrobial properties of the excipients in the NLCs, and thus no synergistic antimicrobial effect is present. Alalaiwe (2018) also found that using blank NLCs do not have an antimicrobial effect on methicillin sensitive or resistant strains of *Staphylococcus aureus*. The MIC value for *P. aeruginosa* ATCC 27853 when treated with meropenem was 0.5 µg/ml and the MBC value was 4µg/ml. This finding is consistent with that of (EUCAST 2023) which reports that the MIC for *P. aeruginosa* ATCC 27853 treated with meropenem is within the range of 0.25-0.5µg/ml.

However, when the meropenem was encapsulated into a NLCs the MIC value increased to 2µg/ml and MBC value was 8µg/ml. Alalaiwe (2018) found that when encapsulating oxacillin into an NLCs, there was an increase in MBC value with methicillin sensitive strain of *Staphylococcus aureus* but a decrease of MBC value when treating a methicillin resistant

strain of *Staphylococcus aureus*. A possible contribution to the decrease in efficacy is that due to the negative surface charge of the ME-NLCs and the overall negative charge of the *P. aeruginosa* bacteria, there might be fewer interactions between ME-NLCs and the test organisms. Tang, Ashcroft *et al.,* (2007) noted that negatively charged bacteria *Escherichia coli* had a greater affinity to nanoparticles with a positive surface charge.

The fluorescence microscopy analysis showed that the ME-NLCs had an antimicrobial effect via the increase of fluorescence intensity of the dead bacteria. The fluorescence microscopy showed an increase of elongated cells from approximately 1% at the 17 hour sample to approximately 5-10% at the 24 hour sample. It has been suggested that after treatment of beta-lactam antibiotics that *P. aeruginosa* makes a morphological change from rod shaped cells to coccus cells (Monahan, Turnbull *et al.,* 2014).This does not appear to be the case. However, this result has been described for other rod-shaped Gram negative bacterium including *E. coli* which shows an increase in surface area to volume ratio when treated with antibiotics that act on the cell wall such as meropenem (Ojkic, Serbanescu *et al.,* 2022).

The efficacy of the ME-NLCs after storage was investigated and it was found that over forty eight hours stored at 20° C the MIC values increased, and the MBC value remained the same. The ME-NLCs stored at 37° C showed that the MIC value remained the same for whole time period of the investigation, but the MBC values remained the same after twenty-four hours and then decreased lower than the MBC value. Therefore, ME-NLCs still have antimicrobial effect after storage of forty-eight hours at both temperatures.

However, this result has not previously been investigated.

Additionally, the kill time curve and release studies also show that the ME-NLCs is relatively fast acting because the in vitro drug release study showed that 30% of the drug was released after the first thirty minutes and levels stay above the MBC value for up to twenty-four hours which could benefit the clinical use of ME-NLCs by increasing time periods between dosages as meropenem is administered every eight hours and is excreted with 70% unchanged.

4.8. Limitations

Limitations to the investigations should be mentioned. In the NLCs preparation the parameters were changed individually while keeping the other parameters the same and therefore inter-variable relationships were not investigated. The degradation of meropenem in aqueous solutions was also a limitation to the overall investigation and but could be investigated in future work to increase stability. An assumption made in the study was that ME-NLCs would have the same effect *in vivo* as that within *in vitro*. This could be investigated in future. Additionally, the release study conducted in an orthophosphate buffer where in further work the investigation would be conducted in a matrix more comparable to blood plasma to inform on the stability and efficacy of the meropenem encapsulated for in vivo studies. Another aspect for consideration is that *P. aeruginosa* colonises the CF lung forming a biofilm whereas this study used organisms in logarithmic phase of growth in broth and therefore the application could be completely different as this was an investigation into the study of NLCs and planktonic bacteria. Further investigation into a wider range of susceptible strains of *P. aeruginosa* may also highlight if the results found in this investigation are repeatable or strain specific as this would benefit the future application of the ME-NLCs. Furthermore, another direction of research for future investigations could be the evaluation

of ME-NLCs for the treatment of meropenem-resistant strains of *P. aeruginosa* to see if the results are consistent with data obtain by Alalaiwe (2018). Alternatively further research could investigate the efficacy of ME-NLCs on other meropenem sensitive bacteria which affect the cystic fibrosis lung, such as Gram positive bacterium *Staphylococcus aureus* or Gram negative bacterium *Burkholderia cepacia* complex.

4.9 Future work

The investigations of the antimicrobial effect of ME-NLC on meropenem sensitive and resistant strains of *P. aeruginosa* could give allow for greater knowledge of mechanism of action of the NLCs. Future investigations for ME-NLCs include the effect on *P. aeruginosa* biofilms and investigations into the efficacy as an antimicrobial treatment against meropenem-resistant strains of *P. aeruginosa* to increase knowledge for application *in vivo*. Additionally, the visualisation of the interactions between ME-NLCs and bacterial cell wall using scanning and transmission electron microscopy to provide insight into possible adaptations for treatment of resistant strains of bacteria.

ME-NLCs could be further optimised by altering the surface for specific binding to the bacterial cell wall using regulatory proteins. Also, the nebulisation of ME-NLCs could allow for testing of bacterial infections of lung cells to further the application for treatment of bacterial infections of the CF lung.

Chapter 5: Conclusion

5. Conclusion

The increase in antibiotic resistance continues to present an obstacle for the treatment of bacterial infections especially for those who are immunocompromised. Research for a drug delivery strategy to optimise the use of existing antibiotics should continue. In this study, a novel approach of encapsulating the hydrophilic antibiotic meropenem in a nanostructured lipid carrier is described. The meropenem nanostructured lipid carriers (ME-NLCs) produced were within the optimum values for each product parameter. The ME-NLCs exhibited a low particle size (178.8nm), polydispersion index (0.283) and a zeta potential of -31mV . The drug encapsulation was calculated at 85.72%. The effect of the ME-NLCs was investigated in Mueller-Hinton media and found that ME-NLCs inhibited the growth of *Pseudomonas aeruginosa* ATCC 27853 at a concentration of 2μg/ml. The ME-NLCs were bactericidal at a concentration of 8μg/ml. Meropenem was released from the ME-NLCs to achieve a concentration greater than the MBC value for a sustained period up to 24 hours. Meropenem showed an increased stability at ambient temperature when encapsulated in the nanostructured lipid carriers compared to aqueous solution.

Chapter 6: References

6. References

Abdelaziz, A.A., Kamer, A.M.A., Al-Monofy, K.B. and al-Madboly, L.A., 2023. Pseudomonas aeruginosa's greenish-blue pigment pyocyanin: its production and biological activities. *Microbial Cell Factories*, Jun 8, vol. 22, no. 1, pp. 110. Available from: https://www.ncbi.nlm.nih.gov/pubmed/37291560 MEDLINE. ISSN 1475-2859. DOI 10.1186/s12934-023-02122-1.

Aflakian, F., Mirzavi, f., Aiyelabegan, H.T., Soleimani, a., Gholizadeh Navashenaq, j., Karimi-Sani, I., Rafati Zomorodi, A. and Vakili-Ghartavol, r., 2023. Nanoparticles-based therapeutics for the management of bacterial infections: A special emphasis on FDA approved products and clinical trials. *European Journal of Pharmaceutical Sciences*, Sep 1, vol. 188, pp. 106515. Available from: https://dx.doi.org/10.1016/j.ejps.2023.106515 PubMed. ISSN 0928-0987. DOI 10.1016/j.ejps.2023.106515.

Ahmad, J., Akhter, S., Rizwanullah, M., Amin, S., Rahman, M., Ahmad, M.Z., Rizvi, M.A., Kamal, M.A. and ahmad, F.J., 2015a. Nanotechnology-based inhalation treatments for lung cancer: state of the art. *Nanotechnology*, Jan 1, vol. 8, no. default, pp. 55-66. Available from: https://www.ncbi.nlm.nih.gov/pubmed/26640374 PubMed. ISSN 1177-8903. DOI 10.2147/NSA.S49052.

Ahmadi, K., Hashemian, A.M., Pouryaghobi, S.M., Akhavan, R., Rozmina, S. and Bolvardi, e., 2016. Antibiotic Resistance Properties of Pseudomonas aeruginosa Isolated From Cases of Superficial Infections at the Emergency Unit. *Jundishapur Journal of Microbiology*, Jan 1, vol. 9, no. 1, pp. e27646. Available from: https://www.ncbi.nlm.nih.gov/pubmed/27833719 PubMed. ISSN 2008-3645. DOI 10.5812/jjm.27646.

Alalaiwe, A., Wang, P., Lu, P., Chen, y., fang, j. and yang, s., 2018. Synergistic Anti-MRSA Activity of Cationic Nanostructured Lipid Carriers in Combination With Oxacillin for Cutaneous Application. *Frontiers in Microbiology*, Jul 4, vol. 9, pp. 1493. Available from: https://www.ncbi.nlm.nih.gov/pubmed/30034381 PubMed. ISSN 1664-302X. DOI 10.3389/fmicb.2018.01493.

Ali, F., Reinert, L., Levêque, J., Duclaux, L., Muller, F., Saeed, S. and Shah, S.S., 2014. Effect of sonication conditions: Solvent, time, temperature and reactor type on the preparation of micron sized vermiculite particles. *Ultrasonics Sonochemistry*, May 1, vol. 21, no. 3, pp. 1002-1009. Available from: https://dx.doi.org/10.1016/j.ultsonch.2013.10.010 PubMed. ISSN 1350-4177. DOI 10.1016/j.ultsonch.2013.10.010.

Almousallam, M., Moia, C. and Zhu, h., 2015. Development of nanostructured lipid carrier for dacarbazine delivery. *International Nano Letters*, Dec 1, vol. 5, no. 4, pp. 241-248. Available from: https://link.springer.com/article/10.1007/s40089-015-0161-8 CrossRef. ISSN 2008-9295. DOI 10.1007/s40089-015-0161-8.

Ashikbayeva, Z., Tosi, D., Balmassov, D., Schena, E., Saccomandi, P. and Inglezakis, v., 2019. Application of Nanoparticles and Nanomaterials in Thermal Ablation Therapy of Cancer. *Nanomaterials*, Aug 24, vol. 9, no. 9, pp. 1195. Available from: https://www.ncbi.nlm.nih.gov/pubmed/31450616 PubMed. ISSN 2079-4991. DOI 10.3390/nano9091195.

Ashiru-Oredope, D., Cunningham, N., Casale, E., Muller-Pebody, B., Hope, R., Brown, C.S., Hopkins, S., Agnew, E., Ashiru-Oredope, D., Bou-Antoun, S., Casale, E., Cunningham, N., Demirjian, A., Gerver,

S.M., Guy, R.L., Hand, K., Hayes, C.V., Henderson, K.I., Hopkins, S., Lecky, D.M., Lochen, a., Mirfenderesky, M., Robotham, J., Squire, H. and Triggs-Hodge, c., 2023. Reporting England's progress towards the ambitions in the UK action plan for antimicrobial resistance: the English surveillance programme for antimicrobial utilisation and resistance (ESPAUR). *Journal of Antimicrobial Chemotherapy*, Aug 19. Available from: https://search.proquest.com/docview/2853944705 CrossRef. ISSN 0305-7453. DOI 10.1093/jac/dkad248.

Aziz, S.A.A.A., Mahmoud, R. and Mohamed, M.B.E.D., 2022. Control of biofilm-producing Pseudomonas aeruginosa isolated from dairy farm using Virokill silver nano-based disinfectant as an alternative approach. *Scientific Reports*, Jun 8, vol. 12, no. 1, pp. 9452. Available from: https://www.ncbi.nlm.nih.gov/pubmed/35676412 PubMed. ISSN 2045-2322. DOI 10.1038/s41598-022-13619-x.

Basak, S., Singh, P. and Rajurkar, M., 2016. Multidrug Resistant and Extensively Drug Resistant Bacteria: A Study. *Journal of Pathogens*, Jan 1, vol. 2016, pp. 4065603-5. Available from: https://dx.doi.org/10.1155/2016/4065603 PubMed. ISSN 2090-3057. DOI 10.1155/2016/4065603.

Bassetti, M., Vena, A., Croxatto, A., Righi, E. and Guery, B., 2018. How to manage Pseudomonas aeruginosa infections. *Drugs in Context*, vol. 7, pp. 212527-18. Available from: https://www.ncbi.nlm.nih.gov/pubmed/29872449PubMed. ISSN 1745-1981. DOI 10.7573/dic.212527.

Bush, K. and Bradford, P.A., 2016. β-Lactams and β-Lactamase Inhibitors: An Overview. *Cold Spring Harbor Perspectives in Medicine*, Aug 1, vol. 6, no. 8, pp. a025247. Available from: https://www.ncbi.nlm.nih.gov/pubmed/27329032 MEDLINE. ISSN 2157-1422. DOI 10.1101/cshperspect.a025247.

Castanheira, M., Simner, P.J. and Bradford, P.A., 2021. Extended-spectrum β-lactamases: an update on their characteristics, epidemiology and detection. *JAC-Antimicrobial Resistance*, Sep 1, vol. 3, no. 3, pp. dlab092. Available from: https://search.proquest.com/docview/2553819697 CrossRef. ISSN 2632-1823. DOI 10.1093/jacamr/dlab092.

Chaudhuri, A., Kumar, D.N., Shaik, R.A., Eid, B.G., Abdel-Naim, A.B., MD, S., Ahmad, A. and Agrawal, A.K., 2022. Lipid-Based Nanoparticles as a Pivotal Delivery Approach in Triple Negative Breast Cancer (TNBC) Therapy. *International Journal of Molecular Sciences*, Sep 3, vol. 23, no. 17, pp. 10068. Available from: https://search.proquest.com/docview/2711394652 CrossRef. ISSN 1422-0067. DOI 10.3390/ijms231710068.

Chen, W., Zhang, Y. and Davies, C., 2017. Penicillin-Binding Protein 3 Is Essential for Growth of Pseudomonas aeruginosa. *Antimicrobial Agents and Chemotherapy*, Jan 1, vol. 61, no. 1. Available from: https://www.ncbi.nlm.nih.gov/pubmed/27821444 MEDLINE. ISSN 0066-4804. DOI 10.1128/AAC.01651-16.

Cho, H., Uehara, T. and Bernhardt, T.G., 2014. Beta-lactam antibiotics induce a lethal malfunctioning of the bacterial cell wall synthesis machinery. *Cell*, Dec 4, vol. 159, no. 6, pp. 1300-1311 ISSN 1097-4172. DOI S0092-8674(14)01448-2 [pii].

Clunes, M.T. and Boucher, R.C., 2007. Cystic fibrosis: the mechanisms of pathogenesis of an inherited lung disorder. *Drug Discovery Today. Disease Mechanisms*, Jan 1, vol. 4, no. 2, pp. 63-72. Available from: https://dx.doi.org/10.1016/j.ddmec.2007.09.001 PubMed. ISSN 1740-6765. DOI 10.1016/j.ddmec.2007.09.001.

Dadgostar, P., 2019. Antimicrobial Resistance: Implications and Costs. *Infection and Drug Resistance*, 20191220, Dec 20, vol. 12, pp. 3903-3910 ISSN 1178-6973. DOI 10.2147/IDR.S234610.

Danaei, M., Dehghankhold, M., Ataei, S., Hasanzadeh Davarani, F., Javanmard, R., Dokhani, A., Khorasani, S. and Mozafari, M.R., 2018. Impact of Particle Size and Polydispersity Index on the Clinical Applications of Lipidic Nanocarrier Systems. *Pharmaceutics*, May 18, vol. 10, no. 2, pp. 57. Available from: https://www.ncbi.nlm.nih.gov/pubmed/29783687 PubMed. ISSN 1999-4923. DOI 10.3390/pharmaceutics10020057.

Delcour, A.H., 2009. Outer membrane permeability and antibiotic resistance. *Biochimica Et Biophysica Acta*, May 1, vol. 1794, no. 5, pp. 808-816. Available from: https://dx.doi.org/10.1016/j.bbapap.2008.11.005 MEDLINE. ISSN 1570-9639. DOI 10.1016/j.bbapap.2008.11.005.

Dhiman, N., AwasthI, R., Sharma, B., Kharkwal, H. and Kulkarni, G.T., 2021. Lipid Nanoparticles as Carriers for Bioactive Delivery. *Frontiers in Chemistry*, Apr 23, vol. 9, pp. 580118. Available from: https://www.ncbi.nlm.nih.gov/pubmed/33981670 PubMed. ISSN 2296-2646. DOI 10.3389/fchem.2021.580118.

Diggle, S.P. and Whiteley, M., 2020. Microbe Profile: Pseudomonas aeruginosa: opportunistic pathogen and lab rat. *Microbiology (Society for General Microbiology)*, Jan 1, vol. 166, no. 1, pp. 30-33. Available from: https://www.ncbi.nlm.nih.gov/pubmed/31597590 PubMed. ISSN 1350-0872. DOI 10.1099/mic.0.000860.

Dincel, D., Sagirli, O. and Topcu, G., 2020. A High-Performance Liquid Chromatographic Method for the Determination of Meropenem in Serum. *Journal of Chromatographic Science*, Jan 23, vol. 58, no. 2, pp. 144-150. Available from: https://www.ncbi.nlm.nih.gov/pubmed/31738410 MEDLINE. ISSN 0021-9665. DOI 10.1093/chromsci/bmz087.

Doi, Y., 2019. Treatment Options for Carbapenem-resistant Gram-negative Bacterial Infections. *Clinical Infectious Diseases : An Official Publication of the Infectious Diseases Society of America*, Nov 13, vol. 69, no. Suppl 7, pp. S565-S575 ISSN 1537-6591. DOI 10.1093/cid/ciz830.

Donaldson, S.H., Laube, B.L., Corcoran, T.E., Bhambhvani, P., Zeman, K., Ceppe, A., Zeitlin, P.L., Mogayzel, P.J.,Jr, Boyle, M., Locke, L.W., Myerburg, M.M., Pilewski, J.M., Flanagan, B., Rowe, S.M. and Bennett, W.D., 2018. Effect of ivacaftor on mucociliary clearance and clinical outcomes in cystic fibrosis patients with G551D-CFTR. *JCI Insight*, 20181220, Dec 20, vol. 3, no. 24, pp. e122695. doi: 10.1172/jci.insight.122695 ISSN 2379-3708. DOI 122695 [pii].

Döring, G., Flume, P., Heijerman, H. and Elborn, J.S., 2012. Treatment of lung infection in patients with cystic fibrosis: Current and future strategies. *Journal of Cystic Fibrosis*, vol. 11, no. 6, pp. 461-479. Available from: https://www.sciencedirect.com/science/article/pii/S1569199312001841 ISSN 1569-1993. DOI 10.1016/j.jcf.2012.10.004.

Duong, V., Nguyen, T. and Maeng, H., 2020. Preparation of Solid Lipid Nanoparticles and Nanostructured Lipid Carriers for Drug Delivery and the Effects of Preparation Parameters of Solvent Injection Method. *Molecules (Basel, Switzerland)*, Oct 18, vol. 25, no. 20, pp. 4781. Available from: https://www.ncbi.nlm.nih.gov/pubmed/33081021 MEDLINE. ISSN 1420-3049. DOI 10.3390/molecules25204781.

Elkateb, H., Cauldbeck, H., Niezabitowska, E., Hogarth, C., Arnold, K., Rannard, S. and Mcdonald, T.O., 2023. High drug loading solid lipid nanoparticles, nanostructured lipid carriers and nanoemulsions for the dual drug delivery of the HIV drugs darunavir and ritonavir. *JCIS Open (Amsterdam)*, Oct, vol. 11, pp. 100087. Available

from: https://dx.doi.org/10.1016/j.jciso.2023.100087 CrossRef. ISSN 2666-934X. DOI 10.1016/j.jciso.2023.100087.

Elmowafy, M., Shalaby, K., Elkomy, M.H., Alsaidan, O.A., Gomaa, H.A.M., Abdelgawad, M.A. and Mostafa, E.M., 2023. Polymeric Nanoparticles for Delivery of Natural Bioactive Agents: Recent Advances and Challenges. *Polymers*, Feb 23, vol. 15, no. 5, pp. 1123. Available from: https://www.ncbi.nlm.nih.gov/pubmed/36904364 PubMed. ISSN 2073-4360. DOI 10.3390/polym15051123.

EUCAST., 2023a. *Antimicrobial susceptibility testing EUCAST disk diffusion method.* , January.

EUCAST., 2023b. *European Committee on Antimicrobial Susceptibility Testing Routine and extended internal quality control for MIC determination and disk diffusion as recommended by EUCAST.* , June.

European Medicines Agency., 1995. *ICH Topic Q 2 (R1) Validation of Analytical Procedures: Text and Methodology.* , June.

Fawaz, S., Barton, S., Whitney, L., Swinden, J. and Nabhani-Gebara, S., 2019. Stability of Meropenem After Reconstitution for Administration by Prolonged Infusion. *Hospital Pharmacy (Philadelphia)*, Jun 1, vol. 54, no. 3, pp. 190-196. Available from: https://journals.sagepub.com/doi/full/10.1177/0018578718779009 PubMed. ISSN 0018-5787. DOI 10.1177/0018578718779009.

Fish, D.N., 2006. Meropenem in the treatment of complicated skin and soft tissue infections. *Therapeutics and Clinical Risk Management*, Dec 1, vol. 2, no. 4, pp. 401-415. Available from: https://www.ncbi.nlm.nih.gov/pubmed/18360652PubMed. ISSN 1176-6336. DOI 10.2147/tcrm.2006.2.4.401.

Fleming, D., Niese, B., Redman, W., VanderpooL, E., Gordon, V. and Rumbaugh, K.P., 2022. Contribution of Pseudomonas aeruginosa Exopolysaccharides Pel and Psl to Wound Infections. *Frontiers in Cellular and Infection Microbiology*, Apr 7, vol. 12, pp. 835754. Available from: https://www.ncbi.nlm.nih.gov/pubmed/35463635 MEDLINE. ISSN 2235-2988. DOI 10.3389/fcimb.2022.835754.

Françoise, A. and Héry-Arnaud, G., 2020. The Microbiome in Cystic Fibrosis Pulmonary Disease. *Genes*, May 11, vol. 11, no. 5, pp. 536. Available from: https://www.ncbi.nlm.nih.gov/pubmed/32403302 MEDLINE. ISSN 2073-4425. DOI 10.3390/genes11050536.

Gao, W., Thamphiwatana, S., Angsantikul, P. and Zhang, L., 2014. Nanoparticle approaches against bacterial infections. *Wiley Interdisciplinary Reviews.Nanomedicine and Nanobiotechnology*, 20140715, vol. 6, no. 6, pp. 532-547 ISSN 1939-0041. DOI 10.1002/wnan.1282.

Ghasemiyeh, P. and Mohammadi-Samani, S., 2018. Solid lipid nanoparticles and nanostructured lipid carriers as novel drug delivery systems: applications, advantages and disadvantages. *Research in Pharmaceutical Sciences*, Aug 1, vol. 13, no. 4, pp. 288-303. Available from: http://www.rpsjournal.net/article.asp?issn=1735-5362;year=2018;volume=13;issue=4;spage=288;epage=303;aulast=Ghasemiyeh;type=0 PubMed. ISSN 1735-5362. DOI 10.4103/1735-5362.235156.

Glen, K.A. and Lamont, I.L., 2021. β-lactam Resistance in Pseudomonas aeruginosa: Current Status, Future Prospects. *Pathogens (Basel)*, Dec 18, vol. 10, no. 12, pp. 1638. Available from: https://www.ncbi.nlm.nih.gov/pubmed/34959593 PubMed. ISSN 2076-0817. DOI 10.3390/pathogens10121638.

Grassi, L., Di Luca, M., Maisetta, G., Rinaldi, A.C., Esin, S., Trampuz, A. and Batoni, G., 2017. Generation of persister cells of pseudomonas aeruginosa and staphylococcus aureus by chemical treatment and evaluation of their susceptibility to membrane-targeting agents. Available from: http://hdl.handle.net/1854/LU-8663116 ISSN 1664-302X. DOI 10.3389/fmicb.2017.01917.

Haiko, J. and Westerlund-Wikström, B., 2013. The Role of the Bacterial Flagellum in Adhesion and Virulence. *Biology*, Oct 25, vol. 2, no. 4, pp. 1242-1267. Available from: https://www.ncbi.nlm.nih.gov/pubmed/24833223 PubMed. ISSN 2079-7737. DOI 10.3390/biology2041242.

Han, H., Bártolo, R., LI, J., Shahbazi, M. and Santos, H.A., 2022. Biomimetic platelet membrane-coated nanoparticles for targeted therapy. *European Journal of Pharmaceutics and Biopharmaceutics*, Mar, vol. 172, pp. 1-15. Available from: https://dx.doi.org/10.1016/j.ejpb.2022.01.004 PubMed. ISSN 0939-6411. DOI 10.1016/j.ejpb.2022.01.004.

He, J., Hong, M., Xie, W., Chen, Z., Chen, D. and Xie, S., 2022. Progress and prospects of nanomaterials against resistant bacteria. *Journal of Controlled Release*, Nov, vol. 351, pp. 301-323. Available from: https://dx.doi.org/10.1016/j.jconrel.2022.09.030 CrossRef. ISSN 0168-3659. DOI 10.1016/j.jconrel.2022.09.030.

Hooper, D.C. and Jacoby, G.A., 2016. Topoisomerase Inhibitors: Fluoroquinolone Mechanisms of Action and Resistance. *Cold Spring Harbor Perspectives in Medicine*, Sep 1, vol. 6, no. 9, pp. a025320. Available from: https://www.ncbi.nlm.nih.gov/pubmed/27449972 MEDLINE. ISSN 2157-1422. DOI 10.1101/cshperspect.a025320.

Horcajada, J.P., Montero, M., Oliver, A., Sorlí, L., Luque, S., Gómez-Zorrilla, S., Benito, N. and Grau, S., 2019. Epidemiology and Treatment of Multidrug-Resistant and Extensively Drug-Resistant Pseudomonas aeruginosa Infections. *Clinical Microbiology Reviews*, 20190828, Aug 28, vol. 32, no. 4, pp. e00031-19. Print 2019 Sep 18 ISSN 1098-6618. DOI 10.1128/CMR.00031-19.

Horna, G. and Ruiz, J., 2021. Type 3 secretion system of Pseudomonas aeruginosa. *Microbiological Research*, May, vol. 246, pp. 126719. Available from: https://dx.doi.org/10.1016/j.micres.2021.126719 PubMed. ISSN 0944-5013. DOI 10.1016/j.micres.2021.126719.

Hou, Y., Zhang, F., Lan, J., Sun, F., LI, J., LI, M., Song, K. and Wu, X., 2019. Ultra-small micelles based on polyoxyl 15 hydroxystearate for ocular delivery of myricetin: optimization, in vitro, and in vivo evaluation. *Drug Delivery*, Jan 1, vol. 26, no. 1, pp. 158-167. Available from: https://www.tandfonline.com/doi/abs/10.1080/10717544.2019.1568624 PubMed. ISSN 1071-7544. DOI 10.1080/10717544.2019.1568624.

Jamieson, C., Allwood, M.C., Stonkute, D., Wallace, A., Wilkinson, A. and Hills, T., 2020. Investigation of meropenem stability after reconstitution: the influence of buffering and challenges to meet the NHS Yellow Cover Document compliance for continuous infusions in an outpatient setting. *European Journal of Hospital Pharmacy*, Mar 1, vol. 27, no. e1, pp. e53-e57. Available from: https://www.ncbi.nlm.nih.gov/pubmed/32296506 PubMed. ISSN 2047-9956. DOI 10.1136/ejhpharm-2018-001699.

Kanamori, H., Weber, D.J. and Rutala, W.A., 2016. Healthcare Outbreaks Associated With a Water Reservoir and Infection Prevention Strategies. *Clinical Infectious Diseases*, Jun 1, vol. 62, no. 11, pp. 1423-1435. Available from: https://www.jstor.org/stable/26371007 MEDLINE. ISSN 1058-4838. DOI 10.1093/cid/ciw122.

Kapoor, G., Saigal, S. and Elongavan, A., 2017. Action and resistance mechanisms of antibiotics: A guide for clinicians. *Journal of Anaesthesiology Clinical Pharmacology*, Jul 1, vol. 33, no. 3, pp. 300-305. Available from: https://www.ncbi.nlm.nih.gov/pubmed/29109626 PubMed. ISSN 0970-9185. DOI 10.4103/joacp.JOACP_349_15.

Kasimanickam, V., Kasimanickam, M. and Kasimanickam, R., 2021. Antibiotics Use in Food Animal Production: Escalation of Antimicrobial Resistance: Where Are We Now in Combating AMR?. *Medical Sciences (Basel)*, Feb 21, vol. 9, no. 1, pp. 14. Available from: https://www.ncbi.nlm.nih.gov/pubmed/33669981 MEDLINE. ISSN 2076-3271. DOI 10.3390/medsci9010014.

Khan, A.A., Mudassir, J., Akhtar, S., Murugaiyah, V. and Darwis, Y., 2019. Freeze-Dried Lopinavir-Loaded Nanostructured Lipid Carriers for Enhanced Cellular Uptake and Bioavailability: Statistical Optimization, in Vitro and in Vivo Evaluations. *Pharmaceutics*, Feb 25, vol. 11, no. 2, pp. 97. Available from: https://www.ncbi.nlm.nih.gov/pubmed/30823545 PubMed. ISSN 1999-4923. DOI 10.3390/pharmaceutics11020097.

Khan, S., Baboota, S., Ali, J., Khan, S., Narang, R.S. and Narang, J.K., 2015a. Nanostructured lipid carriers: An emerging platform for improving oral bioavailability of lipophilic drugs. *International Journal of Pharmaceutical Investigation*, Oct, vol. 5, no. 4, pp. 182-191. Available from: https://pubmed.ncbi.nlm.nih.gov/26682188 https://www.ncbi.nlm.nih.gov/pmc/articles/PMC4674999/ PubMed. ISSN 2230-973X. DOI 10.4103/2230-973X.167661.

Khanolkar, R.A., Clark, S.T., Wang, P.W., Hwang, D.M., Yau, Y.C.W., Waters, V.J. and Guttman, D.S., 2020. Ecological Succession of Polymicrobial Communities in the Cystic Fibrosis Airways. *mSystems*, Dec 1, vol. 5, no. 6. Available from: https://www.ncbi.nlm.nih.gov/pubmed/33262240 PubMed. ISSN 2379-5077. DOI 10.1128/mSystems.00809-20.

Khosa, A., Reddi, S. and Saha, R.N., 2018. Nanostructured lipid carriers for site-specific drug delivery. *Biomedicine & Pharmacotherapy*, vol. 103, pp. 598-613. Available from: https://www.sciencedirect.com/science/article/pii/S0753332218313222 ISSN 0753-3322. DOI 10.1016/j.biopha.2018.04.055.

Knoll, P., Hörmann, N., Nguyen LE, N., Wibel, R., Gust, R. and Bernkop-Schnürch, A., 2022. Charge converting nanostructured lipid carriers containing a cell-penetrating peptide for enhanced cellular uptake. *Journal of Colloid and Interface Science*, Dec 15, vol. 628, pp. 463-475. Available from: https://dx.doi.org/10.1016/j.jcis.2022.07.160 CrossRef. ISSN 0021-9797. DOI 10.1016/j.jcis.2022.07.160.

Kramer, A., Schwebke, I. and Kampf, G., 2006. How long do nosocomial pathogens persist on inanimate surfaces? A systematic review. *BMC Infectious Diseases*, Aug 16, vol. 6, no. 1, pp. 130. Available from: https://www.ncbi.nlm.nih.gov/pubmed/16914034 MEDLINE. ISSN 1471-2334. DOI 10.1186/1471-2334-6-130.

Labauve, A.E. and Wargo, M.J., 2012. Growth and laboratory maintenance of Pseudomonas aeruginosa. *Current Protocols in Microbiology*, May, vol. Chapter 6, pp. Unit 6E.1. ISSN 1934-8533. DOI 10.1002/9780471729259.mc06e01s25.

Lasoń, E., Sikora, E. and Ogonowski, J., 2013. Influence of process parameters on properties of Nanostructured Lipid Carriers (NLC) formulation. *Acta Biochimica Polonica*, Jan 1, vol. 60, no. 4, pp. 773. Available from: https://www.ncbi.nlm.nih.gov/pubmed/24432330 MEDLINE. ISSN 0001-527X. DOI 10.18388/abp.2013_2056.

Laurent, S., Forge, D., Port, M., Roch, A., Robic, C., Vander Elst, L. and Muller, R.N., 2008. Magnetic Iron Oxide Nanoparticles: Synthesis, Stabilization, Vectorization, Physicochemical Characterizations,

and Biological Applications. *Chemical Reviews*, Jun 1, vol. 108, no. 6, pp. 2064-2110. Available from: http://dx.doi.org/10.1021/cr068445e MEDLINE. ISSN 0009-2665. DOI 10.1021/cr068445e.

Lee, A.L., Button, B.M. and Tannenbaum, E.L., 2017. Airway-Clearance Techniques in Children and Adolescents with Chronic Suppurative Lung Disease and Bronchiectasis. *Frontiers in Pediatrics*, 20170124, Jan 24, vol. 5, pp. 2 ISSN 2296-2360. DOI 10.3389/fped.2017.00002 [doi].

Lewis, K., 2008. Multidrug Tolerance of Biofilms and Persister Cells. *Current Topics in Microbiology and Immunology*, vol. 322, pp. 107-131 ISSN 0070-217X.

LI, H., Luo, Y., Williams, B.J., Blackwell, T.S. and XIE, C., 2012. Structure and function of OprD protein in Pseudomonas aeruginosa: from antibiotic resistance to novel therapies. *International Journal of Medical Microbiology : IJMM*, 20120105, Mar, vol. 302, no. 2, pp. 63-68 ISSN 1618-0607. DOI 10.1016/j.ijmm.2011.10.001.

LIAO, C., HUANG, X., WANG, Q., YAO, D. and LU, W., 2022. Virulence Factors of Pseudomonas Aeruginosa and Antivirulence Strategies to Combat Its Drug Resistance. *Frontiers in Cellular and Infection Microbiology*, Jul 6, vol. 12, pp. 926758. Available from: https://search.proquest.com/docview/2694420294 CrossRef. ISSN 2235-2988. DOI 10.3389/fcimb.2022.926758.

Linden, P., 2007. *Safety Profile of Meropenem: An Updated Review of Over 6000 Patients Treated with Meropenem.* Auckland: Adis International, Jan 1, CrossRef. ISBN 0114-5916.

Liou, T.G., 2019. The Clinical Biology of Cystic Fibrosis Transmembrane Regulator Protein: Its Role and Function in Extrapulmonary Disease. *Chest*, 20181022, Mar, vol. 155, no. 3, pp. 605-616 ISSN 1931-3543. DOI S0012-3692(18)32585-6 [pii].

Liu, J., Gong, T., Wang, C., Zhong, Z. and Zhang, Z., 2007. Solid lipid nanoparticles loaded with insulin by sodium cholate-phosphatidylcholine-based mixed micelles: preparation and characterization. *International Journal of Pharmaceutics*, 20070312, Aug 1, vol. 340, no. 1-2, pp. 153-162 ISSN 0378-5173. DOI S0378-5173(07)00242-6 [pii].

Lorusso, A.B., Carrara, J.A., Barroso, C.D.N., Tuon, F.F. and Faoro, H., 2022. Role of Efflux Pumps on Antimicrobial Resistance in Pseudomonas aeruginosa. *International Journal of Molecular Sciences*, Dec 13, vol. 23, no. 24, pp. 15779. Available from: https://www.ncbi.nlm.nih.gov/pubmed/36555423 MEDLINE. ISSN 1661-6596. DOI 10.3390/ijms232415779.

Magiorakos, A.-., Srinivasan, A., Carey, R.B., Carmeli, Y., Falagas, M.E., Giske, C.G., Harbarth, S., Hindler, J.F., Kahlmeter, G., Olsson-Liljequist, B., Paterson, D.L., Rice, L.B., Stelling, J., Struelens, M.J., Vatopoulos, A., Weber, J.T. and Monnet, D.L., 2012. Multidrug-resistant, extensively drug-resistant and pandrug-resistant bacteria: an international expert proposal for interim standard definitions for acquired resistance. *Clinical Microbiology and Infection*, Mar, vol. 18, no. 3, pp. 268-281. Available from: https://dx.doi.org/10.1111/j.1469-0691.2011.03570.xMEDLINE. ISSN 1198-743X. DOI 10.1111/j.1469-0691.2011.03570.x.

Malvern Company., 2018. *https://www.research.colostate.edu/wp-content/uploads/2018/11/ZetaPotential-Introduction-in-30min-Malvern.pdf.* Available from: https://www.research.colostate.edu/wp-content/uploads/2018/11/ZetaPotential-Introduction-in-30min-Malvern.pdf.

Manos, J., 2021. Current and Emerging Therapies to Combat Cystic Fibrosis Lung Infections. *Microorganisms*, 20210903, Sep 3, vol. 9, no. 9, pp. 1874. doi: 10.3390/microorganisms9091874 ISSN 2076-2607. DOI 10.3390/microorganisms9091874 [doi].

Manyi-Loh, C., Mamphweli, S., Meyer, E. and Okoh, A., 2018. Antibiotic use in agriculture and its consequential resistance in environmental sources: potential public health implications. *Molecules*, Mar 30, vol. 23, no. 4, pp. 795. Available from: https://www.ncbi.nlm.nih.gov/pubmed/29601469 PubMed. ISSN 1420-3049. DOI 10.3390/molecules23040795.

Maria Pacifici, G., 2019. Clinical pharmacology of meropenem in infants and children. *Clinical and Medical Investigations*, vol. 4, no. 1 CrossRef. ISSN 2398-5763. DOI 10.15761/CMI.1000178.

Meletis, G., 2016. *Carbapenem resistance: overview of the problem and future perspectives.* London, England: SAGE Publications, Feb, PubMed. ISBN 2049-9361.

Mendez, A.S.L., Steppe, M. and Schapoval, E.E.S., 2003. Validation of HPLC and UV spectrophotometric methods for the determination of meropenem in pharmaceutical dosage form. *Journal of Pharmaceutical and Biomedical Analysis*, Dec 4, vol. 33, no. 5, pp. 947-954. Available from: https://dx.doi.org/10.1016/S0731-7085(03)00366-2 MEDLINE. ISSN 0731-7085. DOI 10.1016/S0731-7085(03)00366-2.

Mhango, E.K.G., Kalhapure, R.S., jadhav, M., Sonawane, S.J., Mocktar, C., Vepuri, S., Soliman, M. and Govender, T., 2017. Preparation and Optimization of Meropenem-Loaded Solid Lipid Nanoparticles: In Vitro Evaluation and Molecular Modeling. *AAPS PharmSciTech*, Aug 1, vol. 18, no. 6, pp. 2011-2025. Available from: https://link.springer.com/article/10.1208/s12249-016-0675-z MEDLINE. ISSN 1530-9932. DOI 10.1208/s12249-016-0675-z.

Miles, A.A., Misra, S.S. and Irwin, J.O., 1938. The estimation of the bactericidal power of the blood. *Epidemiology and Infection*, Nov 1, vol. 38, no. 6, pp. 732-749. Available from: https://dx.doi.org/10.1017/S002217240001158X PubMed. ISSN 0950-2688. DOI 10.1017/S002217240001158X.

Milla, P., Ferrari, F., Muntoni, E., Sartori, M., Ronco, C. and Arpicco, S., 2020a. Validation of a simple and economic HPLC-UV method for the simultaneous determination of vancomycin, meropenem, piperacillin and tazobactam in plasma samples. *Journal of Chromatography. B, Analytical Technologies in the Biomedical and Life Sciences*, Jul 1, vol. 1148, pp. 122151. Available from: https://dx.doi.org/10.1016/j.jchromb.2020.122151 PubMed. ISSN 1570-0232. DOI 10.1016/j.jchromb.2020.122151.

Mitchell, M.J., Billingsley, M.M., Haley, R.M., Wechsler, M.E., Peppas, N.A. and Langer, R., 2021. Engineering precision nanoparticles for drug delivery. *Nature Reviews. Drug Discovery*, Feb 1, vol. 20, no. 2, pp. 101-124. Available from: https://www.ncbi.nlm.nih.gov/pubmed/33277608 MEDLINE. ISSN 1474-1776. DOI 10.1038/s41573-020-0090-8.

Mohareb, A.M., Letourneau, A.R., Sánchez, S.M., Walensky, R.P. and Hyle, E.P., 2021. Addressing Antibiotic Overuse in the Outpatient Setting: Lessons From Behavioral Economics. *Mayo Clinic Proceedings*, Mar, vol. 96, no. 3, pp. 537-542. Available from: https://dx.doi.org/10.1016/j.mayocp.2020.10.033 MEDLINE. ISSN 0025-6196. DOI 10.1016/j.mayocp.2020.10.033.

Monahan, L.G., Turnbull, L., Osvath, S.R., Birch, D., Charles, I.G. and Whitchurch, C.B., 2014. Rapid Conversion of Pseudomonas aeruginosa to a Spherical Cell Morphotype Facilitates Tolerance to Carbapenems and Penicillins but Increases Susceptibility to Antimicrobial Peptides. *Antimicrobial Agents and Chemotherapy*, Apr 1, vol. 58, no. 4, pp. 1956-1962. Available from: https://www.ncbi.nlm.nih.gov/pubmed/24419348 MEDLINE. ISSN 0066-4804. DOI 10.1128/AAC.01901-13.

Mukherjee, S., Ray, S. and Thakur, R.S., 2009. Solid lipid nanoparticles: a modern formulation approach in drug delivery system. *Indian Journal of Pharmaceutical Sciences*, vol. 71, no. 4, pp. 349-358. Available from: https://pubmed.ncbi.nlm.nih.gov/20502539 https://www.ncbi.nlm.nih.gov/pmc/articles/PMC2865805/ PubMed. ISSN 1998-3743. DOI 10.4103/0250-474X.57282.

Mulcahy, L.R., Isabella, V.M. and Lewis, K., 2014. Pseudomonas aeruginosa Biofilms in Disease. *Microbial Ecology*, Jul 1, vol. 68, no. 1, pp. 1-12. Available from: https://www.jstor.org/stable/24542310 MEDLINE. ISSN 0095-3628. DOI 10.1007/s00248-013-0297-x.

Mundekkad, D. and Cho, W.C., 2022. Nanoparticles in Clinical Translation for Cancer Therapy. *International Journal of Molecular Sciences*, Feb 1, vol. 23, no. 3, pp. 1685. Available from: https://www.ncbi.nlm.nih.gov/pubmed/35163607MEDLINE. ISSN 1422-0067. DOI 10.3390/ijms23031685.

Muneer, S., Wang, T., Rintoul, L., Ayoko, G.A., Islam, N. and Izake, E.L., 2020. Development and characterization of meropenem dry powder inhaler formulation for pulmonary drug delivery. *International Journal of Pharmaceutics*, Sep 25, vol. 587, pp. 119684. Available from: https://dx.doi.org/10.1016/j.ijpharm.2020.119684 CrossRef. ISSN 0378-5173. DOI 10.1016/j.ijpharm.2020.119684.

Muraca, G.S., Soler-Arango, J., Castro, G.R., Islan, G.A. and Brelles-Mariño, G., 2021. Improving ciprofloxacin antimicrobial activity through lipid nanoencapsulation or non-thermal plasma on Pseudomonas aeruginosa biofilms. *Journal of Drug Delivery Science and Technology*, Aug, vol. 64, pp. 102644. Available from: https://dx.doi.org/10.1016/j.jddst.2021.102644 CrossRef. ISSN 1773-2247. DOI 10.1016/j.jddst.2021.102644.

Nagaich, U. and Gulati, N., 2016. Nanostructured lipid carriers (NLC) based controlled release topical gel of clobetasol propionate: design and in vivo characterization. *Drug Delivery and Translational Research*, Jun 1, vol. 6, no. 3, pp. 289-298. Available from: https://link.springer.com/article/10.1007/s13346-016-0291-1 MEDLINE. ISSN 2190-393X. DOI 10.1007/s13346-016-0291-1.

National Center for Biotechnology Information, 2023. Meropenem . Available from: https://pubchem.ncbi.nlm.nih.gov/compound/Meropenem#section=EPA-Substance-Registry-Services-Tree.

Nayak, R.P., 2012. Latest in cystic fibrosis. *Missouri Medicine*, vol. 109, no. 2, pp. 127-132. Available from: https://www.ncbi.nlm.nih.gov/pubmed/22675793 MEDLINE. ISSN 0026-6620.

Nguyen, V.H., Thuy, V.N., Van, T.V., Dao, A.H. and Lee, B., 2022. Nanostructured lipid carriers and their potential applications for versatile drug delivery via oral administration. *OpenNano*, Nov, vol. 8, pp. 100064. Available from: https://dx.doi.org/10.1016/j.onano.2022.100064CrossRef. ISSN 2352-9520. DOI 10.1016/j.onano.2022.100064.

NICE, 2023. Meropenem . Available from: https://bnf.nice.org.uk/drugs/meropenem/.

Ojkic, N., Serbanescu, D. and Banerjee, S., 2022. Antibiotic Resistance via Bacterial Cell Shape-Shifting. *mBio*, Jun 28, vol. 13, no. 3, pp. e0065922. Available from: https://www.ncbi.nlm.nih.gov/pubmed/35616332 PubMed. ISSN 2150-7511. DOI 10.1128/mbio.00659-22.

Olbrich, C., Kayser, O. and Müller, R.H., 2002. Lipase degradation of Dynasan 114 and 116 solid lipid nanoparticles (SLN)—effect of surfactants, storage time and crystallinity. *International Journal of Pharmaceutics*, vol. 237, no. 1, pp. 119-128. Available from: https://www.sciencedirect.com/science/article/pii/S0378517302000352 ISSN 0378-5173. DOI https://doi.org/10.1016/S0378-5173(02)00035-2.

Pachori, P., Gothalwal, R. and Gandhi, P., 2019. Emergence of antibiotic resistance Pseudomonas aeruginosa in intensive care unit; a critical review. *Genes & Diseases*, Jun 1, vol. 6, no. 2, pp. 109-119. Available from: https://dx.doi.org/10.1016/j.gendis.2019.04.001 PubMed. ISSN 2352-3042. DOI 10.1016/j.gendis.2019.04.001.

Pang, Z., Raudonis, R., Glick, B.R., Lin, T. and Cheng, Z., 2019. Antibiotic resistance in Pseudomonas aeruginosa: mechanisms and alternative therapeutic strategies. *Biotechnology Advances*, vol. 37, no. 1, pp. 177-192. Available from: https://www.sciencedirect.com/science/article/pii/S0734975018301976 ISSN 0734-9750. DOI 10.1016/j.biotechadv.2018.11.013.

Patel, D., Dasgupta, S., Dey, S., Ramani, Y.R., Ray, S. and Mazumder, B., 2012. Nanostructured Lipid Carriers (NLC)-Based Gel for Topical Delivery of Aceclofenac: Preparation, Characterization and In Vivo Evaluation. *Scientia Pharmaceutica*, Jul, vol. 80, no. 3, pp. 749-764. Available from: https://www.ncbi.nlm.nih.gov/pubmed/23008819 PubMed. ISSN 0036-8709. DOI 10.3797/scipharm.1202-12.

Patra, J.K., das, G., Fraceto, L.F., Campos, E.V.R., Rodriguez-Torres, M.D.P., Acosta-Torres, L.S., Diaz-Torres, L.A., Grillo, R., Swamy, M.K., Sharma, S., Habtemariam, S. and Shin, H., 2018. Nano based drug delivery systems: recent developments and future prospects. *Journal of Nanobiotechnology*, Sep 19, vol. 16, no. 1, pp. 71. Available from: https://www.ncbi.nlm.nih.gov/pubmed/30231877 PubMed. ISSN 1477-3155. DOI 10.1186/s12951-018-0392-8.

Pezeshki, A., Ghanbarzadeh, B., Mohammadi, M., Fathollahi, I. and Hamishehkar, H., 2014. Encapsulation of Vitamin A Palmitate in Nanostructured Lipid Carrier (NLC)-Effect of Surfactant Concentration on the Formulation Properties. *Advanced Pharmaceutical Bulletin*, Dec 1, vol. 4, no. Suppl 2, pp. 563-568. Available from: https://www.ncbi.nlm.nih.gov/pubmed/25671190 PubMed. ISSN 2228-5881. DOI 10.5681/apb.2014.083.

PHE., 5/20/19. *UK SMI TP 39: staining procedures.* 5/20/19, Available from: https://www.gov.uk/government/publications/smi-tp-39-staining-procedures.

PHE, 2018. Pseudomonas aeruginosa infection: mandatory surveillance 2017/18 Summary of the Mandatory Surveillance Annual Epidemiological Commentary 2017/18.

Pottier, M., Gravey, F., Castagnet, S., Auzou, M., Langlois, B., Guérin, F., Giard, J., Léon, A. and Le Hello, S., 2023. A 10-year microbiological study of Pseudomonas aeruginosa strains revealed the circulation of populations resistant to both carbapenems and quaternary ammonium compounds. *Scientific Reports*, Feb 14, vol. 13, no. 1, pp. 2639. Available from: https://www.ncbi.nlm.nih.gov/pubmed/36788252 MEDLINE. ISSN 2045-2322. DOI 10.1038/s41598-023-29590-0.

Public Health England., 2019a. *UK Standards for Microbiology Investigations Catalase test.* , April.

Public Health England, 2019b. UK Standards for Microbiology Investigations Oxidase test, January. Available

from: https://assets.publishing.service.gov.uk/government/uploads/system/uploads/attachment_data/file/771781/TP_26i4.pdf.

Public Health England., 2019c. *UK Standards for Microbiology Investigations Staining procedures.* , May.

Qin, S., Xiao, W., Zhou, C., Pu, Q., Deng, X., Lan, L., Liang, H., Song, X. and Wu, M., 2022. Pseudomonas aeruginosa: pathogenesis, virulence factors, antibiotic resistance, interaction with host, technology advances and emerging therapeutics. *Signal Transduction and Targeted Therapy*, Jun 25, vol. 7, no. 1, pp. 199. Available from: https://search.proquest.com/docview/2680640286 CrossRef. ISSN 2059-3635. DOI 10.1038/s41392-022-01056-1.

Rajpoot, K., Prajapati, S.K., Malaiya , A., Jain, R. and Jain, A., 2022. Meropenem-Loaded Nanostructured Lipid Carriers For Skin and Soft Tissue Infection Caused by Staphylococcus aureus: Formulation, Design, and Evaluation. *AAPS PharmSciTech*, Aug 25, vol. 23, no. 7, pp. 241. Available from: https://link.springer.com/article/10.1208/s12249-022-02381-y CrossRef. ISSN 1530-9932. DOI 10.1208/s12249-022-02381-y.

Reynolds, D. and Kollef, M., 2021. The Epidemiology and Pathogenesis and Treatment of Pseudomonas aeruginosa Infections: An Update. *Drugs (New York, N.Y.)*, Dec 1, vol. 81, no. 18, pp. 2117-2131. Available from: https://link.springer.com/article/10.1007/s40265-021-01635-6 MEDLINE. ISSN 0012-6667. DOI 10.1007/s40265-021-01635-6.

Sharma, A., Gupta, V. and Pathania, R., 2019. Efflux pump inhibitors for bacterial pathogens: From bench to bedside. *Indian Journal of Medical Research (New Delhi, India : 1994)*, Feb 1, vol. 149, no. 2, pp. 129-145. Available from: http://www.ijmr.org.in/article.asp?issn=0971-5916;year=2019;volume=149;issue=2;spage=129;epage=145;aulast=Sharma;type=0 MEDLINE. ISSN 0971-5916. DOI 10.4103/ijmr.IJMR_2079_17.

Singla, A. and Upadhyayula, S., 2022. Nanobiomaterials Administration in Modernization of Biological Science: Current Status and Future Potential. In: *Handbook of Smart Materials, Technologies, and Devices* Cham: Springer International Publishing, pp. 729-777 ISBN 3030842045. DOI 10.1007/978-3-030-84205-5_129.

Sousa De Almeida, M., Susnik, E., Drasler, B., Taladriz-Blanco, P., Petri-Fink, A. and Rothen-Rutishauser, B., 2021. Understanding nanoparticle endocytosis to improve targeting strategies in nanomedicine. *Chemical Society Reviews*, May 7, vol. 5, no. 9, pp. 5397-5434. Available from: https://www.ncbi.nlm.nih.gov/pubmed/33666625 PubMed. ISSN 0306-0012. DOI 10.1039/d0cs01127d.

Studzińska, S. and Buszewski, B., 2013. Effect of mobile phase pH on the retention of nucleotides on different stationary phases for high-performance liquid chromatography. *Analytical and Bioanalytical Chemistry*, Feb 1, vol. 405, no. 5, pp. 1663-1672. Available from: https://link.springer.com/article/10.1007/s00216-012-6590-6 MEDLINE. ISSN 1618-2642. DOI 10.1007/s00216-012-6590-6.

Subramaniam, B., Siddik, Z.H. and Nagoor, N.H., 2020. Optimization of nanostructured lipid carriers: understanding the types, designs, and parameters in the process of formulations. *Journal of Nanoparticle Research : An Interdisciplinary Forum for Nanoscale Science and Technology*, Jun 1, vol. 22, no. 6. Available from: https://link.springer.com/article/10.1007/s11051-020-04848-0 CrossRef. ISSN 1388-0764. DOI 10.1007/s11051-020-04848-0.

Talele, P., Sahu, S. and Mishra, A.K., 2018. Physicochemical characterization of solid lipid nanoparticles comprised of glycerol monostearate and bile salts. *Colloids and Surfaces, B,*

Biointerfaces, Dec 1, vol. 172, pp. 517-525. Available from: https://dx.doi.org/10.1016/j.colsurfb.2018.08.067 MEDLINE. ISSN 0927-7765. DOI 10.1016/j.colsurfb.2018.08.067.

Tang, Y.J., Ashcroft, J.M., Chen, D., Min, G., Kim, C., Murkhejee, B., Larabell, C., Keasling, J.D. and Chen, F.F., 2007. Charge-Associated Effects of Fullerene Derivatives on Microbial Structural Integrity and Central Metabolism. *Nano Letters*, Mar 1, vol. 7, no. 3, pp. 754-760. Available from: http://dx.doi.org/10.1021/nl063020t MEDLINE. ISSN 1530-6984. DOI 10.1021/nl063020t.

Thalhammer, F., Schenk, P., Burgmann, H., El Menyawi, I., Hollenstein, U.M., Rosenkranz, A.R., Sunder-Plassmann, G., Breyer, S. and Ratheiser, K., 1998. Single-Dose Pharmacokinetics of Meropenem during Continuous Venovenous Hemofiltration. *Antimicrobial Agents and Chemotherapy*, Sep 1, vol. 42, no. 9, pp. 2417-2420. Available from: http://aac.asm.org/content/42/9/2417.abstract MEDLINE. ISSN 0066-4804. DOI 10.1128/AAC.42.9.2417.

Tildy, B.E. and Rogers, D.F., 2015. Therapeutic Options for Hydrating Airway Mucus in Cystic Fibrosis. *Pharmacology*, vol. 95, no. 3-4, pp. 117-132. Available from: https://www.karger.com/DOI/10.1159/000377638 ISSN 0031-7012. DOI 10.1159/000377638.

Tooke, C.L., Hinchliffe, P., Bragginton, E.C., ColensO, C.K., Hirvonen, V.H.A., Takebayashi, Y. and Spencer, J., 2019. β-Lactamases and β-Lactamase Inhibitors in the 21st Century. *Journal of Molecular Biology*, Aug 23, vol. 431, no. 18, pp. 3472-3500. Available from: https://dx.doi.org/10.1016/j.jmb.2019.04.002 MEDLINE. ISSN 0022-2836. DOI 10.1016/j.jmb.2019.04.002.

Tripathi, N. and Sapra, A., 2022. Gram Staining. In: *StatPearls* Treasure Island (FL): StatPearls Publishing LLC,Jan DOI NBK562156 [bookaccession].

UK Health Security Agency., 2023. *Start smart then focus: antimicrobial stewardship toolkit for inpatient care settings.* Available from: https://www.gov.uk/government/publications/antimicrobial-stewardship-start-smart-then-focus/start-smart-then-focus-antimicrobial-stewardship-toolkit-for-inpatient-care-settings.

Ukai, H., Imanishi, A., Kaneda, A., Kimura, E., Koyama, M., Morishita, M., Katsumi, H. and Yamamoto, A., 2020. Absorption-Enhancing Mechanisms of Capryol 90, a Novel Absorption Enhancer, for Improving the Intestinal Absorption of Poorly Absorbed Drugs: Contributions to Trans- or Para-Cellular Pathways. *Pharmaceutical Research*, 20201123, Nov 23, vol. 37, no. 12, pp. 248-0 ISSN 1573-904X. DOI 10.1007/s11095-020-02963-0 [doi].

Upadhyay, S.U., Patel, J.K., Patel, V.A. and Saluja, A.K., 2012. Effect of different lipids and surfactants on formulation of solid lipid nanoparticles incorporating tamoxifen citrate. *Journal of Pharmacy & Bioallied Sciences*, vol. 4, pp. S112-S113. Available from: https://pubmed.ncbi.nlm.nih.gov/23066183 https://www.ncbi.nlm.nih.gov/pmc/articles/PMC3467804/ PubMed. ISSN 0975-7406. DOI 10.4103/0975-7406.94161.

Uskoković, V., Castiglione, Z., Cubas, P., Zhu, L., LI, W. and Habelitz, S., 2010. Zeta-potential and Particle Size Analysis of Human Amelogenins. *Journal of Dental Research*, Feb 1, vol. 89, no. 2, pp. 149-153. Available from: https://journals.sagepub.com/doi/full/10.1177/0022034509354455 MEDLINE. ISSN 0022-0345. DOI 10.1177/0022034509354455.

Wong, L.P., Alias, H., Husin, S.A., Ali, Z.B., SIM, B. and Ponnampalavanar, S.S.L.S., 2021. Factors influencing inappropriate use of antibiotics: Findings from a nationwide survey of the general public in Malaysia. *PloS One*, Oct 20, vol. 16, no. 10, pp. e0258698. Available

from: https://search.proquest.com/docview/2583901531 CrossRef. ISSN 1932-6203. DOI 10.1371/journal.pone.0258698.

World Health Organisation., 2021. *https://www.who.int/news-room/fact-sheets/detail/antimicrobial-resistance.*

World Health Organisation, 2016. GLOBAL ACTION PLAN ON ANTIMICROBIAL RESISTANCE. Available from: https://www.who.int/publications/i/item/9789241509763.

Yadav, A.K., Espaillat, A. and Cava, F., 2018. Bacterial Strategies to Preserve Cell Wall Integrity Against Environmental Threats. *Frontiers in Microbiology*, 20180831, Aug 31, vol. 9, pp. 2064 ISSN 1664-302X. DOI 10.3389/fmicb.2018.02064 [doi].

Yagublu, V., Karimova, A., Hajibabazadeh, J., Reissfelder, C., Muradov, M., Bellucci, S. and Allahverdiyev, A., 2022. Overview of Physicochemical Properties of Nanoparticles as Drug Carriers for Targeted Cancer Therapy. *Journal of Functional Biomaterials*, Oct 20, vol. 13, no. 4, pp. 196. Available from: https://search.proquest.com/docview/2756724768 CrossRef. ISSN 2079-4983. DOI 10.3390/jfb13040196.

Yeh, Y., Huang, T., Yang, S., Chen, C. and Fang, J., 2020. Nano-Based Drug Delivery or Targeting to Eradicate Bacteria for Infection Mitigation: A Review of Recent Advances. *Frontiers in Chemistry*, Apr 24, vol. 8, pp. 286. Available from: https://www.ncbi.nlm.nih.gov/pubmed/32391321 PubMed. ISSN 2296-2646. DOI 10.3389/fchem.2020.00286.

Yin, X., Lai, Y., Du, Y., Zhang, T., Gao, J. and LI, Z., 2023. Metal-Based Nanoparticles: A Prospective Strategy for Helicobacter pylori Treatment. *International Journal of Nanomedicine*, Jan 1, vol. 18, pp. 2413-2429. Available from: https://www.ncbi.nlm.nih.gov/pubmed/37192898 MEDLINE. ISSN 1178-2013. DOI 10.2147/IJN.S405052.

Zanichelli, V., Sharland, M., Cappello, B., Moja, L., Getahun, H., Pessoa-Silva, C., Sati, H., Van Weezenbeek, C., Balkhy, H., Simão, M., Gandra, S. and Huttner, B., 2023. The WHO AWaRe (Access, Watch, Reserve) antibiotic book and prevention of antimicrobial resistance. *Bulletin of the World Health Organization*, Apr 1, vol. 101, no. 4, pp. 290-296. Available from: https://search.proquest.com/docview/2799230470 ProQuest Business Collection (Alumni Edition). ISSN 0042-9686. DOI 10.2471/BLT.22.288614.

Zeng, D., Debabov, D., Hartsell, T.L., Cano, R.J., Adams, S., Schuyler, J.A., Mcmillan, R. and Pace, J.L., 2016. Approved Glycopeptide Antibacterial Drugs: Mechanism of Action and Resistance. *Cold Spring Harbor Perspectives in Medicine*, Dec 1, vol. 6, no. 12, pp. a026989. Available from: https://www.ncbi.nlm.nih.gov/pubmed/27663982 MEDLINE. ISSN 2157-1422. DOI 10.1101/cshperspect.a026989.

Zhou, L., Du, S., Wang, T., Wu, S., Guo, Z., Wang, Z. and Zhou, L., 2017. Measurement and correlation of solubility of meropenem trihydrate in binary (water+acetone/tetrahydrofuran) solvent mixtures. *Chinese Journal of Chemical Engineering*, Oct, vol. 25, no. 10, pp. 1461-1466. Available from: https://dx.doi.org/10.1016/j.cjche.2017.05.002 CrossRef. ISSN 1004-9541. DOI 10.1016/j.cjche.2017.05.002.

Ziglam, H.M. and Finch, R.G., 2001. Limitations of presently available glycopeptides in the treatment of Gram-positive infection. *Clinical Microbiology and Infection*, Jan 1, vol. 7, no. 4, pp. 53-65. Available from: https://dx.doi.org/10.1046/j.1469-0691.2001.00059.x MEDLINE. ISSN 1198-743X. DOI 10.1046/j.1469-0691.2001.00059.x.

Zoubari, G., Staufenbiel, S., Volz, P., Alexiev, U. and Bodmeier, R., 2017. Effect of drug solubility and lipid carrier on drug release from lipid nanoparticles for dermal delivery. *European Journal of Pharmaceutics and Biopharmaceutics*, Jan, vol. 110, pp. 39-46. Available from: https://dx.doi.org/10.1016/j.ejpb.2016.10.021 MEDLINE. ISSN 0939-6411. DOI 10.1016/j.ejpb.2016.10.021.

Zwain, T., Alder, J.E., Sabagh, B., Shaw, A., Burrow, A.J. and Singh, K.K., 2021. Tailoring functional nanostructured lipid carriers for glioblastoma treatment with enhanced permeability through in-vitro 3D BBB/BBTB models. *Materials Science & Engineering C*, Feb, vol. 121, pp. 111774. Available from: https://dx.doi.org/10.1016/j.msec.2020.111774 MEDLINE. ISSN 0928-4931. DOI 10.1016/j.msec.2020.111774.